Exploring Passive Dynamics in Legged Locomotion

by

Zhenyu Gan

A dissertation submitted in partial fulfillment
of the requirements for the degree of
Doctor of Philosophy
(Mechanical Engineering)
in the University of Michigan
2018

Doctoral Committee:

Assistant Professor C. David Remy, Chair
Professor Jessy W. Grizzle
Professor Arthur Kuo, University of Calgary
Assistant Professor Shai Revzen
Assistant Professor Ramanarayan Vasudevan

Zhenyu Gan
ganzheny@umich.edu
ORCID iD: 0000-0002-5972-9600

This thesis is dedicated to my parents
for their unconditional love and ceaseless support
through the years I grown up.

ACKNOWLEDGEMENTS

First, I would like to express my gratitude to my Ph.D mentor C David Remy. I learn so much from you not only in conducting rigorous research, giving scientific presentations, and writing papers, but also on how to behave myself and express myself as a person. You are my role model in so many ways and I am very lucky to follow you as a student.

I also want to thank my colleagues in the RAMlab. Especially I want to thank my good friend, Yevgeniy Yesilevskiy, for being so patient and considerate of me, and bringing me so much laughter. I will never forget the time we worked together in the lab. Thank you to Jeff Koller for teaching me so many things about US. Thank you also to Petr Zaytsev who helped me a lot in writing and shared with me so many interesting stories. I also want to thank Wei Zhou, Haoyue Tang, Ziyuan Jiao, and Chang Liu for helping me on developing models and conducting experiments.

Thanks to all my friends in Ann Arbor, there are so many precious memories in the past six years. Especially, my good friends Yihao Zheng and Molong Duan who helped me in countless ways. Weiyu Cao and Wubing Qin who were constantly available and providing me support.

Most importantly, I want to thank my family. Mom and Dad, you have been a constant source of support no matter what happened. Your encouragements always motivate me to become a better person. And also my wife, Jiangliu Dong, I know you have sacrificed so much to stay with me. I am in your debt for the rest of my life.

TABLE OF CONTENTS

LIST OF FIGURES

Figure

LIST OF TABLES

Table

LIST OF APPENDICES

Appendix

LIST OF ABBREVIATIONS

AOA Angle of Attack

COM Center of Mass

GRF Ground Reaction Force

IP Inverted Pendulum

SLIP Spring Loaded Inverted Pendulum

EOM Equations of Motion

SEAs Series Elastic Actuators

SQP Sequential Quadratic Programming

BVP Boundary Value Problem

ABSTRACT

A common observation among legged animals is that they move their limbs differently as they change their speed. The observed distinct patterns of limb movement are usually referred to as different gaits. Experiments with humans and mammals have shown that switching between different gaits as locomotion speed changes, enables energetically more economical locomotion. However, it still remains unclear why animals with very different morphologies use similar gaits, where these gaits come from, and how they are related. This dissertation approaches these questions by exploring the natural passive dynamic motions of a range of simplified mechanical models of legged locomotion.

Recent research has shown that a simple bipedal model with compliant legs and a single set of parameters can match ground reaction forces of both human walking and running. As first contribution of this dissertation, this concept is extended to quadrupeds. A unified model is developed to reproduce many quadrupedal gaits by only varying the initial states of a motion. In addition, the model parameters are optimized to match the experimental data of real horses, as measured by an instrumented treadmill. It is shown that the proposed model is able to not only create similar kinematic motion trajectories, but can also explain the ground reaction forces of real horses moving with different gaits.

In order to reveal the mechanical contribution to gaits, the simplistic bipedal and quadrupedal models are then augmented to have passive swing leg motions by including torsional springs at the hip joints. Through a numerical continuation of periodic motions, this work shows that a wide range of gaits emerges from a simple

bouncing-in-place motion starting with different footfall patterns. For both, bipedal and quadrupedal models, these gaits arise along one-dimensional manifolds of solutions with varying total energy. Through breaking temporal and spatial symmetries of the periodic motions, these manifolds bifurcate into distinct branches with various footfall sequences. That is, passive gaits are obtained as different oscillatory motions of a single mechanical system with a single set of parameters. By reproducing a variety of gaits as a manifestation of the passive dynamics of unified models, this work provides insights into the underlying dynamics of legged locomotion and may help design of more economical controllers for legged machines.

CHAPTER I

Introduction

1.1 Motivation

An animal's ability to move from one place to another in the environment is one of the most fundamental features that differs it from any other creatures on earth. It enables animal species to harvest more resources, expand their colonies, and find more suitable environments. In order to locomote to a specific destination, one has to overcome the constraints enforced by the environment and utilize energy. Therefore in nature, a large number of animals exhibit remarkable locomotion abilities while maintaining low energy expenditure. As for terrestrial animals, the most important constraint is the consistent pull of gravity. Some species develop different numbers of limbs to move their bodies.

A very common observation of legged animals, including humans, is that at different speeds, they move their limbs differently. The different patterns of limb movement are usually called *gaits*. These gaits can also be characterized by a specific footfall sequence (*Alexander*, 1984; *Hildebrand*, 1989), a typical Ground Reaction Force (GRF) profile (*Alexander*, 1980), or by how gravitational, potential, and kinetic energy are exchanged over the course of a stride (*Cavagna et al.*, 1976). Despite vast differences in morphology, the gaits of many animals are strikingly similar (*Alexander*, 1982). Bipeds, such as humans and birds, prefer to *walk* at low speeds and to *run* at higher

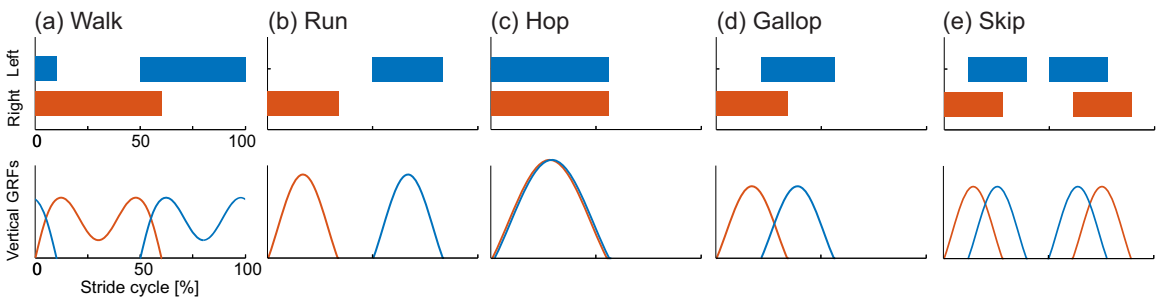

Figure 1.1: The footfall patterns (upper row) and the GRF profiles (lower row) of several bipedal gaits are shown in this figure. The filled bars in the footfall pattern indicate the stance phase of each leg during one stride cycle. And the curves represent the magnitude of the vertical component of the GRFs during stance.

speeds (Fig. 1.1). Quadrupedal mammals, across many species, *walk*, *trot*, and *gallop*. Some other gaits are less common: red kangaroos, for example, are known to *hop* (*Dawson and Taylor*, 1973), and some primates such as lemurs tend to *skip* at a large range of speeds (*Franz et al.*, 2005; *Demes et al.*, 1999). These less common gaits are also observed in humans in special situations such as fast turning, descending stairs, or in low gravity environments (*Minetti*, 1998; *Fiers et al.*, 2012; *Pavei et al.*, 2015).

Modeling and simulating the dynamics of locomotion in all its detail, however, requires multi-body models with a large number of degrees of freedom, the correct handling of intermittent ground contact with collisions, and the modeling of a substantial amount of soft-body motion. These models have to incorporate neural control and they must account for the highly non-linear characteristics of muscle actuation. For many purposes, such a detailed representation is not necessary. On the contrary, while complex models could precisely represent all the details of locomotion in nature, they would have difficulties revealing the underlying principles. Because of this, locomotion research often relies on simplistic models (*Cavagna and Kaneko*, 1977; *McGeer*, 1990; *Holmes et al.*, 2006). These models are highly abstract approximations of reality, often reducing the entire system to a single point mass. Still, they are able to capture the many essential features of the dynamics of locomotion.

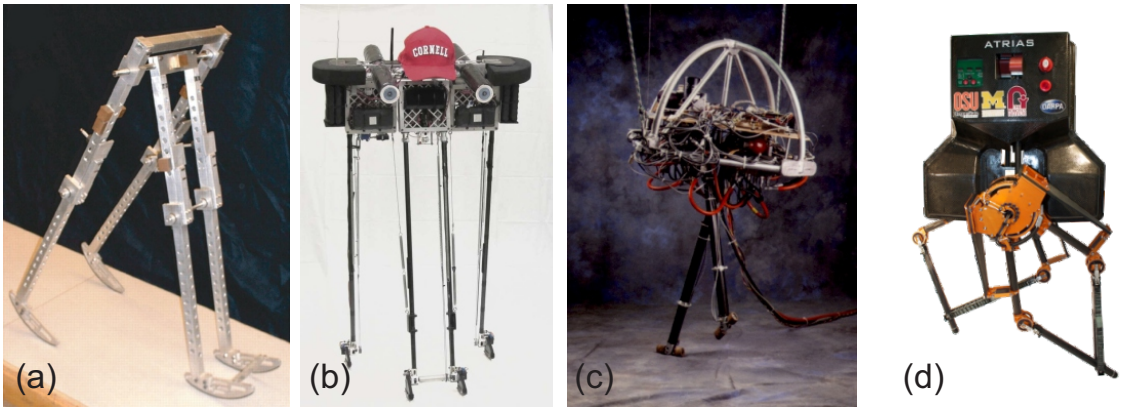

Figure 1.2: Several efficient robots that are designed based on the principles of passive dynamics: (a) a copy of the McGeer's passive dynamic walker with knee joints, (b) Cornell Ranger developed by Biorobotics and Locomotion Lab, (c) MIT 3D Biped, and (d) ATRIAS built by the Oregon State University.

Among these simple models, people found some mechanical systems can exhibit stable periodic motions under certain conditions without the help of external actuators or controllers. This type of system is driven by its internal mechanism and the interaction with the environment such as gravity, inertia, and collisions which is often referred as *passive dynamics*. These passive models have been widely studied and used to predict the relationships among speed, stride length, and stride frequency in legged systems (*Blickhan*, 1989; *Kuo*, 2001). They also have been used as templates for the design (*Collins et al.*, 2005; *Rezazadeh et al.*, 2015), motion generation (*Mordatch et al.*, 2010), and control (*Hereid et al.*, 2014) of legged robots. For example, the passive dynamic walker designed by McGeer (*McGeer*, 1990) as shown in Fig. 1.2(a) can exhibit stable walking motion pattern on an adjusted ramp. The damping and collision losses during each step are compensated exactly by the changes in the gravitational energy. The Cornell Ranger pictured in Fig. 1.2(b) can walk indoors for 65.2 km without recharging its battery.

All these passive models and walking machines, however, are designed to reproduce only one specific gait. On the other hand, animals in nature are able, with a single

structure, to locomote with different gaits across a range of velocities. In order to analyze these locomotion patterns and design similar motions for legged robots, it is valuable to find a single unified model to explain the underlying mechanics of all common gaits. An important step in this direction was to show that a single compliant bipedal model could explain ground reaction forces of both, walking *and* running with a single set of parameters (*Geyer et al.*, 2006). They were able to show that this model can explain the dynamics of both bipedal walking and running. Their work suggests that these two gaits are different dynamical modes of the same system, oscillating at different energy levels. However, there does not exist a passive model that is able to reproduce all gaits observed in nature.

In the past few years, I have been wondering why there exist such a large number of gaits in nature? Why do animals of different species, regardless of their morphology, tend to switch to the same gait at similar Froude numbers (*Vaughan and O'Malley*, 2005)? As for roboticists, can we design legged systems that could exhibit similar motion patterns? How and when should we command legged robots to switch from one gait to another?

1.2 State of the art

Legged animal locomotion is usually very complex, and sometimes it is difficult to distinguish with human eyes. As a result, the study of legged locomotion was almost impossible until the invention of the camera. In the 1880s, Muybridge used banks of cameras to capture successive images of animals and humans in motion (*Muybridge*, 2012a,b). With these images, researchers could look at each frame of the whole stride cycle and analyze the phases and footfall sequences of animal gaits. Starting in 1965, M. Hildebrand developed a criteria to classify gaits by three numbers, the time lag of footfall of forefeet or rearfeet, the time lag of footfall of ipsilateral feet, and the duty factor (*Hildebrand*, 1965, 1989). He compared over 150 different species of animals

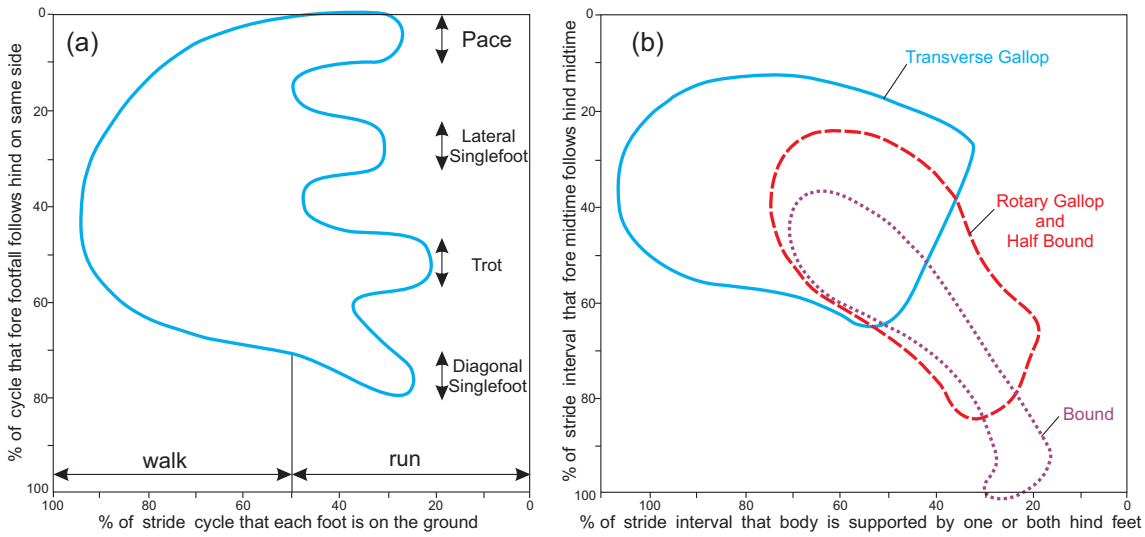

Figure 1.3: These figures are adapted from the Hildebrand Gait Graph for (a) quadrupedal symmetrical gaits and (b) quadrupedal asymmetrical gaits.

using this method. The gaits were categorized into two groups: symmetrical gaits and asymmetrical gaits, and analyzed separately. In the symmetrical gaits, left legs and right legs basically do the same thing just half stride out of phase. For example, quadrupedal walking, trotting, or pacing. On the other hand, in asymmetrical gaits, legs move differently during the whole stride. Such as bounding and galloping. This method allowed for a graphical classification of gaits in a so-called *gait graph* (Fig. 1.3), and Hildebrand's results suggested that the range of possible gaits in this graph can be represented as a continuum, rather than a set of isolated regions. For example, the regions of symmetrical gaits of vertebrates in the graph form a four pronged figure as shown in Fig. 1.3(a). While certain components of this shape, have been explained in (*Hildebrand*, 1985), the reasons for its exact shape remain unclear.

Several simplistic models have been proposed to emulate the underlying dynamics of walking and running. For example, *Mochon and McMahon* (1980b) demonstrated that rather than constantly controlling values of each state in the model and forcing all joints to follow predefined trajectories, the Inverted Pendulum (IP) can closely

resemble bipedal walking. In this model, the whole body is represented as two stiff pendulums. During stance phase, the system is vaulting over a stiff leg with fixed length while the other leg is swinging forward as shown in Fig. 1.4(a). Under proper initial conditions, this passive model can demonstrate stable periodic walking gait patterns on a ramp without the help of additional actuators and controllers. In each step, the collision losses are exactly compensated by the changes of gravitational energy caused by the Center of Mass (COM) descent. This discovery in legged locomotion has lead to the creation of a number of highly efficient walking robotic devices (*Bhounsule et al.*, 2012; *Collins et al.*, 2005). Similar models have been to extended to quadrupeds to identify walking gaits, and to investigate their dynamics and stability (*Smith and Berkemeier*, 1997; *Remy et al.*, 2009). The main body and the legs in these models were represented by rigid links. Since motion was based on inverted pendulum walking that requires an instantaneous transfer of support, the range of possible gaits was severely limited. Inverted pendulum walking by itself is not able to capture the rich variety of gaits and locomotion patterns that can be found in nature.

In addition to the rigid leg models, a spring-mass model (*Blickhan*, 1989; *Farley et al.*, 1993) has been used to describe the dynamics of running. This model assumes that the total mass of the legged system is located in a single point mass that is connected via a massless linear spring to a massless foot. During stance, the point mass pivots in a downward arch about the contact point as illustrated in Fig. 1.4(b). Since the leg has no mass, no swing dynamics exist, and it is assumed that the leg simply moves to a predefined Angle of Attack (AOA) α during swing. As opposed to stiff legged systems, which require an instantaneous transfer of support, the two legs can conduct touch down and lift off independently, such that a double stance phase as well as an airborne phase is possible. This spring-mass model is utilized to explain the basic mechanics of two legged runners and trotting quadrupeds (*Farley et al.*, 1993; *Full and Koditschek*, 1999).

In recent research, a *unified* Spring Loaded Inverted Pendulum (SLIP) model was proposed to explain the underlying dynamics of bipedal walking and running (*Geyer et al.*, 2006). It is based on the spring-mass model (*Farley et al.*, 1993; *Full and Koditschek*, 1999), but it has *two* legs. As opposed to stiff legged systems, which require an instantaneous transfer of support, the two legs can conduct touch down and lift off independently, such that a double stance phase is possible. As shown in Fig. 1.4(c), the double stance phase takes place between the first two frames. By using this model, they could reproduce more realistic GRFs as well as the COM trajectories for both gaits. The GRFs that are predicted by this model closely resemble those of human walking and running (*Lee and Farley*, 1998), and the model is able to explain the characteristic double hump in the vertical GRFs of human walking (*Pandy*, 2003).

While this unified SLIP model has been instrumental in understanding the dynamics of bipedal gaits, it has a key simplifying assumption inherited from the spring-mass model: after lift off, each leg instantaneously goes to a predefined AOA and remains there until the foot hits the ground again. This modeling choice is problematic for two reasons: first, in gaits with flight phases such as running, two legs cannot be fully distinguished when they have exactly the same landing angle which will lead to incorrect footfall sequence without proper selection of the stance leg. Additionally, due to lack of swing leg dynamics, this model has infinitely many periodic motions including motions with infinitely short, nonphysical swing times (*Rummel et al.*, 2009). When the leg stiffness both legs are fixed, in order to identify the entire solution manifold of this SLIP model, one has to continuously change the AOA and the totally energy stored in the system. However, the structure of periodic solutions from this model seems to be very complex. In addition to common walking and running, there exists an continuous region of footfall sequences such as walking gait pattern with one, two, three maxima in the GRF profiles, running gait without flight phases,

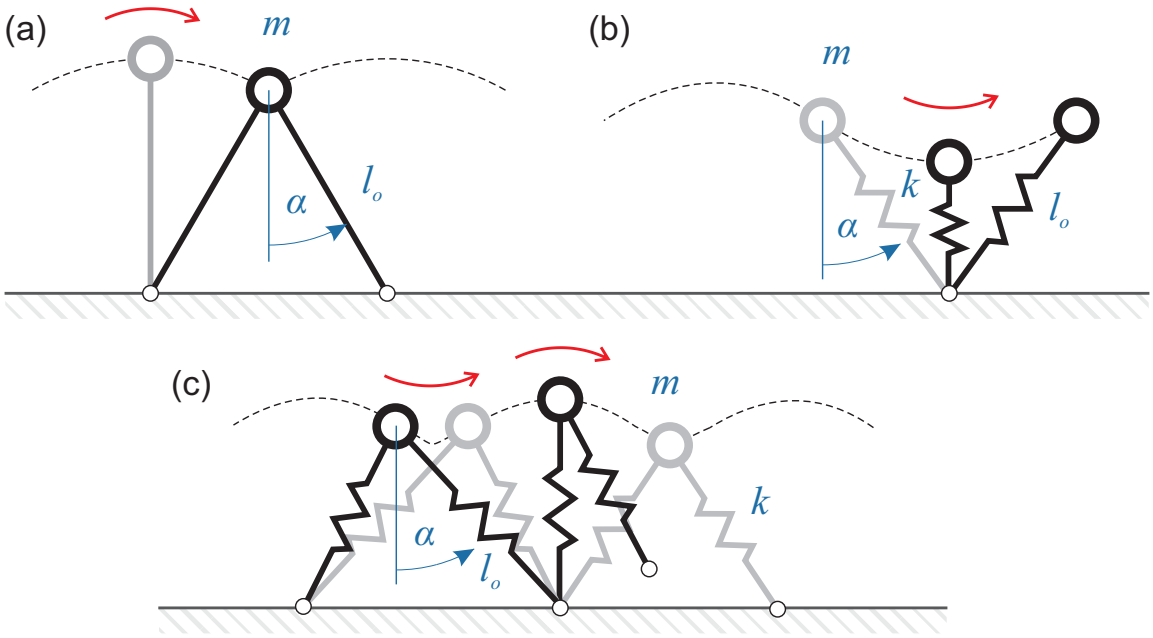

Figure 1.4: Several simplistic models that are used to study the bipedal walking and running. The IP model shown in (a) are used to emulate the ballistic walking gait, whereas the spring-mass model plotted in (b) resembles running or hopping gaits. (c) illustrates the Geyer bipedal SLIP model walking with double stance phases. Parameters of the models in these figures include AOA α, leg stiffness k, original leg length l_o, and total body mass m.

and gaits with asymmetrical limb forces (*Rummel et al.*, 2009, 2010). Moreover, to find more complex bipedal gaits like skipping *Minetti* (1998), each leg needs to have two different AOA. This will add another dimension to the solution manifold, which makes it almost impossible to identify all solutions from this SLIP model.

1.3 Thesis outline

In this work, I seek to explain the relationships among gaits by using a model-based approach and investigating the idea that all gaits are a manifestation of the underlying natural passive dynamics of a legged system. Therefore, the proposed dissertation will focus on modeling and exploring gaits of passive models with compliant legs.

Motivated by the Geyer bipedal SLIP model, in Chapter II, the concept of unified model is extended to quadrupeds. This quadrupedal model includes a rigid torso and four linear springs as legs. Gaits are identified in a gait creation framework (*Remy et al.*, 2011), such that the contact sequence is only influenced by the starting values of the numerical integration. By varying these values, the unified quadrupedal model is able to reproduce a large number of gaits observed in nature passively including trotting, pacing, walking, tölting, bounding, and galloping. In order to validate to what degree this model can explain the quadrupedal locomotion and ensure that the model is not oversimplified, in Chapter III, optimization is conducted to match the experimentally obtained vertical GRFs of the real horses at walking, trotting, and tölting. It has been shown that despite the model simplicity, the model does not only produce qualitatively similar motion patterns, but can quantitatively match the underlying dynamics with high R-square values.

To include even more bipedal gaits other than just walking and running, in Chapter IV, a new augmented bipedal SLIP model with swing leg motions is developed. In this model, the AOA for each leg is no longer a free parameter but a function of the initial conditions which leaves the total energy stored in the system as a single system

parameter that can be altered. By using numerical continuation techniques (*Allgower and Georg*, 2003), it is shown that all bipedal gaits including bipedal hopping, skipping, galloping can be originated through various bifurcations and continuations from in-place bouncing of a single model.

In Chapter V, similar techniques have been implemented on a quadrupedal model. With the same set of parameter values as adopted in the bipedal model, an examination of the *dynamic similarity* (*Alexander and Jayes*, 1983) between these two models is presented. Additionally, it has been shown these passive quadrupedal gaits are sensitive to the value of main body inertia. Some shifts in the gait branches are observed when the main body inertia varies.

Finally, in Chapter VI, some preliminary results in quadrupedal symmetrical gaits are shown. The identified passive gaits are further compared to the animal gaits observed in nature. Potential implementations and embodiment of the passive solutions from both bipedal and quadrupedal models developed in the thesis are also discussed.

CHAPTER II

A Passive Dynamic Quadruped that Moves in a Large Variety of Gaits

2.1 Introduction

[1] Passive dynamic walkers and runners (*Cavagna and Kaneko*, 1977; *McGeer*, 1990; *Seyfarth et al.*, 2002) have been studied extensively with simplistic conceptual models. These models have been used to identify the basic dynamics of locomotion, predict energetic efficiency, and quantify first order stability of the resulting motion. Researchers in this field have been focused primarily on passive dynamic quadrupeds with stiff legs (*Smith and Berkemeier*, 1997; *Remy et al.*, 2009, 2010) to investigate the inverted-pendulum walking and stability of two and three dimensional systems. However, stiff legged systems require an instantaneous transfer of support, which means that for stiff-legged quadrupeds exactly two of the four legs are on the ground at all times. Therefore the range of possible gaits was severely limited. This restricts the models to symmetrical gaits with a duty factor of $\beta = 0.5$. Another drawback of stiff legged models is the fact that such an inverted pendulum model fails to match the motion of the center of mass in human bipedal walking (*Lee and Farley*, 1998), and that it cannot explain the characteristic double hump in the vertical ground reaction

[1] This chapter has been previously published in 2014 IEEE/RSJ International Conference on Intelligent Robots and Systems (IROS 2014) (*Gan and Remy*, 2014a).

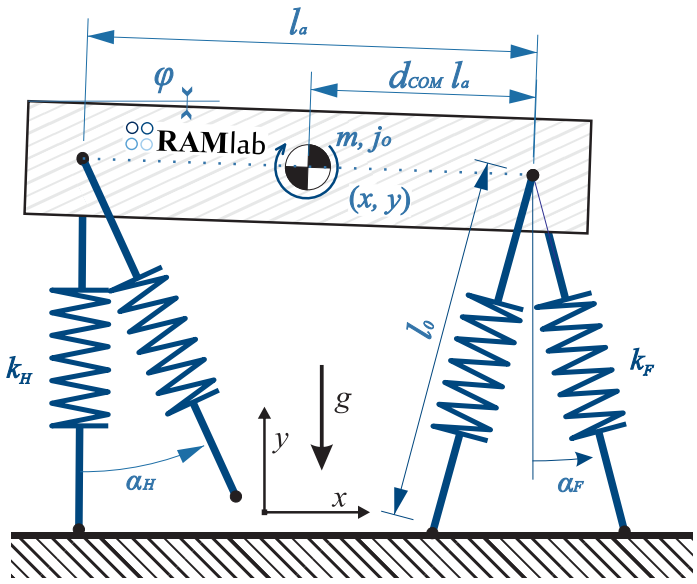

Figure 2.1: This conceptual quadrupedal model with an extended main body and four massless elastic legs, can predict a wide variety of passive dynamics gaits.

forces (*Pandy*, 2003).

Recent research has shown that a compliant bipedal model can explain ground reaction forces of both, human walking *and* running with a single set of parameters (*Geyer et al.*, 2006). Their research suggests that not stiff, but compliant legs are fundamental to the dynamics of walking. In this interpretation, walking and running are just two separate dynamic modes of the same system that is driven by its natural mechanical dynamics.

In this chapter, I extended such an elastic model to quadrupedal locomotion. Elasticity plays an important role in quadrupedal locomotion in nature (*McGuigan*, 2003), and elastic leg designs have found their way into a number of quadrupedal robotic prototypes (*Remy et al.*, 2012; *Poulakakis et al.*, 2005). I modeled this conceptual quadruped with a single rigid body with three degrees of freedom. Four massless elastic legs are mounted at the shoulder and hip, that –during swing– go to a predefined Angle of Attack (AOA). With this simple structure, our model is able to produce a wide range of gaits; –simply by setting appropriate initial states and

system parameters. Such periodic motions were identified in a numerical framework for gait creation (*Remy et al.*, 2010). With this, I was able to identify trotting, pacing, walking, toelting, bounding, and galloping within a single quadrupedal model. In the present chapter, I modified the methodology of the gaits creation (*Remy et al.*, 2010) for compliant leg model. Details of the compliant quadrupedal model and framework are shown in the following section. It has been also demonstrated that this model could reproduce a wide range of gaits such like walking, trotting, and toelting. For each gait, the footfall sequence and vertical Ground Reaction Forces (GRFs) and compare the gaits identified by the simplistic model with the gaits of the horse in nature.

2.2 Methods

While the simplistic model that I consider in this chapter is very similar in its structure to the established Spring Loaded Inverted Pendulum (SLIP) models of bipedal locomotion, the fact that it has an extended main body and that it is resting on *four* legs requires a number of adjustments to the standard methodology of passive dynamic gait identification. In particular, we introduce a swing time t_{swing}, during which a leg is not able to engage in ground contact. This creates a well defined contact pattern.

2.2.1 Gait Creation

For gait creation, I introduce a vector $\mathbf{X} = [\bar{\mathbf{q}}_o, \dot{\mathbf{q}}_o, \mathbf{z}_o]^{\mathrm{T}}$ and a vector $\mathbf{p}$ that contain all initial states and all system parameters that are necessary to define a gait. $\mathbf{X}$ includes a subset of the initial generalized coordinates $\bar{\mathbf{q}}_o$ and all generalized speeds $\dot{\mathbf{q}}_o$ at the beginning of a stride. Similarly, $\mathbf{z}_o$ defines the discrete states at the beginning of a stride. Discrete states have a derivative of 0 and hence no velocity is associated with them. The generalized coordinate vector $\mathbf{q} = [x, y, \varphi]^{\mathrm{T}}$ contains

the horizontal and vertical position (x, y) of the Center of Mass (COM), and the orientation of the main body φ. A stride is assumed to always start at an initial horizontal position of $x = 0$. x is hence excluded from the variable vector $\mathbf{X}$. The continuous dynamics of the model are governed by a set of differential Equations of Motion (EOM):

$$\ddot{\mathbf{q}} = f\left(\mathbf{q}, \dot{\mathbf{q}}, \mathbf{z}, \mathbf{p}\right). \tag{2.1}$$

In addition to the continuous dynamics, discrete changes to the system state occur every time a foot touches down or leaves the ground. We refer to such instances as *events*. They are defined mathematically by the directional zero crossing of an event function e:

$$e\left(\mathbf{q}, \dot{\mathbf{q}}, \mathbf{z}, \mathbf{p}\right) = 0, \quad \text{with} \quad \dot{e} > 0. \tag{2.2}$$

One event is defined as the *terminal* event $e^\star$ and marks the end of a stride. Since our models are collision-free, the continuous states $\mathbf{q}$ and $\dot{\mathbf{q}}$ do not change during events. Only discrete states $\mathbf{z}$ change according to a event-handler function

$$\mathbf{z}^+ = g\left(\mathbf{q}, \dot{\mathbf{q}}, \mathbf{z}^-, \mathbf{p}\right), \tag{2.3}$$

where the indices $-$ and $+$ indicate the states right before and right after the event. The discrete state vector $\mathbf{z}$ is given by $\mathbf{z} = [\mathbf{phase}, \mathbf{pos}_x]^{\mathrm{T}}$ and contains two kinds of discrete states: A first set of states is used to track the *phase* of each leg i ($phase_i \in [1, 2, 3]$). These variables describe the current leg configuration. A second set of discrete states $pos_{x,i}$ is used to record the horizontal position at which a foot touched the ground. From these positions I can calculate the spring forces that the stance legs exhibit, and I can monitor whether foot placement is periodic over the course of multiple strides.

To simulate the *hybrid dynamics* of a single stride, I start with the initial state values $\mathbf{q}_o$, $\dot{\mathbf{q}}_o$ and $\mathbf{z}_o$ at time $t = 0$. State derivatives are computed according to

the EOM (2.1) and are being integrated while monitoring for events (2.2). Each time an event is detected, it is processed by the appropriate event handler function (2.3), before integration is continued with the new values of the discrete states $\mathbf{z}^+$. This process is repeated until the terminal event $e^\star$ is triggered which marks the end of the stride at time t_{stride}. With this, I can define a stride-to-stride mapping $\mathbf{X}^{k+1} = \mathrm{P}\left(\mathbf{X}^k,\ \mathbf{p}\right)$, which conducts the simulation of a single stride starting from the values $\mathbf{X}^k$ at the beginning of a stride. It returns the values $\mathbf{X}^{k+1}$ at the end of the stride. This stride-to-stride mapping reduces the definition of a periodic gait to the implicit equation:

$$\mathrm{P}\left(\mathbf{X}^\star, \mathbf{p}^\star\right) - \mathbf{X}^\star = 0. \tag{2.4}$$

First order stability of such a periodic gait can be assessed via the eigenvalues of the Monodromy Matrix $\mathbf{J}$ which is the partial derivative of P with respect to the continuous and discrete states, evaluated at the periodic solution:

$$\mathbf{J} = \left.\frac{\partial \mathrm{P}}{\partial \mathbf{X}}\right|_{\mathbf{X}^\star, \mathbf{p}^\star}. \tag{2.5}$$

$\mathbf{J}$ describes how a disturbance $\Delta\mathbf{X} = \mathbf{X} - \mathbf{X}^\star$ evolves from step to step:

$$\Delta\mathbf{X}^{k+1} = \mathbf{J} \cdot \Delta\mathbf{X}^k. \tag{2.6}$$

If all eigenvalues are smaller than one, the disturbance in the initial states will decay exponentially.

2.2.2 The Simplistic Model

The simplistic model that I use in this study consists of a rigid main body and four massless elastic legs as shown in Fig. 2.1. It is a planar model and motion is restricted to the sagittal plane. The main body measures l_1 from hip to shoulder. It has a point-

mass of m_o and an inertia of j_o. The COM can be displaced along the anteroposterior axis to represent different weight distributions. A parameter $d_{COM}(0 < d_{COM} < 1)$ is used to continuously shift the COM from the shoulder ($d_{COM} = 0$) to the hip ($d_{COM} = 1$). The distances from the COM to the shoulder and hip are given by:

$$l_F = l_1 \cdot d_{COM} \tag{2.7}$$

$$l_H = l_1 \cdot (1 - d_{COM}) \tag{2.8}$$

So the shoulder and hip positions could be calculated as:

$$x_F = x + l_F \cdot cos(\varphi); \quad x_H = x - l_H \cdot cos(\varphi) \tag{2.9}$$

$$y_F = y + l_F \cdot sin(\varphi); \quad y_H = y - l_H \cdot sin(\varphi) \tag{2.10}$$

The legs are modeled as massless springs with a uncompressed length of l_o. They are connected to the main body at the hip and shoulder via rotational joints. Front legs and hind legs have different spring stiffnesses of k_F and k_H, respectively. There is no damping in the springs and rotational joints. Since the legs have no mass, there are also no collision losses. The model is energetically conservative. Feet are modeled as points with no geometrical extension and I assume that ground friction is infinitely large; that is, the feet never slip on the ground.

Parameter values of the quadruped model are given in units normalized relative to total mass of the model m_o, uncompressed leg length l_o and gravity g (*Hof*, 1996). As these three quantities are removed from the set of adjustable parameters, the results of this research are irrelevant of the mass or size of a specific system.

2.2.3 System Dynamics

Each leg that is in stance creates a force F_i on the main body. This force acts along the direction of the leg with a magnitude proportional to the leg compression. The

Table 2.1: The proportions of the model roughly represent the dimensions and mass properties of a Crossbred horse.

Param.	Value	Unit	Description
m_o	1	$[\cdot]$	Total mass
l_o	1	$[\cdot]$	Uncompressed leg length
g	1	$[\cdot]$	Gravitational constant
l_a	1	$[\mathrm{l_o}]$	Main body length
j_o	0.18	$[\mathrm{m_o l_o^2}]$	Main body inertia
k_F	21	$[\mathrm{m_o g / l_o}]$	Front leg spring stiffness
k_H	19	$[\mathrm{m_o g / l_o}]$	Hind leg spring stiffness
α_F	0.21	[rad]	Front AOT
α_H	0.25	[rad]	Hind AOT
d_{COM}	0.5	$[\cdot]$	Offset of the COM
t_{swing}	0.4	$[\sqrt{\mathrm{l_o / g}}]$	swing time

current length and angle of the stance leg are continuously updated in the integration of eq (2.1):

$$l_i = \sqrt{(x_{F,H} - pos_{x,i})^2 + y_{F,H}^2} \tag{2.11}$$

$$\gamma_i = arctan(\frac{pos_{x,i} - x_{F,H}}{y_{F,H}}) \tag{2.12}$$

Once I get the current lengths and angles for the stance legs, the corresponding forces and torques exerting on the main body could be calculated as following equations:

$$F_i = k_{F,H} \cdot (l_o - l_i) \tag{2.13}$$

$$M_i = F_i \cdot l_{F,H} \cdot cos(\varphi - \gamma_i) \tag{2.14}$$

Because this is a single body system, the EOM is reduced to three fully decoupled differential equations:

$$\ddot{x} = \frac{-1}{m_1} \sum_i F_i \cdot \sin(\gamma_i) \tag{2.15}$$

$$\ddot{y} = \frac{1}{m_1} \sum_i F_i \cdot \cos(\gamma_i) - g \tag{2.16}$$

$$\ddot{\phi} = \frac{1}{j_1} \sum_i M_i \tag{2.17}$$

Each leg is in one of three discrete phases $phase_i$: *ready to touch town* (1), *stance* (2), or *swing* (3). Because the ground is a unilateral constraint, a stance leg will lift off the ground contact when the current length equals to its uncompressed leg length. Since the legs have no mass, it is assumed that they go to a pre-defined AOA during swing. In contrast to other implementations of the SLIP model, it is assumed that after lift off, leg swing does not happen instantaneously and that the AOA is only reached after a certain swing time t_{swing}. Before this time has passed, a leg will not engage in ground contact so that swing legs will not affect the main body dynamics.

The transition between these phases is detected via the following event detection functions:

$$e_{i,1} = l_o \cdot cos(\alpha_{F,H}) - y_i \tag{2.18}$$

$$e_{i,2} = l_i - l_o \tag{2.19}$$

$$e_{i,3} = t_i - t_{swing} \tag{2.20}$$

In the corresponding event handler functions, the phase of the involved leg is updated to its new value. At touchdown, the contact position pos_x is updated according to

$g_{i,1}$, and at liftoff, the time measurement of the swing phase is reset.

$$g_{i,1} : phase_i^+ = 2; \quad pos_{x,i}^+ = x + l_{f,b} \cdot cos(\alpha_{F,H}); \tag{2.21}$$

$$g_{i,2} : phase_i^+ = 3; \quad t_i^+ = 0; \tag{2.22}$$

$$g_{i,3} : phase_i^+ = 1; \tag{2.23}$$

When computing the first order stability of a gait with eqs. (2.5) and (2.6), I have to consider that not all discrete states cause a disturbance. For example, the positions of the contact points $pos_{x,i}$ of feet that are not on the ground do not influence the motion. For this reason, only the non-zero eigenvalues are reported throughout this chapter. Their number varies from gait to gait, depending on how many feet are on the ground during the terminal event $e^\star$.

2.3 Results

[2] With the methodology described above, I was able to identify a large variety of symmetrical and asymmetrical gaits by numerically solving equation (2.4) with different initial guesses. Each gait is defined by a vector $\mathbf{X}$ that contains the full information about the continuous and discrete states, as well as about all system parameters. The order of ground contact, which is the main characterization of a gait, is an outcome of these initial states and parameters, and not enforced through additional constraints. The continuous generalized coordinates and velocities for all gaits are shown in Table 2.2, the discrete states in Table 2.3, and the system parameters in Table 2.4.

All gaits that were found within this chapter are dynamically unstable. For most gaits, the spectral radius of the Monodromy Matrix is about 4. That means that an unstable disturbance grows by a factor of 4 during a stride. While actual self-stability

[2] Videos of all gaits are available at https://youtu.be/3EMNoW1vrEg

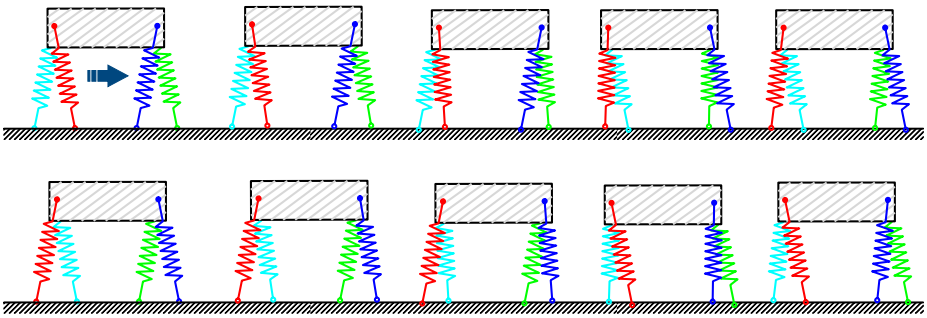

Figure 2.2: 10 consecutive frames of a full stride of a trotting gait.

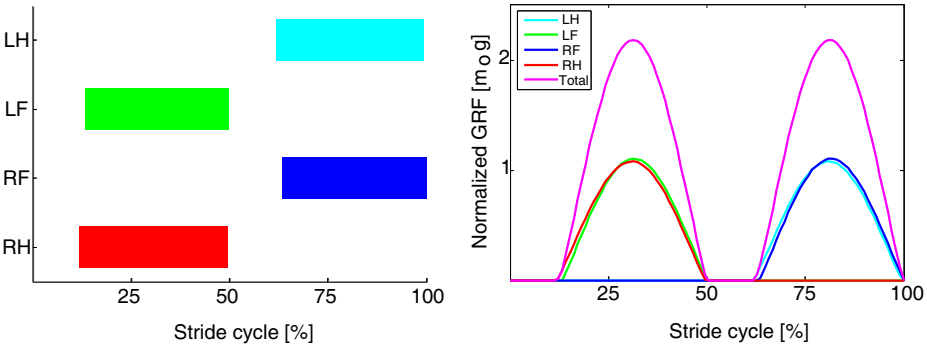

Figure 2.3: Footfall sequence and GRFs of a trotting gait.

would be very desirable, such a rate of disturbance growth can probably be tolerated by a closed loop control system in a robotic application. The only exception to this is the toelting gait, which is highly unstable with a spectral radius of 273.

2.3.1 Symmetrical gaits

In symmetrical gaits, the left and right side of a legged system are performing the same motion, but with a phase difference of half a stride. This greatly facilitates gait synthesis, since only a half stride must be simulated, after which the left and right side of the model can simply be switched. The AOA is identical for left and right legs such that only two parameters, α_F and α_H, were defined for the AOA.

2.3.1.1 Trotting and Pacing

Since the employed model is planar, the labels of left and right legs can be assigned arbitrarily to each leg. A two-beat gait with an air phase can thus be interpreted as a trotting gait if diagonal pairs of legs move together (Fig. 2.2) or as a pacing gait if two legs on the same side move together.

The vertical ground reaction forces (Fig. 2.3, shown for trotting) show a characteristic single hump that corresponds to a single compression cycle of the leg spring. This result is very similar to previous studies which employed more complex models (*Herr and McMahon*, 2000). Furthermore, by a slight adjustment of the system parameters, I can identify ground reaction forces that perfectly match those recorded from crossbreed horses (*Weishaupt et al.*, 2004; *Gan and Remy*, 2014b). The average velocity for trotting and pacing is $0.66\sqrt{l_o g}$ and the non-zero eigenvalues of the Monodromy Matrix are $(4.06, 1, 0.56 \pm 0.27i)$.

2.3.1.2 Walking

Walking is a four-beat gait. In nature it only exists in a *lateral sequence* with the following touch-down order: right hind leg, right front leg, left hind leg, left front leg. We hence used this order when defining left and right legs. The resulting motion is shown in Fig. 2.4. Walking is the slowest gait that I found. With an average velocity of $0.25\sqrt{l_o g}$ it is only half as fast as trotting and pacing. The non-zero eigenvalues of the Monodromy Matrix of walking are $(-2.70 \pm 1.04i, 1, 0.54 - 0.66 \pm 1.37i)$.

In contrast to trotting and pacing, in walking, each leg spring will undergo *two* compression cycles. This double-oscillation results in the characteristic double hump in the vertical GRFs (*Pandy*, 2003) (Fig. 2.5).

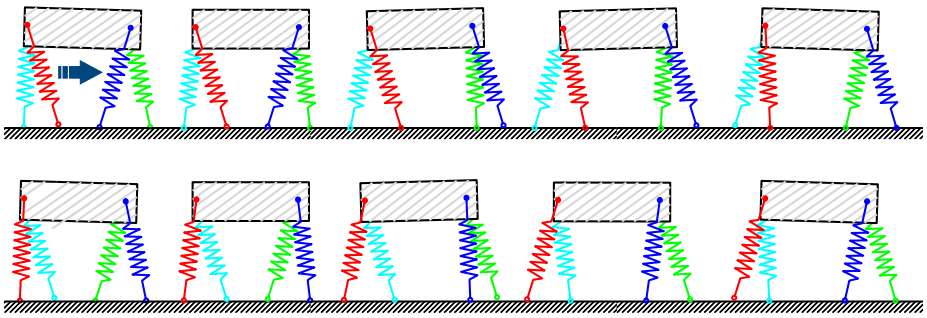

Figure 2.4: 10 consecutive frames of a full stride of a walking gait.

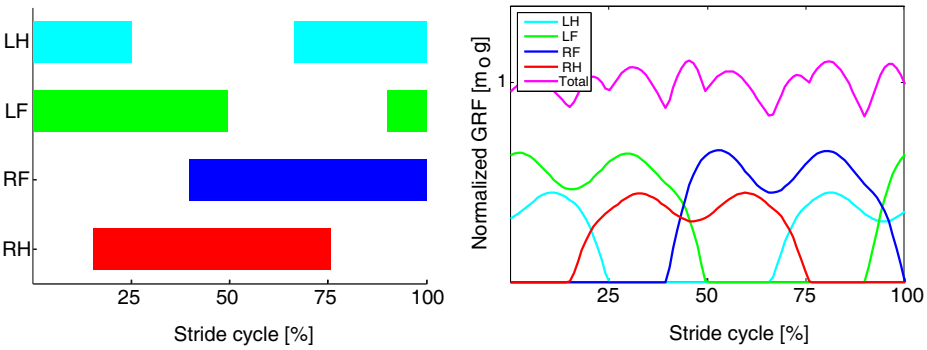

Figure 2.5: Footfall sequence and GRFs of a walking gait.

2.3.1.3 Toelting

Toelting is a gait that is unique to Icelandic horses. Like the walking gait, it is a four beat gait. Yet it has the ground reaction force profile of a running gait in which the leg springs undergo only a single compression cycle (Fig. 2.7). In this gait, the main body shows only very small rotations and a very limited vertical movement (Fig. 2.6). In nature, this makes this gait very comfortable for a rider, and one can see that it might be equally beneficial in a robotic application in which a fast and efficient, yet steady motion is desired. In terms of locomotion velocity, toelting (average speed $0.69\sqrt{l_o g}$) is comparable to trotting and pacing. As a downside, toelting is the most unstable gait that I observed. The non-zero eigenvalues of the Monodromy Matrix are $(273.57, 1, 0.68, 0.14, -0.04, -0.10)$.

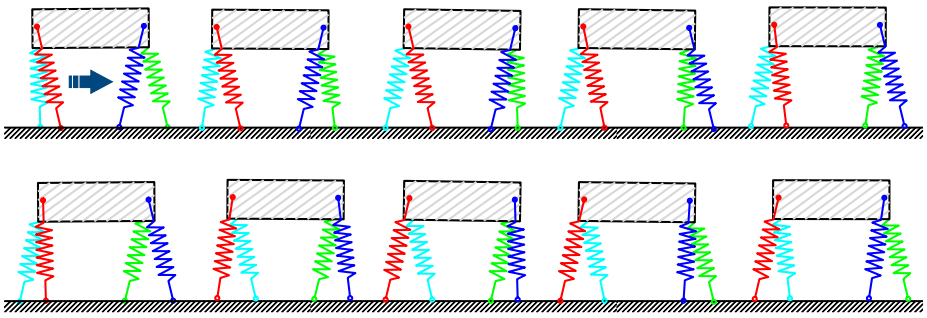

Figure 2.6: 10 consecutive frames of a full stride of a toelting gait.

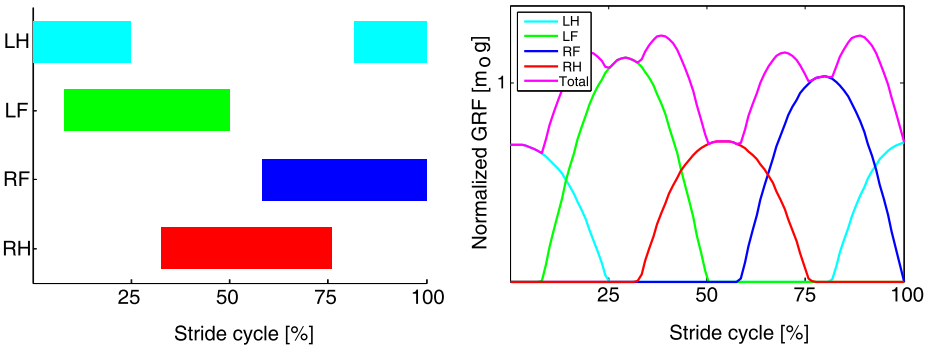

Figure 2.7: Footfall sequence and GRFs of a toelting gait.

2.3.2 Asymmetrical gaits

In contrast to symmetrical gaits, the stance phases of the left and right leg pairs are unevenly spaced in time for asymmetrical gaits. This means that a different AOA must be assigned to each individual leg and that a full stride must be simulated to identify a gait. Instead of using two parameters α_F and α_H, for the AOA, four parameters α_{LH}, α_{RH}, α_{LF}, and α_{RF} are required. Asymmetrical gaits include bounding and galloping gaits.

2.3.2.1 Bounding

In a bounding gait, the two front legs and the two hind legs move in unison (Fig. 2.9). Such bounding gaits are not very frequent in nature, but a couple of robots with elastic legs have implemented these gaits; including the MIT quadruped (*Raibert et al.*, 1986) and the Scout II robot (*Poulakakis et al.*, 2005). The appeal

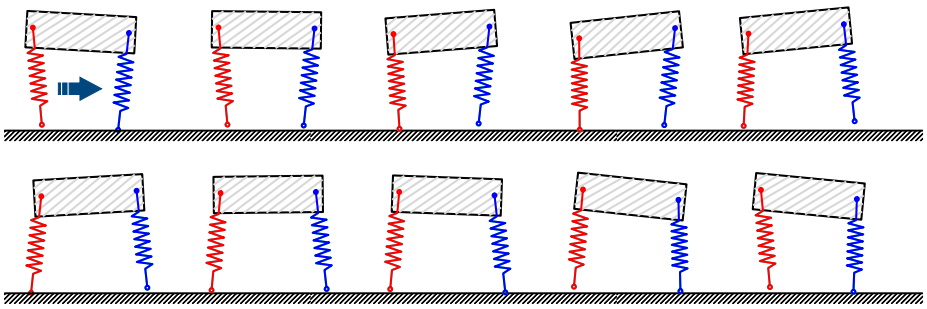

Figure 2.8: 10 consecutive frames of a full stride of a bounding gait.

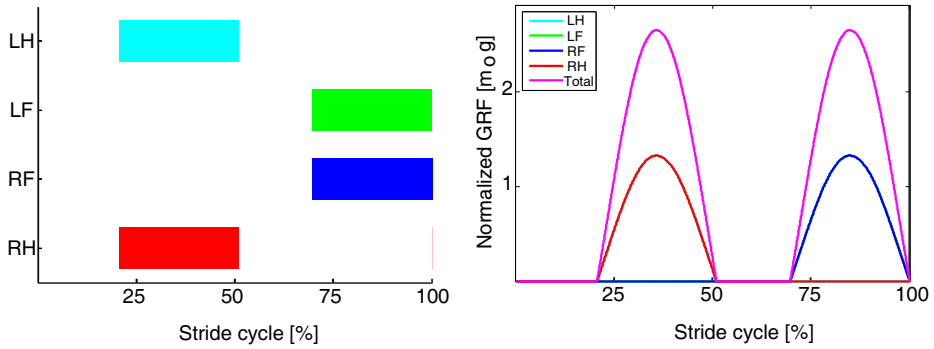

Figure 2.9: Footfall sequence and GRFs of a bounding gait.

from this gait comes from the fact that by moving both legs together the control problem is greatly simplified, and no rolling motion is created. However, a substantial pitching motion is introduced (Fig. 2.8) and bounding is comparatively slow (average speed $0.41\sqrt{l_o g}$). The non-zero eigenvalues of the Monodromy Matrix of bounding are $(5.66, 1.54, 1, 0.19)$.

2.3.2.2 Galloping

Galloping, is the fastest gait that I was able to identify. With a velocity of $1.49\sqrt{l_o g}$ it is more than twice as fast as trotting, pacing, and toelting. For the galloping gait that I identified, the non-zero eigenvalues of the Monodromy Matrix are $(3.40, 1, 0.32 \pm 0.45i)$. Depending on the assignment of left and right legs, I can produce both a rotary and a transverse gallop. The transverse gallop is more common in horses and hence depicted in Fig. 2.10.

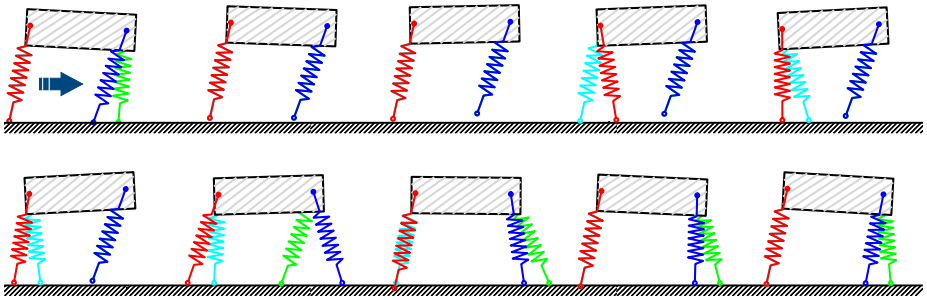

Figure 2.10: 10 consecutive frames of a full stride of a galloping gait.

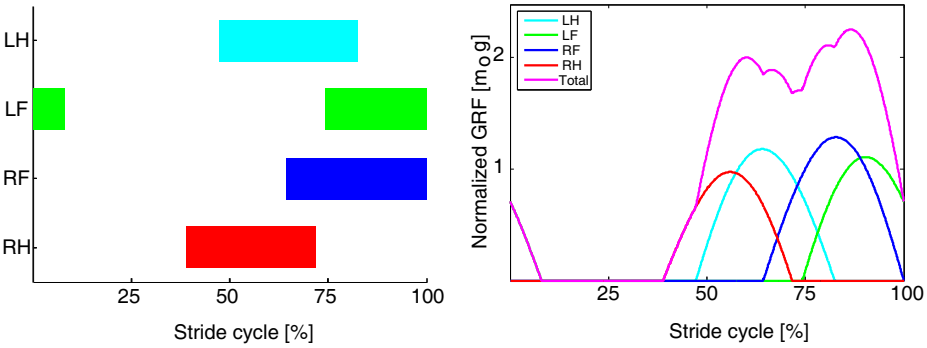

Figure 2.11: Footfall sequence and GRFs of a galloping gait.

Table 2.2: Values of continuous states for each gait.

Gaits	$\dot{x}$	y	$\dot{y}$	φ	$\dot{\varphi}$
Trotting	0.6742	0.9805	0.1011	0.0013	0.0052
Pacing	0.6742	0.9805	0.1011	0.0013	0.0052
Walking	0.2551	0.9670	0.0102	-0.0284	0.0616
Toelting	0.6869	0.9667	0.0262	0.0024	0.0115
Bounding	0.4138	1.0237	0.1683	-0.0560	0.3325
Galloping	1.4920	0.9640	0.2727	-0.0511	0.1311

Table 2.3: Values of discrete states for each gait.

Gaits	ph_{LH}	ph_{RH}	ph_{LF}	ph_{RF}	pos_{LH}	pos_{RH}	pos_{LF}	pos_{RF}
Trotting	3	1	1	3	-0.7088	-1.2472	-0.2318	0.3066
Pacing	1	3	1	3	-1.2472	-0.7088	-0.2318	0.3066
Walking	2	1	2	3	-0.5754	-1.0730	-0.6622	0.1646
Toelting	2	1	1	3	-0.5642	-1.1567	-0.4284	0.1810
Bounding	1	1	3	3	-0.9426	-0.9426	0.4068	0.4068
Galloping	3	3	2	3	-1.2093	-1.4859	0.3914	0.1292

Table 2.4: Values of model parameters for each gait.

Gaits	l_a	j_o	k_f	k_b	α_{LH}	α_{RH}	α_{LF}	α_{RF}	d_{COM}	t_{swing}
Trotting	1.00	0.60	20.00	21.00	0.20	0.20	0.20	0.20	0.50	0.51
Pacing	1.00	0.60	20.00	21.00	0.20	0.20	0.20	0.20	0.50	0.51
Walking	1.00	0.42	20.02	21.54	0.30	0.30	0.30	0.30	0.53	0.63
Toelting	1.04	0.61	21.13	24.29	0.27	0.27	0.25	0.25	0.58	0.40
Bounding	1.00	0.60	20.00	20.00	0.09	0.09	0.11	0.11	0.50	0.61
Galloping	1.00	0.49	12.02	12.54	0.34	0.22	0.42	0.35	0.53	0.81

2.4 Discussion and Conclusion

This chapter introduced the model of a conceptual quadruped with elastic legs, and identified a large variety of passive dynamics gaits. In particular, I was able to create all primary quadrupedal gaits that are found in nature; including walking, trotting, pacing, toelting, bounding, and galloping. The different ground contact sequences of these gaits emerged thereby solely from the initial model states and model parameters. Our work shows that all these gaits can be created completely passively with a single model, and allows us to extend the ideas of passive dynamic locomotion to a large range of quadrupedal gaits. This insight provides an invaluable vantage point for the design of energy efficient quadrupedal robots.

Even though the different gaits are based on the same model, they have different properties, such as locomotion speed or stability. In an abstract sense, different gaits can be interpreted as different *modes* of elastic oscillations that propel the legged

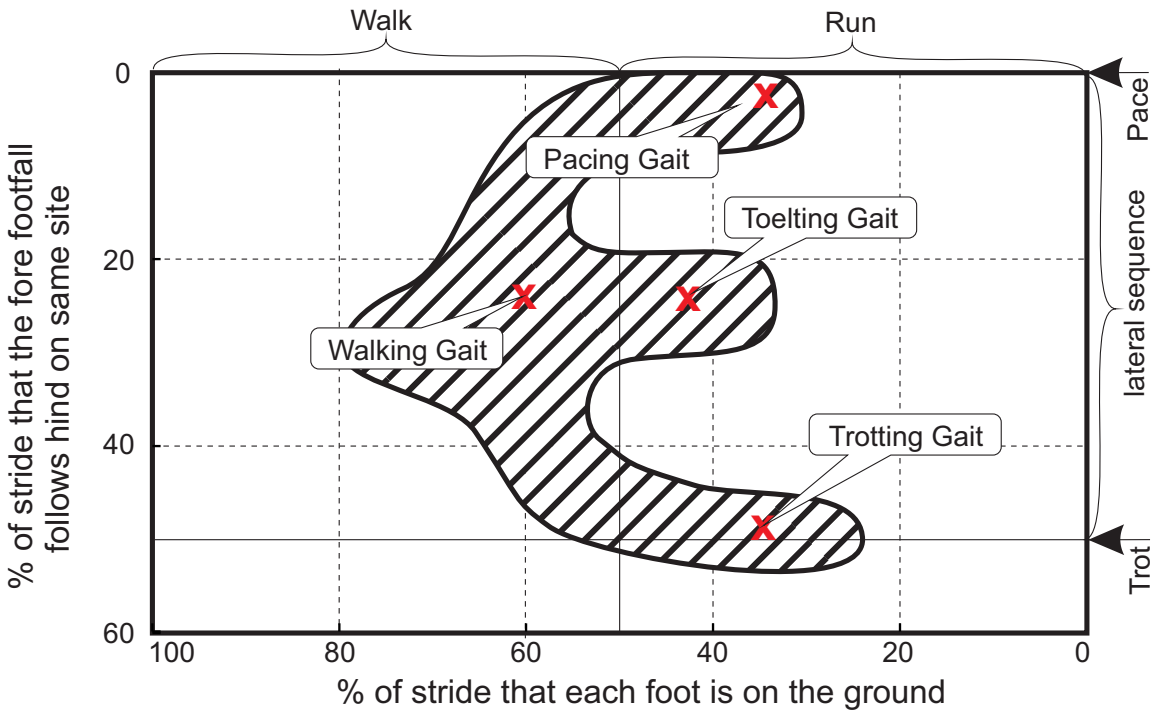

Figure 2.12: The four symmetrical passive dynamic gaits that were identified in this study are compared with the range of gaits found in horses. This range is illustrated by the shaded region, which is adapted from Hildebrand. Our results span the full range of possible symmetrical gaits that are found in nature.

system forward. These modes can be observed most clearly in the transition from walking to trotting, in which the leg springs go from a double compression stance phase to a single compression stance phase. By using different modes of locomotion, gait properties can thus be adjusted without compromising efficiency.

The results presented in this chapter are, however, only the tip of the iceberg. We deliberately restricted ourselves to only identifying example motions for the most important gaits that are found in nature. In the gait graph of Fig. 2.12, these results are compared to symmetrical horse gaits. While our results span the whole range of possible gaits, it is evident, that a much larger variety of motions is possible and being used in nature. Furthermore, it is possible, that in technical applications additional gaits might proof beneficial. Our research confirms the expectation that

even more gaits exist. While I only report one exemplary gait for each footfall pattern, I was able to create a continuous variety of gaits by changing the initial states $\mathbf{q}$, $\dot{\mathbf{q}}$ and model parameters $\mathbf{p}$. This result suggest that, in addition to finding a periodic motion via eq. (2.4), it is possible to optimize a merit function in the process. With this, one can try to mimic the ground contact patterns of gaits that are found in nature (*Gan and Remy*, 2014b) or optimize first order stability of the legged system (*Mombaur et al.*, 2005). Knowledge about such *optimal* passive dynamic walkers will be extremely useful in robotic applications, and might also teach us about gaits in nature. For example, it might explain the range of gaits used by horses, as it is shown in Fig. 2.12.

CHAPTER III

Passive Dynamics Explain Quadrupedal Walking, Trotting, and Tölting

3.1 Introduction

[1] In the previous chapter, a unified model with compliant legs is developed which is capable of reproducing a large number of quadrupedal motions that are similar to animal gaits observed in nature. This is not surprising, given that the compliance of the locomotor apparatus plays such an important role in quadrupedal locomotion in nature. *McGuigan* (2003), for example, pointed out that the long flexor tendons of the horse's limbs can store and release elastic energy during the stance phase, similar to a spring. Their experiments showed that during weight-bearing the limb changes its length by flexion of limb joints, particularly the metacarpophalangeal joint, and therefore can be modeled as a compression spring. *Clayton et al.* (2000) showed that metacarpophalangeal joint angles changed proportionally with peak vertical Ground Reaction Force (GRF).

The current chapter is based on this insight, and investigates to what extend this passive model can explain the animal locomotion in nature. To obtain a well-defined sequence of ground contact, three distinct phases for each leg are defined: *stance*,

[1] This chapter has been previously published in the Journal of computational and nonlinear dynamics (*Gan et al.*, 2015).

swing, and *ready for touch down*. In the *ready for touch down* phase each leg goes to a predefined angle of attack, similar to the Spring Loaded Inverted Pendulum (SLIP) model. This phase is, however, preceded by an extended *swing* phase in which the legs cannot make contact. Introducing this *swing* phase allowed us to prevent feet from striking the ground prematurely. This variation of the original SLIP model was necessary to enable a coordinated motion of the four legs. The model is implemented in a numerical framework for gait creation (*Gan and Remy*, 2014a) using a single-shooting approach. The contact sequence was thereby an outcome of the numerical integration, and was not determined a priory. With this, a wide variety of gaits can be found by simply changing the initial states and system parameters. Furthermore, by numerically fitting the model-predicted GRFs to experimentally obtained data, appropriate values for these states and parameters can be identified automatically. These data was obtained on an instrumented high-speed treadmill.

With this approach, I am able to produce realistic walking, trotting, and tölting with a *single* conceptual model. Furthermore, the model-predicted vertical GRFs closely matched the recorded GRFs of walking and trotting Warmblood horses, and of tölting Icelandic horses. These results suggest that the different quadrupedal gaits that are found in nature are potentially just different oscillation modes of the same dynamic system. The paper highlights the significance of natural dynamic motions and of elastic energy storage in quadrupedal locomotion.

The mathematical details of the gait creation are similar to the previous chapter. A quantitatively comparison between the identified motion and morphological parameters to those of horses is reported. A sensitivity study is conducted to examine how well different parameters can be identified by the methodology and how much influence they have on a particular gait. As a possible extension to the simplistic model presented above, an extended model with an articulated head-neck segment is evaluated. This model predicts the GRFs of walking more accurately.

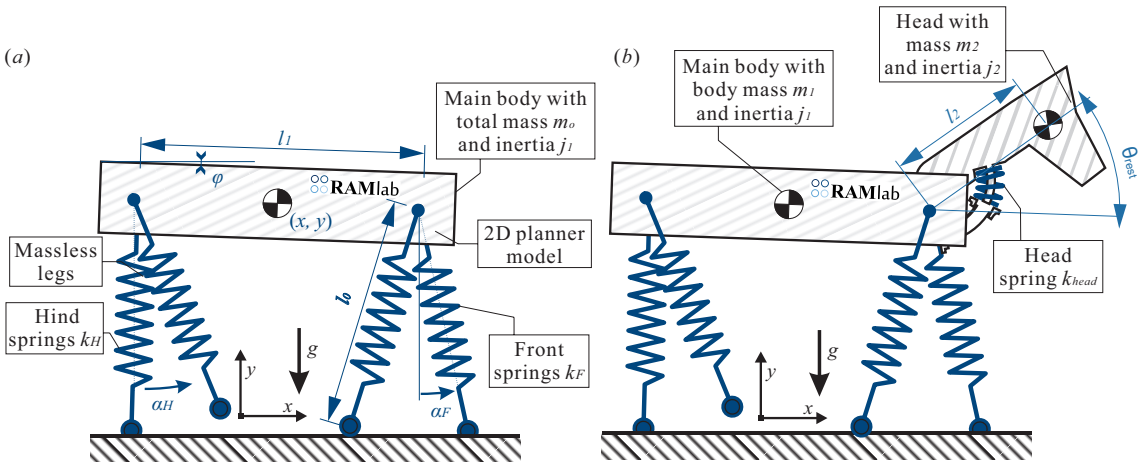

Figure 3.1: A simplistic model that essentially consists of a single distributed mass on four mass-less springs is able to explain the dynamics of quadrupedal walking, trotting, and tölting (shown in a). In addition, I studied an extended version that includes a head-neck segment connected to the body by a rotational joint with a torsional spring (shown in b).

3.2 Methods

In this section, I introduce the theoretical framework and the simplistic models that are used to generate periodic motions that optimally predict experimentally recorded GRFs. The methodology is based on the previous work on gait creation (*Gan and Remy*, 2014a). The gait creation and the details of the model is presented in section 2.2.

3.2.1 Models

The simplistic model is identical to the one shown in the previous chapter which consists of a rigid main body and four massless elastic legs (Fig. 3.1a). It is planar with all motion being restricted to the sagittal plane.

Head and neck motion play an important role in quadrupedal locomotion. To make sure this model is not oversimplified, I additionally studied a headed model (Fig. 3.1b) in which I use a second rigid body to represent head and neck. This body

Table 3.1: List of model parameters for both headless and headed models. All values are normalized with respect to total mass m_o, uncompressed leg length l_o, and the gravitational constant g

Param.	Unit	Description
m_o	$[\cdot]$	Total mass
l_o	$[\cdot]$	Uncompressed leg length
g	$[\cdot]$	Gravitational constant
l_1	$[\mathrm{l_o}]$	Main body length
j_1	$[\mathrm{m_o l_o^2}]$	Main body inertia
k_F	$[\mathrm{m_o g / l_o}]$	Forelimb spring stiffness
k_H	$[\mathrm{m_o g / l_o}]$	Hind limb spring stiffness
α_F	[rad]	fore angle of attack
α_H	[rad]	Hind angle of attack
d_{COM}	$[\mathrm{l_o}]$	Offset of the COM of the main body
t_{swing}	$[\sqrt{\mathrm{l_o / g}}]$	swing time
m_1	$[\mathrm{m_o}]$	Main body mass
m_2	$[\mathrm{m_o}]$	Head mass
l_2	$[\mathrm{l_o}]$	Head length
j_2	$[\mathrm{m_o l_o^2}]$	Head inertia
k_{head}	$[\mathrm{m_o g l_o / rad}]$	Head-neck spring stiffness
θ_{rest}	[rad]	Head resting angle

is connected to the shoulder via a rotational joint with a torsional spring. Head and neck have a mass of m_2 and an inertia of j_2. The stiffness of the head-neck spring is k_{head}. During locomotion, head and neck passively rotate about the shoulder joint. There is no damping associated with this joint. The resting angle is θ_{rest} and the spring creates a torque of $M_{head} = k_{head}(\theta_{rest} - \theta)$. Since all masses are normalized to total body mass m_o, the main body mass is given by $m_1 = m_o - m_2$ and is thus not part of the free parameter vector.

3.2.2 System Dynamics

The Equations of Motion (EOM) are stated in the canonical form

$$\mathbf{M}(q)\ddot{q} + \mathbf{h}(q,\ \dot{q}) = \boldsymbol{\tau}, \tag{3.1}$$

where $\mathbf{M}(q)$ is the mass matrix, $\mathbf{h}(q, \dot{q})$ are the Coriolis, centrifugal, and gravitational terms, and $\boldsymbol{\tau}$ is the vector of generalized forces. The latter is created by the spring forces of all legs i that are in stance. These forces act along the direction of the leg γ_i with a magnitude F_i that is proportional to the leg compression $l_o - l_i$. The stiffness of this spring is given by k_i. The vector of generalized forces $\boldsymbol{\tau}$ is computed as a projection of the spring forces $\boldsymbol{\tau} = \sum_i \mathbf{J_i}^T F_i$ with

$$\mathbf{J}_i = [-\sin(\gamma_i),\ \cos(\gamma_i),\ d_i \cdot cos(\varphi - \gamma_i)] \tag{3.2}$$

for the headless model. As this model is a single body system, the mass matrix is simply a diagonal matrix with entries $\mathbf{M} = diag(m_1,\ m_1,\ j_1)$, and $\mathbf{h}$ only contains the gravitational forces: $\mathbf{h} = [0,\ -m_o g,\ 0]^T$. The equations of motion for the headed model are a bit more involved. They were derived using Euler-Lagrange equations, and the components $\mathbf{M}$, $\mathbf{h}$, and $\mathbf{J}_i$ are reported in Appendix A.

3.2.3 Experimental Data

The experimental data were recorded on an equine high-speed treadmill (Mustang 2200, Kagra AG) instrumented with piezoelectric force transducers (Type Z17135, Kistler Instruments) and able to measure vertical GRF of all four limbs simultaneously (*Weishaupt et al.*, 2002). Recordings were made with a clinically sound and treadmill-adapted Warmblood riding horse (withers height: 1.74 m, m_o: 660 kg) at walk (1.7 m/s) and trot (3.4 m/s) and an Icelandic horse (withers height: 1.35 m, 355 kg) at the tölt (3.3 m/s). Both horses showed representative breed-specific movement patterns. The active leg length was set to be $l_o = 0.135 \times m_o^{0.37}$, which equaled to about 85 % of the horses' withers height (*Griffin*, 2004). In contrast to real horses, the model has the same leg length for all four limbs. Data collection lasted 20 seconds at a sampling frequency of 480 Hz. Force-time histories were analyzed with in-house

developed software (HP2, Equine Performance Centre, University of Zurich) which allowed automatic extraction of force, time and spatial parameters for each limb separately. Twenty succeeding motion cycles per horse were analyzed and averaged. Force parameters were normalized to the horse's body weight.

3.2.4 Optimization

During the simulation of a stride, I also compute the simulated GRFs $\mathrm{F}_{sim}(t, \mathbf{X}, \mathbf{p})$. They are a function of time t and depend on the parameters $\mathbf{p}$ and on the states at the beginning of the stride as defined by $\mathbf{X}$. $\hat{\mathrm{F}}(t)$ denotes the experimentally obtained GRFs that were recorded from actual horses. To quantify how well the simplistic model predicts the experimentally obtained GRFs, I define the residual:

$$\mathrm{c}(\mathbf{X}, \mathbf{p}) = \int_0^1 \left\| \mathrm{F}_{sim}(s, \mathbf{X}, \mathbf{p}) - \hat{\mathrm{F}}(\hat{s}) \right\|^2 dt. \tag{3.3}$$

The integral uses a normalized time $s = \frac{t}{t_{stride}}$ ($\hat{s} = \frac{t}{\hat{t}_{stride}}$) which runs from 0 to 1 for both the simulated and the experimentally recorded stride. This normalization allowed an easier comparison of simulated and experimental data. One should note, that this means that the cost has no notion of *absolute* time. Since the primary goal of this research is the prediction of the correct footfall sequence (i.e., of *relative* time) as well as of the correct shapes of the vertical GRFs, I deemed this an acceptable simplification. The value of the integrated residual is used as a cost function in a constrained optimization problem:

$$\begin{aligned} &\min\{\mathrm{c}(\mathbf{X}, \mathbf{p})\} \\ s.t. \quad &\mathrm{P}(\mathbf{X}, \mathbf{p}) - \mathbf{X} = 0 \end{aligned} \tag{3.4}$$

that finds states and parameters that optimally predict experimentally recorded GRFs. The optimization problem is solved numerically with the MATLAB opti-

mization toolbox using a Sequential Quadratic Programming (SQP) algorithm (*Remy et al.*, 2011).

3.2.5 Sensitivity Analysis

To be able to judge how well each parameter could be identified by the optimization approach, I conducted a detailed sensitivity study for each gait. Looking at a single initial condition X_j (or a single parameter p_j) at a time, I varied its value by some δX (δp) and then fixed it while optimizing all other states and parameters. Assuming that $\mathbf{x}^\star$ and $\mathbf{p}^\star$ are solutions to the optimization problem (3.4) (with a final cost value of $c^\star$), this is equivalent to stating a new optimization problem with an additional constraint:

$$\begin{aligned} & \min \{\mathrm{c}(\mathbf{X}, \mathbf{p})\} \\ s.t. \quad & \mathrm{P}(\mathbf{X}, \mathbf{p}) - \mathbf{X} = 0 \\ & X_j = X_j^\star + \delta X_j \end{aligned} \tag{3.5}$$

The cost value c at the solution of this optimization problem is a direct function of δX_j. The increase in cost from $c^\star$ to $c(\delta X_j)$, indicates how sensitive the process is with regard to X_j; or -in other words- how well a particular state can be identified. If the variation of a certain state does create a large increase in cost, it means that the state can be identified clearly in the original optimization. If, on the other hand, a certain state does not create an increase in cost, it can be changed without reducing the quality of the fit. Such a state cannot be identified by the proposed method. We can draw similar conclusions about parameters p_j.

Table 3.2: Coefficients of determination (R^2) of the model-predicted GRFs. Values are listed for both, the model without a head and that with an articulated head and neck.

Gaits	left hind	right hind	left fore	right fore
Headless Walk	0.922	0.897	0.958	0.957
Headless Tölt	0.979	0.986	0.998	0.967
Headless Trot	0.999	0.998	0.999	0.999
Headed Walk	0.978	0.971	0.982	0.977
Headed Tölt	0.967	0.962	0.992	0.989
Headed Trot	0.999	0.998	0.999	0.999

3.3 Results

We applied the methods and models described in Section 3.2 to synthesize three different gaits: Walk and trot of Warmblood horses, as well as tölt of Icelandic horses. We were able to produce all three gaits with the same conceptual model, while accurately predicting the experimentally recorded contact timing and SLIPs (Table 3.2). Mathematically, the three gaits are defined by their initial continuous and discrete states (as given by $\mathbf{X}$, Table 3.3 & 3.4) as well as their system parameters (given by $\mathbf{p}$, Table 3.5 & 3.6). The complete motion evolves fully from these values.

In this section, I highlight some key-features of the algorithm, report on the properties of the three identified gaits, and discuss the sensitivity of the solutions with respect to individual model parameters and initial states. Furthermore, I analyze the results obtained by a model with an articulated head-neck segment, and quantify how important this additional model component is in the prediction of the ground contact forces.

3.3.1 Identified Motions and Parameters

For the optimization problem of eq. (3.4) to converge, one must find a suitable initial guess for $\mathbf{X}$. This initial guess must show a footfall sequence that is similar to the experimentally recorded data and must result in a motion that is fairly close to being periodic. Particularly problematic are *missed* or *redundant* events; that is, feet that either do not touch the ground at all or that make contact more than once. The timing of the swing phase (defined by t_{swing}) was tuned towards avoiding these situations. Missed or redundant events otherwise cause discontinuities in the root function $\mathrm{P}(\mathbf{X}, \mathbf{p}) - \mathbf{X} = 0$, which makes it impossible for the SQP solver to converge. Since I was relying on a single shooting method for optimization, the regions of possible initial model states are quite narrow. It thus took some directed trial and error to find appropriate initial guesses for the model states.

Once a suitable initial guess has been determined, the optimization converged in less than 1 minute on a standard Desktop PC. One should note that the optimization problem of eq. (3.4) is non-convex. There is no guarantee that the SQP solution represents a global minimum. To avoid local minima as much as possible, I conducted optimization starting from multiple initial guesses. In combination with the sensitivity study of Section 3.2.5, this gave us some confidence that these solutions are globally optimal. As an example of the periodic continuous state trajectories that result from this process, the motion of the main body and the head-neck segment are shown over a full stride of walking, tölting, and trotting in Figure 3.2.

The most characteristic property of a gait, the footfall sequence is given by the discrete **phase** states (Fig. 3.3). The transition from *ready for touch down* ($phase_i = 1$) to *stance* ($phase_i = 2$) is detected kinematically. A *touch-down* event happens if the contact foot height goes to zero. During this event, the horizontal position of the contact point ($pos_{x,i}$, shown by the solid line) is updated to reflect the new contact point. *Lift-off* is also detected kinematically. A leg leaves the ground, if it would be

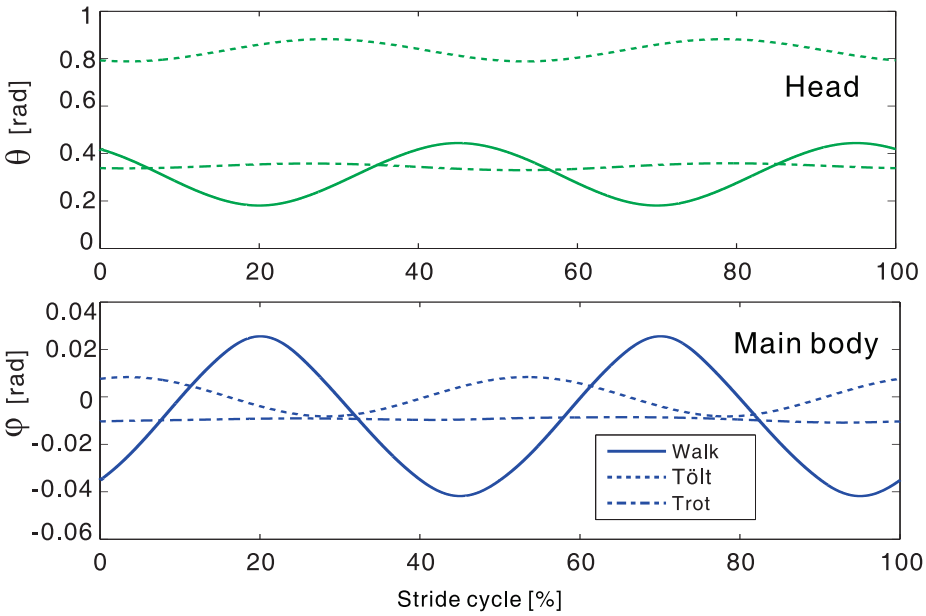

Figure 3.2: Head-neck angle (top), and main body angle (bottom) of a single stride at walk, tölt, and trot for the headed model. Oscillation amplitudes change with gait and are most pronounced in the walk. Generally, the head and torso angles are 180 ° out of phase. That is, the head is low if the shoulders are high. A similar behavior is observed in horses.

extending beyond its rest length l_o. At this moment the timer that measures swing time (illustrated by the red dotted lines) is reset to zero and a *swing* phase of duration t_{swing} is initiated ($phase_i = 3$). A timer triggers the *swing over* event when its value equals to t_{swing}. From a dynamic point of view, there is no distinction between *swing* and the *ready for touch down* phase. In both cases, the legs are assumed to be in the air and are not creating any forces on the main body. The difference is that during the *swing* phase the leg is not able to engage in ground contact. This prevents feet from striking the ground prematurely and enables a coordinated motion of the four legs.

In this framework, the end of a stride is marked by the *lift-off* of the right forelimb (the *terminal event* $e^\star$). Since legged motion is periodic, one should note that any event or relative time point in the cyclic movement might serve as a stride boundary. Our particular choice implies that the right forelimb must always be started in *swing*,

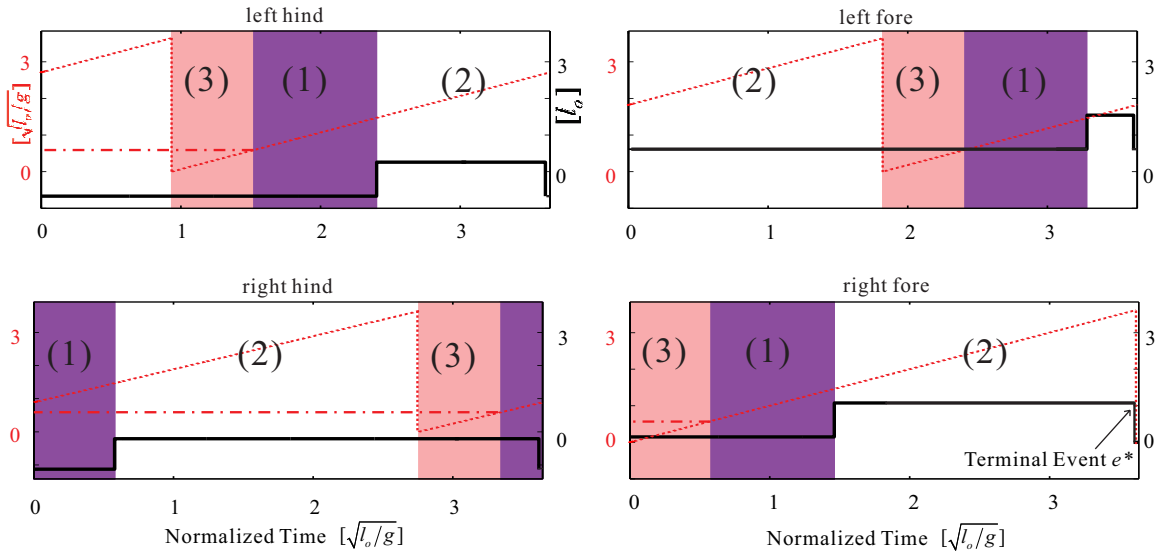

Figure 3.3: The discrete states of all four limbs are shown for a single stride of walking of the headless model. The different phases of each leg are *ready for touch down* (1), *stance* (2), and *swing* (3). At the beginning of *swing*, a timer is started (dotted red line) that triggers the transition into *ready for touch down* once it reaches t_{swing}. All four limbs share the same t_{swing} value that is illustrated by red dash-dotted line. The associated waiting period prevents feet from striking the ground too early and allows for a coordinated motion of the model's legs. The absolute horizontal position of the foot on the ground (solid black line) is only updated at touchdown and remains constant throughout the other phases. At the terminal event, the forward motion is removed from this variable, making it periodic from step to step.

right after lift-off. The initial phases of the other legs can be defined freely, and each different combination results in a different footfall pattern. To achieve quadrupedal *walking*, for example, I have to start the two left limbs in *stance* and the right hind limb in *swing* (Table 3.4).

To better visualize the result, a sequence of animated frames of the walking gait is shown in Figure 3.4 [2]. For purposes of visualization, the swing legs are shown as being retracted and moving gradually towards the AOA; despite the fact that in the mathematical model swing happens instantaneously. Once the limbs are ready for

[2]Videos of all gaits are available at https://youtu.be/Xd-Yw26YDnE

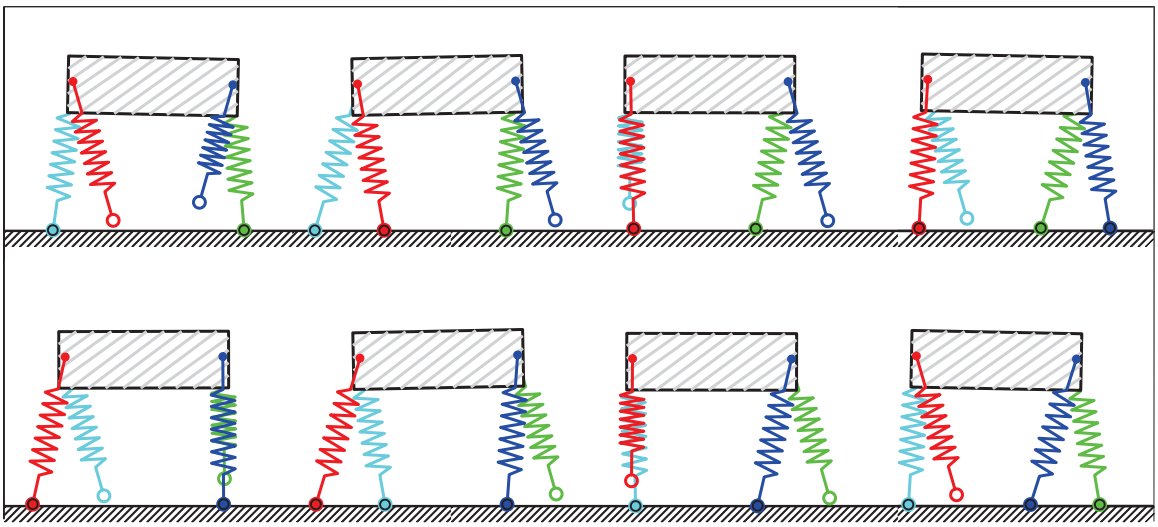

Figure 3.4: 8 consecutive frames of a full stride of headless walking. The model is moving left to right. Uncompressed legs with open circles indicate legs that are *ready for touch-down* ($phase_i = 1$), filled circles indicate legs that are in *stance* ($phase_i = 2$), and retracted legs are in *swing* ($phase_i = 3$).

touch down, they are shown as being uncompressed and at the AOA. Finally, a leg that is in stance is indicated by a filled circle at the foot. At this time, the spring is engaged and creates force.

3.3.1.1 Walk

The walk is a symmetrical four-beat gait with the footfall sequence: right hind, right fore, left hind, left fore. Phases of bipedal support alternate with tripedal support phases, and the vertical SLIP show the characteristic double hump that results from a mid-stance relieve (Fig. 3.5a, b). During walking, the leg springs undergo two compression-extension cycles that create this force profile. The mechanism is similar to what can be observed in the bipedal SLIP model (*Geyer et al.*, 2006). The double-compression of each leg is accompanied by a pronounced pitching motion (-1.45° $+1.23^\circ$) of the main body (φ in Fig. 3.2). The walk had a velocity of $0.255\sqrt{l_o g}$ in simulation, compared to $0.457\sqrt{l_o g}$ in the experimental data.

The model accurately predicts the sequence and timing of the contact events. Furthermore, the model-predicted SLIP for each individual foot roughly match the experimental data ($R^2 > 0.89$) (Table 3.2).

3.3.1.2 Tölt

The tölt is a symmetrical four-beat gait that is unique to Icelandic horses. It has the same footfall sequence as a walking gait. In contrast to walking, however, the legs spend less time on the ground and phases of double support alternate with phases of single support. Furthermore, each limb only undergoes a single compression cycle. The ground reaction forces have a single hump, similar to a bipedal running gait (Fig. 3.5c, d). Apart from the lift-off of the hind limbs, the model correctly predicts the footfall sequence, contact timing, and vertical GRFs. Individual GRFs are predicted with $R^2 > 0.96$.

Similar to walking, a clear but less pronounced pitching motion ($-0.47^\circ \ +0.48^\circ$) of the main body can be observed. Even though the GRFs (and thus the spring compression) peak at almost twice the maximum value as for walking, the main body height y is fairly constant over the course of a stride. It only varies by $0.0058\, l_o$. Intra-stride horizontal velocity $\dot{x}$ is also nearly constant in this gait, and therefore velocity variability is the least among the gaits ($0.0317\sqrt{l_o g}$). In reality, the steady vertical and horizontal motion make this gait very comfortable for a rider. In simulation, the tölt had a velocity of $0.681\sqrt{l_o g}$, compared to a velocity of $0.975\sqrt{l_o g}$ recorded in the experiments.

3.3.1.3 Trot

The trot is a symmetrical two-beat gait, in which diagonal limb pairs move together. Phases of double support alternate with suspension phases. The vertical GRFs (Fig. 3.5e, f) show characteristic single humps that correspond to a single

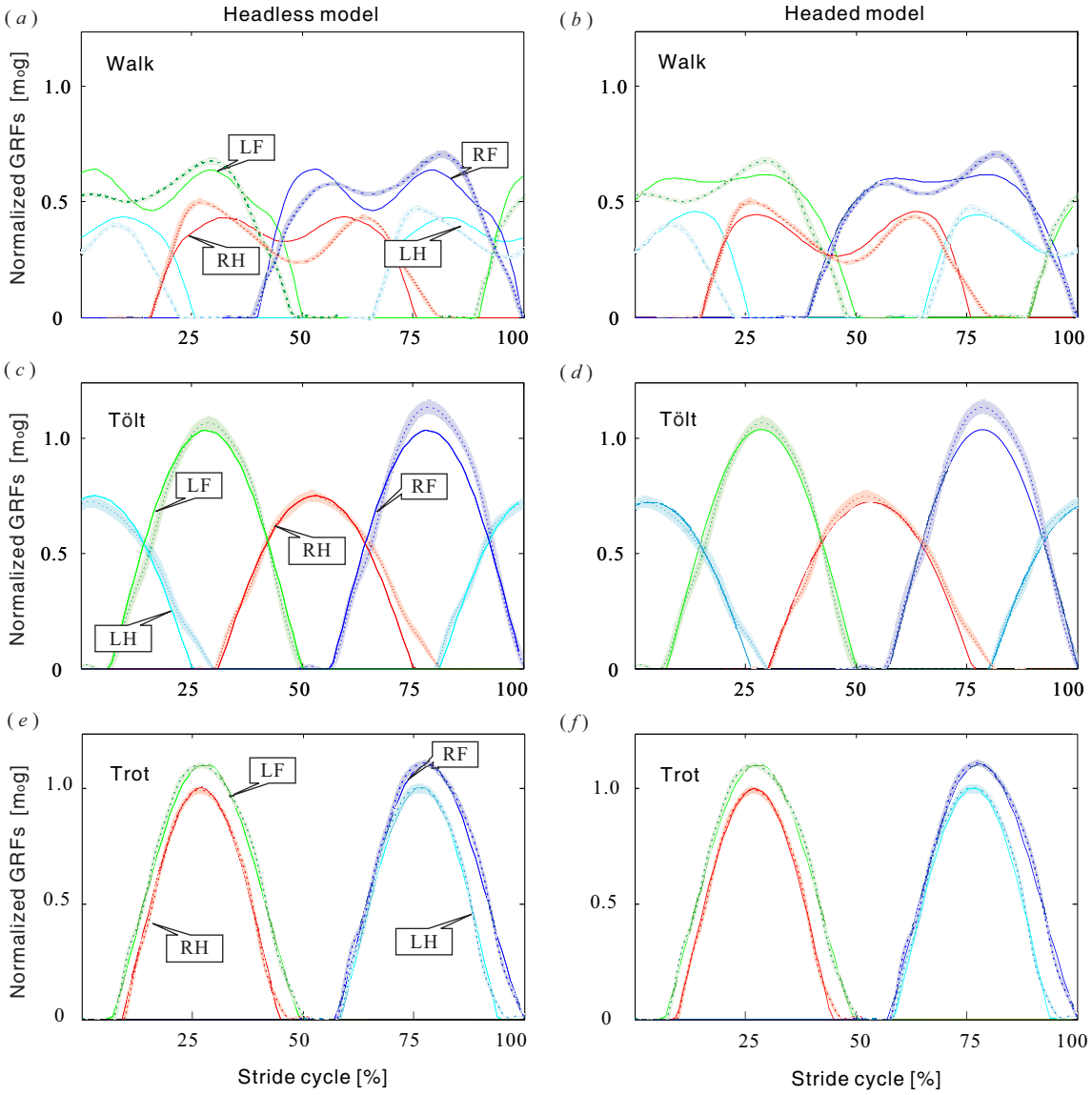

Figure 3.5: Experimentally recorded vertical GRFs (dotted lines ±1 std.) are compared to forces predicted by the headless model (solid lines, shown on the left) and to those predicted by the model with an articulated head and neck (solid lines, shown on the right). Shown are the results for walking (top), tölting (center), and trotting (bottom). Both models correctly predict the footfall pattern, timing, and the general shape of the force curves for all gaits. Quantitatively, a better fit is produced by the headed model, especially for the hind limbs at walk (see also Table 3.2). RH, RF, LH and LF stand for right hind, right fore, left hind, and left fore respectively.

Table 3.3: Optimal initial continuous states for each gait. Please refer to Figure 2.1 for coordinate definitions

Gaits	$\dot{x}[\sqrt{\mathrm{l_o g}}]$	$y[\mathrm{l_o}]$	$\dot{y}[\sqrt{\mathrm{l_o g}}]$	φ[rad]	$\dot{\varphi}[\sqrt{\mathrm{g/l_o}}]$	θ[rad]	$\dot{\theta}[\sqrt{\mathrm{g/l_o}}]$
Headless Walk	0.2601	0.9670	0.0100	-0.0208	0.0566	·	·
Headless Tölt	0.6818	0.9685	0.0148	0.0082	0.0349	·	·
Headless Trot	0.5701	0.9862	0.0417	-0.0126	0.0065	·	·
Headed Walk	0.3236	0.9604	-0.0045	-0.0351	0.0731	0.4186	-0.2921
Headed Tölt	0.8737	0.9656	0.0182	0.0076	0.0334	0.7927	-0.1942
Headed Trot	0.6490	0.9866	0.0393	-0.0103	0.0064	0.3388	-0.0329

compression cycle of the leg spring. This result is similar to previous studies, which employed models that are more complex (*Herr and McMahon*, 2000). Of the three gaits, the trot is the gait that can be best approximated with this conceptual model. The overall GRFs are predicted with an R^2 value of more than 0.99. Similarly, the model predicts the contact sequence and the timing of touchdown and lift-off events with great accuracy. It is even able to account for the small differences in the contact timing and GRF-profiles between the two diagonal leg pairs. There is no visible pitching motion of the main body, yet a very pronounced vertical movement of about 0.04 leg lengths in y. Simulated trotting had a velocity of $0.559\,\sqrt{l_o g}$. Experimentally, this velocity was $0.893\,\sqrt{l_o g}$.

3.3.2 Sensitivity of Initial States and Parameters

For the sensitivity analysis of walking and trotting, each initial state and parameter value was varied by $\pm 1\,\%$. For tölting, which proved to be much more sensitive to both, states and parameters, I only varied their values by $\pm 0.05\,\%$. We excluded both the horizontal position x and the vertical position y from the analysis. The horizontal position x has no influence on the GRFs, and changing the vertical position y violates the lift-off condition at the terminal event $e^\star$. The results of the sensitivity study are shown in Figures 3.6.

Table 3.4: Initial discrete states for each gait. Listed are for each leg the phases ('ready for touch down' (1),'stance' (2), or 'swing' (3)), and the horizontal foot positions in absolute coordinates. RH, RF, LH and LF stand for right hind, right fore, left hind, and left fore respectively. For legs that are in the air, the foot position records where the foot was before lift-off. Note that all gaits start with the right forelimb in swing

Gaits	$phase_{LH}[\cdot]$	$phase_{RH}[\cdot]$	$phase_{LF}[\cdot]$	$phase_{RF}[\cdot]$	$pos_{LH}[\mathrm{l_o}]$	$pos_{RH}[\mathrm{l_o}]$	$pos_{LF}[\mathrm{l_o}]$	$pos_{RF}[\mathrm{l_o}]$
Headless Walk	2	1	2	3	-0.6708	-1.1352	0.6121	0.1477
Headless Tölt	2	1	1	3	-0.5441	-1.0850	-0.3414	0.1995
Headless Trot	3	1	1	3	-0.7688	-1.2293	-0.2419	0.2304
Headed Walk	2	1	2	3	-0.5519	-1.0877	0.6611	0.1253
Headed Tölt	2	1	1	3	-0.5364	-1.1057	-0.2537	0.3156
Headed Trot	3	1	1	3	-0.7914	-1.2533	-0.0792	0.3960

Table 3.5: Optimal main body parameter choices for each gait. Please note that d_{COM} only reflects the main-body COM, not the overall value. It is smaller for the headed model, since there is additional mass in the head-neck segment

Gaits	$m_1[\mathrm{m_o}]$	$l_1[\mathrm{l_o}]$	$j_1[\mathrm{m_o l_o^2}]$	$k_H[\mathrm{m_o g/l_o}]$	$k_F[\mathrm{m_o g/l_o}]$	$\alpha_H[\mathrm{rad}]$	$\alpha_F[\mathrm{rad}]$	$d_{COM}[\cdot]$	$t_{swing}[\sqrt{\mathrm{l_o/g}}]$
Headless Walk	1.00	1.06	0.28	18.31	24.69	0.28	0.28	0.59	0.58
Headless Tölt	1.00	1.01	0.42	20.60	24.88	0.24	0.24	0.57	0.41
Headless Trot	1.00	0.96	0.80	21.46	19.83	0.16	0.20	0.56	0.50
Headed Walk	0.87	0.95	0.25	14.26	15.50	0.33	0.33	0.52	0.55
Headed Tölt	0.89	1.13	0.67	18.65	23.33	0.27	0.25	0.51	0.42
Headed Trot	0.86	1.15	1.15	25.18	21.87	0.16	0.20	0.49	0.43

In terms of sensitivity, there is quite some variability between different states and parameters. The forward velocity $\dot{x}$, for example, can be identified quite clearly, whereas the final cost value (or degree of fitting) is much less sensitive to the vertical velocity $\dot{y}$ and the pitch states φ and $\dot{\varphi}$. This holds for all three gaits. Related to the forward velocity, the AOA (for both, forelimbs and hind limbs) shows a larger sensitivity for all gaits and can thus be identified clearly.

Of the physical parameters, the quantity that can be identified best is the horizontal position of the center of mass (d_{COM}). Its value has a direct impact on the fore-aft distribution of the vertical GRFs and it is thus explicitly influencing the cost function. For walking and tölting, one can additionally identify the length and inertia of the main body, which are coupled to the vertical GRFs via the pitching dynamics of the main body. For trotting (which has hardly any pitching motion) these parameters cannot be identified accurately.

3.3.3 Headed Model

The same three gaits could be identified for the headed model. The initial continuous and discrete states for all gaits are listed in Tables 3.3 and 3.4, and the parameters in Tables 3.5 and 3.6. The resulting SLIPs are shown in Figures 3.5. To assess the ability of this model to match the experimentally recorded vertical SLIPs, the R^2 values are compared to those of the headless model in Table 3.2.

For the tölting and trotting gait, no clear improvement in the fitting to the experimental vertical SLIPs was observed. Head and neck dynamics only play a minor role in these gaits, and the simplistic model without a head is good enough to explain the underlying motion. For walking, on the other hand, the head and neck motion does play an important role. Compared with the optimal solution of the headless model, the model with head improves the correlations of the SLIPs of all four limbs significantly. On average, the fit improved by 4.35 %. In particular, the asymmetry

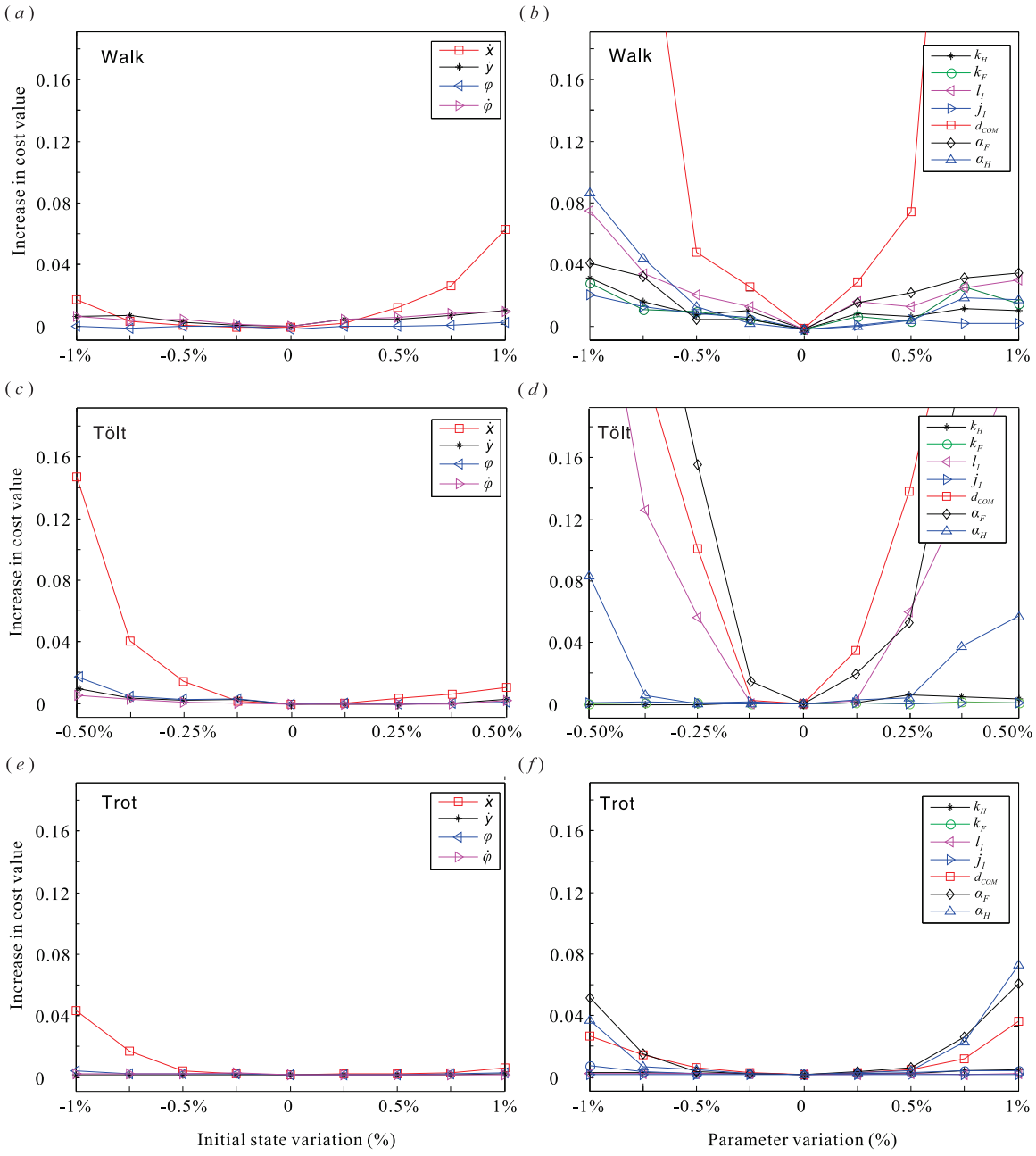

Figure 3.6: Shown is the increase in cost (quantifying the difference between model-predicted and experimentally measured vertical GRFs) as a function to variations in states (shown on the left) and parameter choices (shown on the right). Results are shown for walking (top), tölting (center), and trotting (bottom). This analysis highlights which states and parameters can be predicted well by matching of the vertical GRFs (indicated by a high sensitivity) and which cannot be predicted well (indicated by a low sensitivity).

Table 3.6: Optimal choices for the head parameters for each gait.

Gaits	$m_2[\mathrm{m_o}]$	$l_2[\mathrm{l_o}]$	$j_2[\mathrm{m_o l_o^2}]$	$k_{head}[\mathrm{m_o g l_o/rad}]$	$\theta_{rest}[\mathrm{rad}]$
Headed Walk	0.13	0.69	0.07	1.30	0.38
Headed Tölt	0.11	0.51	0.22	3.25	0.85
Headed Trot	0.14	0.74	0.11	2.37	0.39

in the midstance relieve between forelimbs and hind limbs can only be explained with the additional head dynamics.

This observation also becomes clear when looking at the magnitude of the head motion. At the trot and tölt, the neck joint only rotates by 1.7 and 5.4 degrees, respectively. For walking, a rotation of over 15.1 degrees can be observed (Fig. 3.2) . With respect to parameters, the most notable change in the obtained solution is a decrease of d_{COM} (Table 3.5). Since the mass of the head would shift the overall location of the center of mass forward, the displacement of the main body COM (which is given by d_{COM}) is smaller as in the head-less case. This ensures that the impulse distribution and *overall* COM is still matching the experimental data.

3.4 Discussion and Conclusion

In this paper, we presented a simplistic passive dynamic model that is able to create realistic quadrupedal walking, tölting, and trotting motions. By choosing appropriate system parameters and initial states through an optimization process, the model is able to closely match the GRFs of walk and trot in Warmblood horses and of tölt in Icelandic horses. We investigated the sensitivity of the obtained solutions with respect to all states and parameters, and evaluated the improvement in fitting GRFs when including an additional head and neck segment.

3.4.1 Generating Multiple Gaits with a Single Model

Our proposed model generates this variety of different gaits primarily by altering the initial continuous and discrete states of the system. The resulting motions, footfall patterns, and GRFs emerge from these initial conditions through a numerical integration of the dynamics. Our finding suggests that quadrupedal gaits are merely different dynamic modes of the same structural system and that we can interpret different gaits as different nonlinear elastic oscillations that propel an animal forward. These different oscillation modes create a large variety of locomotion types and allow for varying properties (such as different locomotion velocities) that can be exploited by the animal.

The main determinant for a particular gait (or footfall pattern) are the initial phase choices (Table 3.4). For walk, the model starts with both left limbs in stance; for tölt, only the left hind limb is in stance; and for trot all legs are in the air. The *ready for touch down* phase indicates additionally which feet are able to strike the ground next. For walk this is the right hind limb, and for tölt and trot the right hind limb and left forelimb. The exact timing of these footfalls, however, is determined by the continuous states. Remember that all gaits are assumed to start at lift-off of the right forelimb.

In addition to the starting conditions, the motion is influenced by the system parameters. Some of these parameters, such as the angles of attack α or the rest angle of the neck θ_{rest} would represent a conscious choice of the animal and are expected to change from gait to gait. Other parameters are fixed physical properties that would not vary in a real horse. Yet, in this study, we did allow all values to change, in order to account for the fact that the experimental data was recorded from different horses. Despite being unconstrained, the main parameters (such as the main body length l_1, leg stiffness k, or COM position d_{com}) had very similar values for the three gaits (Tables 3.5 & 3.6).

A detailed analysis of the stability of the obtained motions was not the focus of this work. However, a quick check of the Floquet-multipliers revealed that all reported motions are unstable in a linear approximation. Values varied from 3.2 for headless walking to 247 for the headless tölt. That means, while the gaits that we identified are periodic, continuous locomotion can only be maintained in the complete absence of disturbances. Even a tiny deviation from the periodic orbit will eventually lead to a fall. With this in mind, the presented motions can only be considered as nominal. For continuous locomotion, they must be stabilized through appropriate active feedback control.

The main methodological improvement that enabled us to find multiple gaits within a single model was the introduction of a 'swing phase' in the simulation. In this phase, the feet are unable to engage in ground contact. This facilitated the intrinsic coordination of complex motion patterns and allowed us to include all four limbs in the simulation at the same time. This made it unnecessary to make additional assumptions (such as synergies and symmetries (*Full and Koditschek*, 1999)), or to artificially reduce the complexity of the model (e.g., to a single spring mass system (*Farley et al.*, 1993) or to the lateral half of a quadruped (*Chatzakos and Papadopoulos*, 2007)). In contrast to these examples in which the models could only be used for the parametric analysis of *specific* gaits (such as a trotting or bounding), the proposed model can produce a much larger number of gaits; including the complex motions of four-beat walking and tölting. At the same time, the complexity of the simulation and the number of necessary parameters remains at an absolute minimum. Despite this simplicity, the model does not only produce qualitatively different motion patterns, but can quantitatively match recorded vertical GRFs with high accuracy. Particularly the GRFs of trotting and tölting can be predicted almost perfectly. Larger residuals were only obtained when identifying walking, but could be alleviated by adding a head-neck segment to the model.

Table 3.7: Comparison of simulated and experimental stride time.

Gaits	Experiments [s]	Simulation [s]
Headless Walk	1.129	1.402
Headless Tölt	0.523	0.548
Headless Trot	0.825	0.649
Headed Walk	1.129	1.281
Headed Tölt	0.523	0.536
Headed Trot	0.825	0.569

3.4.2 Stride Time

The cost function in eq. 3.3 uses a normalized time to speed up the optimization process and to get better convergence. The goal of this research was to identify the footfall sequence and shapes of vertical GRFs for different gaits of horses in nature by using simple models. Stride time was thus not my primary concern. However, for comparison, the absolute stride time (in seconds) is listed in Table 3.7 for both the optimized simulated results and the experimental data. Larger discrepancies can be observed in the trotting gait of both headless and headed models as well as in headless walk.

3.4.3 Model Limitations and Comparison to Biology

Naturally, a simplistic model has to make some approximations and can never fully explain all observed dynamics. In the following, I compare these results to the locomotion of horses in nature and discuss the limitations that are inevitable when using such strongly simplified models.

The passive nature of the models prevents an active contribution to the motion; for example, during an active push-off. The lift-off of all limbs shows a pronounced break-over phase in the experimentally recorded GRFs. In nature, this prolongation of the stance phase is caused by the hoof tilting actively shortly before lift-off. Such an effect

cannot be replicated in our models, where the point-feet predict abruptly vanishing vertical GRFs. The break-over influence is visible in all gaits but most prominent at tölt in the hind limbs (Fig. 3.5c, d). This may be caused by the comparatively larger range of the limb angle in Icelandic horses compared to Warmblood horses; especially while tölting (*Weishaupt et al.*, 2014; *Bogisch et al.*, 2014).

Since our models are planar, they are unable to replicate motions that happen outside the sagittal plane. As the experimental GRFs are mostly symmetric with respect to left and right, this did not cause any major problems. The only exemption are the forelimb forces of the tölt, in which the experimentally measured peak force of the right side was significantly higher than the peak force of the left side (Fig. 3.5c, d). This is potentially caused by a lateral torso motion. Such an asymmetric loading cannot be produced with the planar symmetrical model. This does not mean that we can only generate symmetrical gaits. For example, there is an asymmetry regarding the leg phasing of the diagonal legs at trot in the experimental data. For the left diagonal (LF, RH) the impact of the RH limb is slightly delayed with reference to the LF impact, while the legs of the right diagonal (RF, LH) impacted nearly synchronously. This behavior can be replicated in simulation and explained by a small difference in the main body pitch between the two diagonal stances (Fig. 3.5e, f). Even a small amount of such pitch influences the relative timing of fore and hind footfall. Furthermore, we have shown in related work that our planar model can produce the footfall patterns associated with asymmetric gaits such as bounding or galloping (*Gan and Remy*, 2014a).

In terms of methodology, I based the gait identification on the replication of vertical GRFs. Our cost function was the difference between measured and model-predicted GRFs. This is a reasonable choice, since the GRFs contain substantial gait information; including contact sequences, footfall timing, and center of mass dynamics. Yet, when comparing the model-predicted optimal parameter choices and

resulting motion characteristics to values reported from biology, one should keep in mind that not all parameters can be identified with the same accuracy by the optimization method. We evaluated this effect in a sensitivity study that investigated how well each state and parameter could be identified. The GRFs of the trot, for example, are clearly dependent on the center of mass position d_{COM}, but they are not very sensitive to the main body length l_1 and inertia j_1 (Fig. 3.6f). This means that d_{COM} can be accurately identified, while this method does not allow clear conclusions about the values of l_1 and j_1. This is not surprising. At trot, the main body is mostly leveled and not undergoing a large amount of pitch. Since length and inertia are parameter values that can only manifest themselves in the GRFs if the main body is pitching, they are consequently not reflected in the analysis of a trot. At walk and tölt, on the other hand, a pronounced pitching motion exists, and the analysis is very sensitive to l_1 and j_1 (Fig. 3.6b, d).

An interesting result of the sensitivity study was the low predictability of the leg stiffness values. Independent of the chosen gait, it was shown that the leg stiffness could not be predicted through the analysis of the GRFs. This is surprising, since the leg stiffness appears to be one of the most fundamental model properties and should have a direct influence on the GRFs. However, a simultaneous adaptation of the motion (most notably through the vertical velocity $\dot{y}$ and the pitch states φ and $\dot{\varphi}$) can compensate for this effect, such that the combination of leg stiffness and vertical motion cannot be resolved from the GRFs alone. Furthermore, this effect might also be amplified by the normalization of stride duration in eq. (3.3). Having no absolute time in the model potentially degrades the correct identification of frequencies.

In terms of identifying motions and parameters, some limitations might arise from the fact that we were experimentally limited to *vertical* contact forces. Consequently, we had only limited knowledge about the fore-aft motion. Characteristics that relate to this motion could not be identified very well. For example, the model-predicted

forward velocities differed substantially from the experimentally recorded values. At walk, the model-predicted speed was about half of the experimentally measured. This shortcoming is likely a consequence of the missing horizontal contact information.

Furthermore, redundancies in the model can make it difficult to identify values reliably. This can be seen, for example, with respect to the head-neck parameters. In order to match experimental GRFs, the optimizer had to synchronize the head-neck motion with the pitching of the main body. The two motions must be exactly out of phase at tölt and especially at walk (Fig. 3.2). That is, the natural frequency of the neck oscillation must be matched to the overall stride frequency. Through this link of morphology, motion, and contact forces, the optimizer can establish estimates of parameter values through matching of the GRFs. Yet, since four morphologic parameters (head length l_2, head and neck stiffness k_{head}, head mass m_2, and inertia j_2) all influence the natural frequency of the head motion, it becomes difficult to determine all these parameters at the same time. This is reflected in the large variability that some of these parameters have for the three different gaits (Table 3.6).

Even with these limitations, parameters were often close to values reported in biology (using (*Vorstenbosch et al.*, 1997) as my main reference). This holds, for example, for the overall COM position at walk of 59 % of the main body (in the headless case this is identical to d_{COM}, Table 3.5), compared to a value of 58.2 % in Warmblooded horses (*Waldern et al.*, 2009). For trotting the model predicts 56 % compared to 57.0 %. Similarly, the model predicts a main body length l_1 between $0.95\,l_o$ and $1.15\,l_o$ which compares to values of about $0.8\,l_o$ in horses. This list includes even more detailed parameters, such as the relative amount of the head and neck mass. The predicted value of 11 %-14 % (Tables 3.5 & 3.6) only slightly overestimates values from the existing literature, where head-neck mass was determined as about 8 % of body weight (*Buchner et al.*, 1997). While the optimization outcomes are not exact predictions, they show that the model parameters are in the right ballpark.

CHAPTER IV

All Common Bipedal Gaits Emerge from a Single Passive Model

4.1 Introduction

[1] While the Geyer Spring Loaded Inverted Pendulum (SLIP) model has been instrumental in understanding bipedal gaits, it has a key simplifying assumption inherited from the simple SLIP: after a leg lifts off the ground, it instantaneously goes to a predefined Angle of Attack (AOA) and remains there until the foot hits the ground again. This modeling choice is problematic for several reasons: First, it represents a control parameter rather than a passive dynamic motion. In addition, the AOA likely needs to be actively adapted to enable different gaits. Moreover, one can find infinitely many periodic motions by changing the AOA, including motions with infinitely short, nonphysical swing times (*Rummel et al.*, 2009). Furthermore, since in the SLIP model leg swing happens instantaneously, the footfall timing of two or more independent legs needs additional considerations, such as the introduction of a phase timer for each leg (*Gan and Remy*, 2014a). Similar to the AOA, the choices of timing parameters are arbitrary and represent control rather than dynamics. Finally, as there is a single AOA for both legs, the model is unable to replicate some bipedal

[1] This chapter has been previously submitted to the Journal of the Royal Society Interface (*Gan et al.*, 2018b).

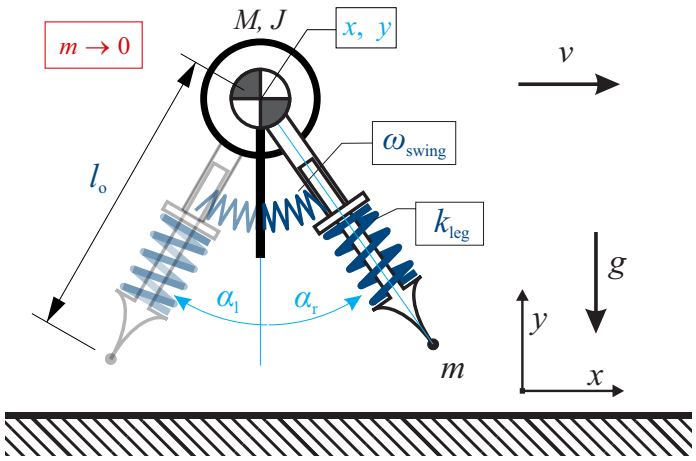

Figure 4.1: This figure shows the passive bipedal model with swing leg dynamics used in this study. By taking the limit of $m \to 0$, collision losses at touchdown are eliminated and therefore the resulting model is energetically conservative. A continuation method is utilized to identify all possible passive periodic motions of this model, as they emerge from bouncing in place. Solutions lie, as a function of energy, along one dimensional manifolds that bifurcate into different branches with distinctly different motions. In doing so, almost all of the bipedal gaits found in nature and robotics can be identified.

gaits, such as bipedal skipping or galloping (leaping), in which the two legs usually need different angles of attack. In order to understand the passive dynamic motion underlying the different gaits, it is thus necessary that leg swing is also a function of the natural mechanical dynamics. The way this is done in this work is very similar to the method proposed by (*O'Connor*, 2009) in which a torsional spring is added at the hip joint. The legs are therefore subjected to passive oscillations during swing.

In the following sections, I introduce a fully passive model that fulfills the requirements stated above. I systematically identify all period-one periodic motions of this model that emerge from simple bouncing in place with certain footfall patterns, and which branch off via bifurcations detectable with the numerical continuation techniques (*Allgower and Georg*, 2003; *Rosa and Lynch*, 2014). Periodic motions lie, as a function of energy, along one dimensional manifolds that bifurcate into different branches with distinctly different motions. It is demonstrated that the model is able

to reproduce almost all of the bipedal gaits found in nature and robotics by gradually breaking symmetries in periodic solutions. In addition to walking and running, these include several gaits not present in prior models, such as hopping, skipping, or bipedal galloping. All these gaits originate through bifurcations and continuations from in-place bouncing of a single model with a single set of parameter values.

4.2 Methods

4.2.1 Model Description

The bipedal model used in this work (Fig. 4.1), is an extension of the work by (*Geyer et al.*, 2006), and is similar to the model proposed by (*O'Connor*, 2009). It consists of a main body with mass M and inertia J. The vertical and horizontal positions of the Center of Mass (COM) of the main body, and the main body's pitch angle are given by the variables x, y, and φ, respectively. Each of the two legs (with index $i \in [l, r]$) is modeled as a massless linear spring with length l_i, rest leg length l_o, spring stiffness k_{leg}, no damping, and a point mass m at the foot. Each leg is connected, through a frictionless hip joint (with joint angle α_i), to the COM of the main body. Torsional springs with stiffness k_{swing} and no damping are added to these joints. The springs are uncompressed when the respective leg is pointing straight down. Rather than defining a value for k_{swing} directly, I prescribe a leg swing frequency ω_{swing}, and derive:

$$k_{\text{swing}} = \omega_{\text{swing}}^2 m l_o^2. \tag{4.1}$$

While this model is energetically conservative during flight, it would lose energy when a foot's velocity is brought to zero in a touch-down collision. With such losses, it would be impossible to identify passive periodic gaits. To resolve this issue, I take the limit of m going towards zero ($m \to 0$), similar to the method used in (*Garcia*, 1998; *O'Connor*, 2009). This implies that $k_{\text{swing}} \to 0$ as the swing frequency ω_{swing}

remains unchanged. Furthermore, the inertia of the main body becomes very large compared to the inertia of the feet ($J \gg ml_o^2$), such that I can neglect any main body pitch and assume $\varphi \equiv 0$. Finally, the legs exert forces onto the main body only when they are compressed in stance; during swing, the main body motion is independent of the leg motion (but not the other way around). Since the leg stiffness k_{leg} is finite, infinitely fast oscillations of the leg length (around l_o) would occur while the leg is in the air. For viability, I ignore these oscillations and assume that the leg length is constant during swing ($l \equiv l_o$).

4.2.2 Equations of Motion

Based on these assumptions, I develop the Equations of Motion (EOM) for the model. For the main body, they are:

$$\ddot{x} = F_x/M, \tag{4.2a}$$

$$\ddot{y} = F_y/M - g, \tag{4.2b}$$

where F_x and F_y are the components of the combined leg force $\mathbf{F}$.

During the swing phase of each leg, the leg angle acceleration is given by

$$\ddot{\alpha}_i = \frac{1}{l_o^2 m}\left(-\ddot{x} m l_o \cos(\alpha_i) - (g + \ddot{y}) m l_o \sin(\alpha_i) - k_{\text{swing}}\alpha_i\right), \tag{4.3}$$

which, in the limit $m \to 0$, and by substitution of (4.1) and (4.2), becomes:

$$\ddot{\alpha}_i = \frac{-\cos(\alpha_i) F_x l_o - \sin(\alpha_i) F_y l_o}{M l_o^2} - \alpha_i \omega_{\text{swing}}^2. \tag{4.4}$$

During stance of each leg, a kinematic constraint is introduced on the leg length, leg angle, and the associated velocities. I assume that there is no sliding of the foot during the stance phase and use the variable s_i to record the horizontal foot positions

on the ground. With this, the leg angle and leg length during stance can be computed as:

$$\alpha_i = \arctan\left(\frac{s_i - x}{y}\right), \tag{4.5}$$

$$l_i = \sqrt{(x - s_i)^2 + y^2}. \tag{4.6}$$

The forces exerted by the stance legs are:

$$F_i = k_{\text{leg}} \cdot (l_o - l_i), \tag{4.7a}$$

$$F_x = \sum_i -F_i \sin(\alpha_i), \tag{4.7b}$$

$$F_y = \sum_i F_i \cos(\alpha_i). \tag{4.7c}$$

The transition between stance and swing of the individual legs is monitored via zero crossings of two event functions, $e_{i,1}$ and $e_{i,2}$. A *touch-down* event happens when the height of the COM is equal to the vertical projection of the leg length. A foot leaves the ground (the *lift-off* event) when the leg reaches its rest length.

$$\text{touch-down event: } e_{i,1} = l_o \cos(\varphi + \alpha_i) - y, \tag{4.8a}$$

$$\text{lift-off event: } e_{i,2} = \sqrt{(x - s_i)^2 - y^2} - l_o. \tag{4.8b}$$

At touch-down, I record the new foot position on the ground, which is given by

$$s_i = x + l_o \sin(\alpha_i). \tag{4.9}$$

Also note that during touch-down, the leg velocities $\dot{l}_i$ and $\dot{\alpha}_i$ are discontinuous. During lift-off, $\dot{\alpha}_i$ remains unchanged, while $\dot{l}_i$ is set to 0.

It is important to note this model has no way to change its leg length during swing

(as humans and animals do by bending their knees). Instead, the leg length is fixed to l_o during the swing phase. To simulate swing when the COM is so low that the foot has to go through the ground, I simply ignore some of the touch-down events. The choice of whether to enforce a touch-down or allow the leg to swing through, is somewhat arbitrary in that it does not follow from the model's dynamics. As I demonstrate later in this work, this choice plays an important role in the evolution of, and distinction between different gaits. The contact events I consider are either specified explicitly in Section 4.2.3, or follow uniquely from the continuation of existing solutions.

In order to keep the solutions general, I normalize all state and parameter values with respect to M, g, and l_o (*Hof*, 1996). The only parameters that I had to select for the proposed model were the leg stiffness $k_{\text{leg}} = 20\, {}^{Mg}/_{\text{l}_\text{o}}$ and the swing frequency $\omega_{\text{swing}} = \sqrt{5}\,\sqrt{{}^{g}/_{\text{l}_\text{o}}}$. These dimensionless values are comparable to the existing hardware (*Smit-Anseeuw et al.*, 2017b).

4.2.3 Gait Creation

I define a gait as a periodic motion in which all states except for the horizontal position x return to their original values after one full *stride*. I further assume that the stride begins at the instance of a right leg touch-down $e_{r,1}$. This event provides the Poincaré section for a limit cycle analysis. The state at the beginning of the stride (at the Poincaré section) is $\mathbf{X^o} = [\dot{x}_o, y_o, \dot{y}_o, \alpha_{l,o}, \dot{\alpha}_{l,o}, \alpha_{r,o}, \dot{\alpha}_{r,o}]^T$. Starting at this initial state (and setting the body horizontal position $x_o = 0$), I obtain a trajectory over a full stride through a numerical integration that is terminated when the subsequent touch-down event of the right leg is registered. This process yields the Poincaré map P that maps the initial states $\mathbf{X^o}$ to final states $\mathbf{X'}$ at the end of the stride. A function $\mathbf{\Phi} : \mathbb{R}^7 \to \mathbb{R}^7$ enforces periodicity:

$$\mathbf{\Phi} := \mathrm{P}\left(\mathbf{X}^\star\right) - \mathbf{X}^\star = 0. \tag{4.10}$$

Gaits are defined by states $\mathbf{X}^\star$ at the Poincaré section that are solutions to this implicit equation. Since the system is energetically conservative, only six of the seven periodicity constraints are independent. This means that solutions to (4.10) evolve along one-dimensional manifolds on the Poincaré section.

Some bipedal gaits in nature, such as walking, running, and skipping, are classified as *symmetrical* gaits. That is, the legs on each side perform exactly the same motion, just 180 ° out of phase (*Alexander*, 1984). To simplify computation of such symmetrical gaits, I cut the simulation of these gaits in half and terminate the integration at left leg touch-down $e_{l,1}$. To obtain a full stride, I then repeat the first half of the motion but with the left and right legs switched. For the *asymmetrical* gaits (hopping and bipedal galloping) integration was continued to the next right leg touch-down event, simulating a full stride.

Beyond the definition of the continuous states, I also have to define which leg is initially in stance and which is in swing. Since the Poincaré section is defined as right leg touch-down, the right leg is always initially in stance. This leads to two possible cases: *single stance*, in which the left leg is initially in the air, and *double stance* in which it is on the ground. Each case leads to a distinct dynamic behavior of the system and also imposes a different number of constraints on the continuous states.

4.2.4 Continuation and Bifurcations

I find branches of periodic solutions by solving a 1D *continuation problem* (*Dankowicz and Schilder*, 2013). That is, given a known solution $\mathbf{X}_n^\star$, I numerically search for an adjacent solution $\mathbf{X}_{n+1}^\star$ on the same branch, and, by iteratively repeating this process, discover the entire branch. At each iteration, I constrain the next solution $\mathbf{X}_{n+1}^\star$ to be a fixed distance d away from $\mathbf{X}_n^\star$ in the direction that is similar to the

previous step. That is, I find $\mathbf{X}^{\star}_{n+1}$ by solving:

$$\begin{aligned} \mathbf{\Phi}\left(\mathbf{X}^{\star}_{n+1}\right) &= 0, \\ \left\|\mathbf{X}^{\star}_{n+1} - \mathbf{X}^{\star}_{n}\right\| &= d, \\ \left(\mathbf{X}^{\star}_{n+1} - \mathbf{X}^{\star}_{n}\right)^{T}\left(\mathbf{X}^{\star}_{n} - \mathbf{X}^{\star}_{n-1}\right) &> 0. \end{aligned}$$

Solving (4.11) numerically is sensitive to having a good initial guess of $\mathbf{X}^{\star}_{n+1}$. I generate such a guess based on the Floquet analysis of the Poincaré map. Suppose that for a given periodic trajectory $\mathbf{X}^{\star}_{n}$, there exists another trajectory $\mathbf{X}^{\star}_{n+1}$ nearby. Then a small disturbance in the direction of $\mathbf{X}^{\star}_{n+1}$ remains unchanged after one stride (after such disturbance, the passive system stays on the new periodic trajectory). Mathematically, this means that one of the Floquet multipliers[2] $\lambda_{n,i}$ of the system at $\mathbf{X}^{\star}_{n}$ is equal to $+1$, and the corresponding eigenvector $\boldsymbol{v}_{n,i}$ is approximately directed towards $\mathbf{X}^{\star}_{n+1}$. Therefore, I use $\mathbf{X}^{o}_{n+1} = \mathbf{X}^{\star}_{n} \pm d \cdot \boldsymbol{v}_{n,i}$ as the initial guess for numerically solving the problem (4.11). The step size d was carefully tuned during the search in order to identify periodic solutions, especially at turning points.

The continuation algorithm searches for adjacent periodic solutions associated with a Floquet multiplier equal to $+1$ on the same branch. For every solution in this branch, this is a stationary eigenvalue and the corresponding eigenvector is tangential to the branch. However, at some points along the branch, there may be more than one unit-multiplier. This happens when at least one of the other Floquet multipliers crosses the unit circle with a real value of $+1$ (*Dankowicz and Schilder*, 2013). The additional unit multipliers at such a bifurcation point usually have eigenvectors that are not tangential to the original branch of solutions. Another distinct branch of solutions is thus connected to the original branch at such bifurcation points. I run

[2]Floquet multipliers are eigenvalues of the Monodromy matrix $\mathbf{J}$, which is the partial derivative of the Poincaré map P with respect to the system states, evaluated at the periodic solution. $\mathbf{J}$ provides linear approximations to the changes in small disturbances to the system state from stride to stride which is described in the equation (2.5).

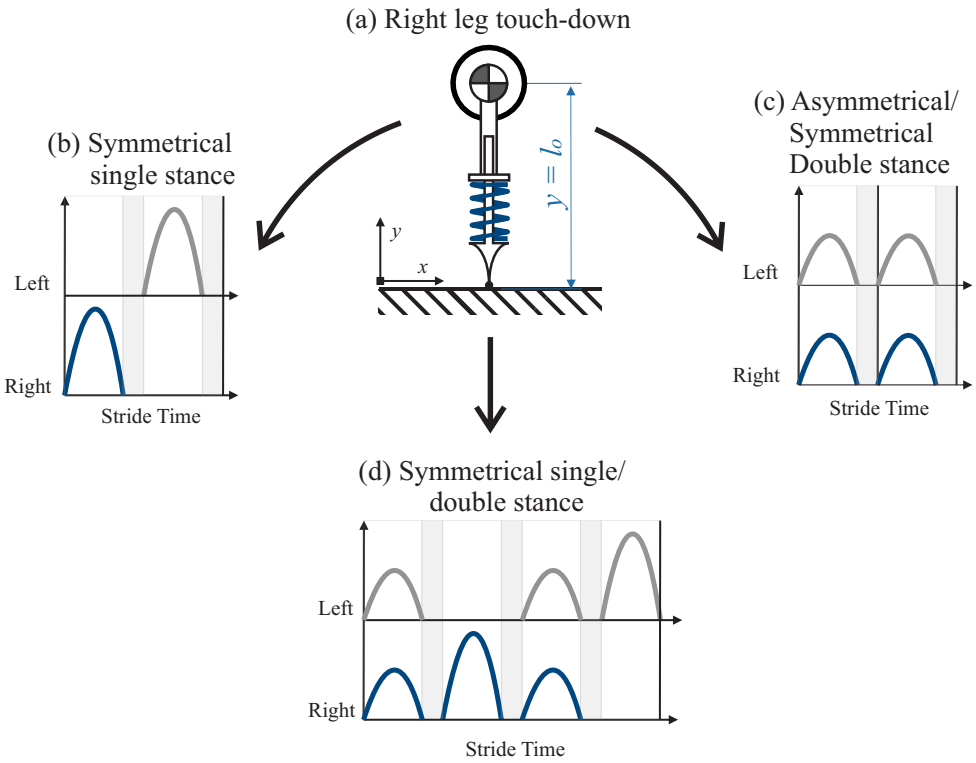

Figure 4.2: This study considers three fundamentally different footfall patterns (shown here together with the corresponding vertical ground reaction forces) that originate from different contact considerations at the moment of touch-down (a). By choosing different combinations of supporting legs, the following three footfall sequences emerge: (b) single stance (running), (c) double stance (hopping), and (d) the combination of the previous two cases which includes both double stance and single stance in alternation.

a separate instance of the continuation algorithm to discover all periodic solutions along each new branch.

New branches originate at *bifurcation points* and *turning points* which were detected by a change in the null space dimension of the fréchet derivative of $\mathbf{\Phi}$ (*Hermann and Saravi*, 2016). Instead of determining the type of bifurcation points by applying the Lyapunov-Schmidt reduction and evaluating the values of its coefficients, I categorized them by considering the changes in stability and the number of solutions in the neighborhood of the bifurcation.

4.2.5 Start of the Search

The search for gaits was initiated with the most trivial motion that fulfills the requirements for a gait: bouncing in place with the lowest energy possible. The initial state for this motion is $\mathbf{X}_o = [0, l_o, 0, 0, 0, 0, 0]$, there is no forward speed, both legs are pointing down and are motionless, and the vertical height is equal to l_o with no vertical velocity. When started in this state, the model undergoes a purely vertical cycle of leg compression and decompression, followed by an infinitesimally short flight phase before reaching the initial state again. This oscillation can happen either on one leg or on both legs, depending on whether I assume the initial state $\mathbf{X}_o$ to be in (right leg) single stance or in double stance. Based on this distinction, I define four different footfall patterns which lead to different types of gaits:

- *Symmetrical single stance.* The right leg enters stance while the left leg does not. In the simplified model this means that the left leg is allowed to go through the ground at the initial instant. After one vertical oscillation and an infinitesimally short flight phase, the roles of the left and right leg are switched (Fig. 4.2b).

- *Asymmetrical double stance.* Both legs are fully synchronized: they start in stance phase and lift off the ground at the same time. This is shown as the first half of the footfall pattern in Fig. 4.2c.

- *Symmetrical double stance.* Both legs are fully synchronized as in the previous case, but after one oscillation (at the next touch-down) the legs are switched. This gait is shown as the whole gait cycle in Fig. 4.2c. The switching of the legs has no effect on this in-place motion, which is identical to the asymmetrical double stance. But this formal distinction from the asymmetrical double stance leads to different gaits when the legs become desynchonized.

- *Symmetrical single/double stance.* As shown in Fig. 4.2d, this gait combines the first two cases, where a single stance phase alternates with a double stance

phase. The legs are switched when the left leg touch-down is triggered at the beginning of the double stance phase.

4.3 Results

In the following, I present the periodic motions identified by the continuation analysis for this model. Solutions are discussed according to the footfall sequences from which they originate and are reported by stating the initial state $\mathbf{X}_o$ from which the periodic motion evolves. These initial states are plotted in a three-dimensional projection of the state space (showing the vertical velocity $\dot{y}$, horizontal velocity $\dot{x}$, and the angle of the right leg α_r at the Poincaré section) to visualize the evolution and connection of individual solution branches and to highlight bifurcation points. For some selected periodic motions, I also present a visualization of the motion and show the vertical GRFs [3].

I numerically report the most important bifurcation points and explicitly state their eigenvectors. Due to the contact constraints, not all of the seven initial states can be chosen freely. Since the right leg is uncompressed at touch-down (which defines the Poincaré section), the initial vertical position is fully determined by the right leg angle, $y_o = l_o \cos(\alpha_{r,o})$, and the right leg angle rate $\dot{\alpha}_{r,o}$ is fully determined by the COM position (i.e. the angle $\alpha_{r,o}$) and velocity according to eq. (4.5). In addition, in initial *double stance*, the left leg velocity $\dot{\alpha}_{l,o}$ is also no longer a free variable and, similar to $\dot{\alpha}_{r,o}$, is determined by the COM position and rate and the left leg angle. The reported states and eigenvectors thus have five dimensions for initial *single stance* and only four dimensions for initial *double stance*. At bifurcation points, I describe the multidimensional eigenspace to the eigenvalue of +1 by reporting a set of independent eigenvectors that are tangential to the resulting solution branches.

[3] Please see the multimedia file at https://youtu.be/3W30TnUGj9U for a video showing these motions.

4.3.1 Symmetrical Single Stance

Periodic motions emerging from the symmetrical single stance footfall pattern are shown in Fig. 4.3. They originate from bouncing-in-place (point S, red circle) and can be generally classified as *running-in-place* (branch ***RP***) and different types of *running forward/backward* (branches ***R1***-***R6***).

4.3.1.1 Running-in-Place (Branch RP):

At the starting point S –the initial bouncing-in-place motion– the eigenvector $\boldsymbol{v_s}$ corresponding to the eigenvalue of 1 is pointing in the $\dot{y}$ direction (see Table 4.1), corresponding to adjacent solutions with different vertical velocities $\dot{y}$ at touch-down, but otherwise unchanged behavior. Positive initial velocities $\dot{y}_o > 0$ are impossible, since they correspond to lift-off, violating the touch-down condition at the Poincaré section. The ***RP*** branch thus extends from $\dot{y}_o = 0\,\sqrt{\mathrm{gl_o}}$ towards negative vertical velocities, corresponding to *running-in-place* with increasingly longer flight phases with a higher apex height and stance phases with a greater spring compression (grey line in Fig. 4.3). The branch is limited to $\dot{y}_o > -\sqrt{k_{\mathrm{leg}} l_o^2/M - 2gl_o} = -4.24\,\sqrt{\mathrm{gl_o}}$. At this point, the leg spring fully compresses during stance ($l_i = 0$), leading to a singularity in eq. (4.5). Note that Fig. 4.3 only shows part of this branch for $\dot{y}_o > -2\,\sqrt{\mathrm{gl_o}}$. Along the ***RP*** branch, I find 13 bifurcations points. The first five (points A-E in Fig. 4.3) are reported in Table 4.1.

4.3.1.2 Running Forward and Backward (Branches R1-R6):

The additional eigenvectors with an eigenvalue of $+1$ at bifurcations A-E all have components in the $\dot{x}$, α_i, and $\dot{\alpha}_l$ directions. The new solutions that stem from them thus incorporate horizontal velocity and leg swing, and correspond to *running forward/backward* gaits. The resulting branches (labeled ***R2***-***R6***) extend symmetrically for both negative and positive velocities $\dot{x}$ (only the positive velocity range is shown

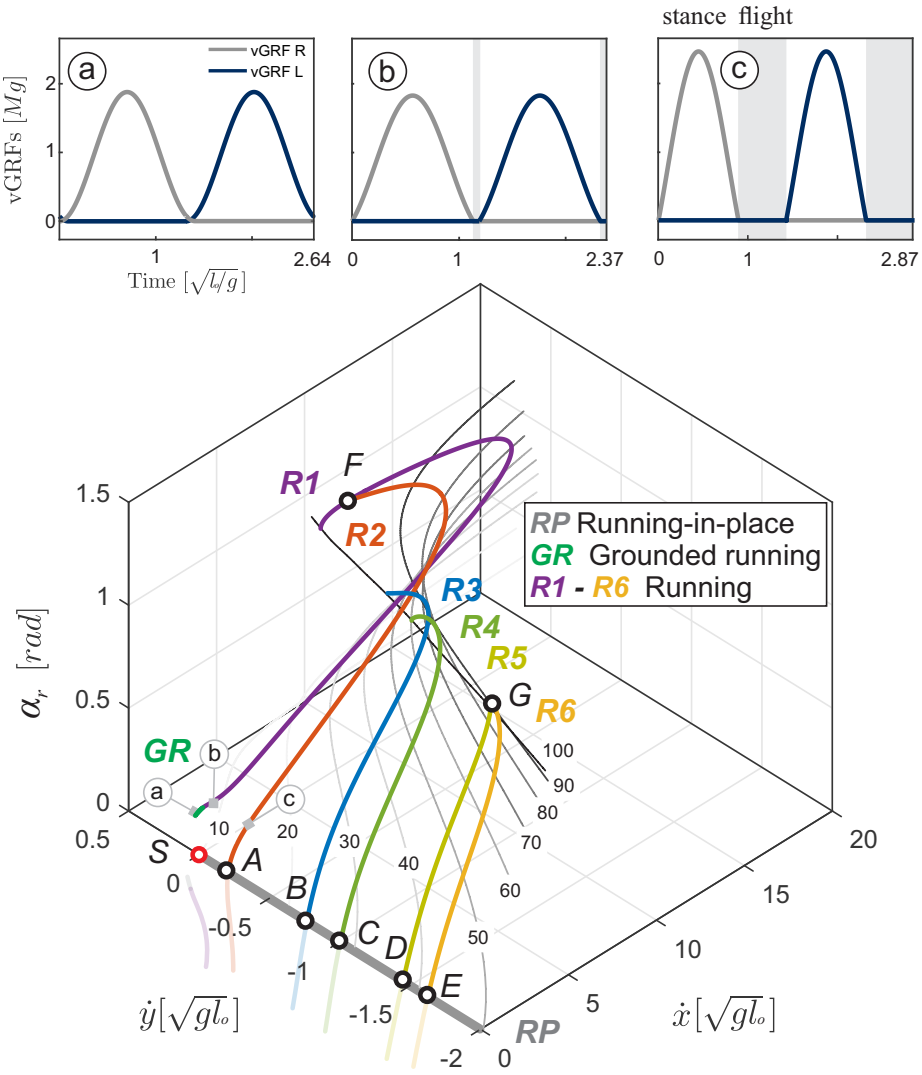

Figure 4.3: Visualization of periodic motions that emerge from bouncing-in-place (red circle, S) with a *symmetrical single stance* (as shown in Fig. 4.2b). Solutions can be classified into running-in-place gaits with different vertical heights (grey line, ***RP***), and running forward/backward gaits (***R1 - R6***) which differ primarily by the number of swing leg oscillations in the associated solutions. Black circles (A-G) denote bifurcations points that connect the solution branches. The numbers on the grey isolines denote the largest leg compression in a stride as a percentage of leg length. The inserts show the ground reaction forces of a sample running motion along ***R2*** (c), as well as the transition to grounded running (when the flight phase disappears) along ***R1*** (a) & (b). Several successive frames of solution (c) are presented in Fig. 4.4.

Table 4.1: Initial states and eigenvectors associated with a Floquet multiplier of +1 at selected bifurcation points for motions emerging from *Symmetrical Single Stance*.

States	S	A		B		C		D		E		F		G	
$\dot{x}_o$	0	0.00		0.00		0.00		0.00		0.00		6.38		4.17	
$\dot{y}_o$	0	-0.21		-0.77		-1.01		-1.45		-1.63		-0.27		-1.56	
$\alpha_{l,o}$	0	0.00		0.00		0.00		0.00		0.00		-0.66		-0.96	
$\dot{\alpha}_l$	0	0.00		0.00		0.00		0.00		0.00		3.01		1.52	
$\alpha_{r,o}$	0	0.00		0.00		0.00		0.00		0.00		1.50		1.18	
eVec	$\boldsymbol{v}_S$	$\boldsymbol{v}_{A1}$	$\boldsymbol{v}_{A2}$	$\boldsymbol{v}_{B1}$	$\boldsymbol{v}_{B2}$	$\boldsymbol{v}_{C1}$	$\boldsymbol{v}_{C2}$	$\boldsymbol{v}_{D1}$	$\boldsymbol{v}_{D2}$	$\boldsymbol{v}_{E1}$	$\boldsymbol{v}_{E2}$	$\boldsymbol{v}_{F1}$	$\boldsymbol{v}_{F2}$	$\boldsymbol{v}_{G1}$	$\boldsymbol{v}_{G2}$
$\Delta\dot{x}$	0	0	0.75	0	0.80	0	0.78	0	0.85	0	0.86	0.98	0.01	0.08	0.05
$\Delta\dot{y}$	1	1	0.00	1	0.00	1	0.00	1	0.00	1	0.00	-0.03	0.12	-0.12	0.11
$\Delta\alpha_l$	0	0	-0.48	0	0.37	0	0.28	0	-0.31	0	-0.31	0.14	-0.70	0.36	-0.34
$\Delta\dot{\alpha}_l$	0	0	0.28	0	0.36	0	-0.49	0	-0.32	0	0.30	0.14	-0.70	0.92	-0.94
$\Delta\alpha_r$	0	0	0.36	0	0.30	0	0.29	0	0.29	0	0.28	0.01	0.03	-0.06	0.03
Branch	***RP***	***RP***	***R2***	***RP***	***R3***	***RP***	***R4***	***RP***	***R5***	***RP***	***R6***	***R1***	***R2***	***R5***	***R6***

in Fig. 4.3). Moving along these branches, maximal leg compression during stance (shown as isolines in Fig. 4.3) increases until the branches terminate in the singularity of a full leg compression.

Motions along the branch ***R2***, which extends from bifurcation point A, are most reminiscent of bipedal running gaits in nature. A representative motion (solution labeled (c)) on this branch is shown in Fig. 4.4. Trajectories of the leg angles α_i essentially follow a quasi-sinusoidal profile (shown for a forward speed of $0.5\sqrt{\mathrm{gl_o}}$ in Fig. 4.5, red lines). For motions along ***R2***, after lift-off, the swing leg first moves backward, then swings forward to be in front of the main body, and retracts backward before hitting the ground. Such 'swing leg retraction' is also observed in human running (*Seyfarth et al.*, 2003), and, has the beneficial property that the foot closely matches the ground-speed at touchdown.

The periodic motions on the other running branches differ primarily in when the swing leg hits the ground. Motions along the branches ***R3*** and ***R4*** represent running gaits in which the swing leg performs *two* oscillations during swing (blue and green lines in Fig. 4.5). The solutions differ in when the touch-down event is triggered:

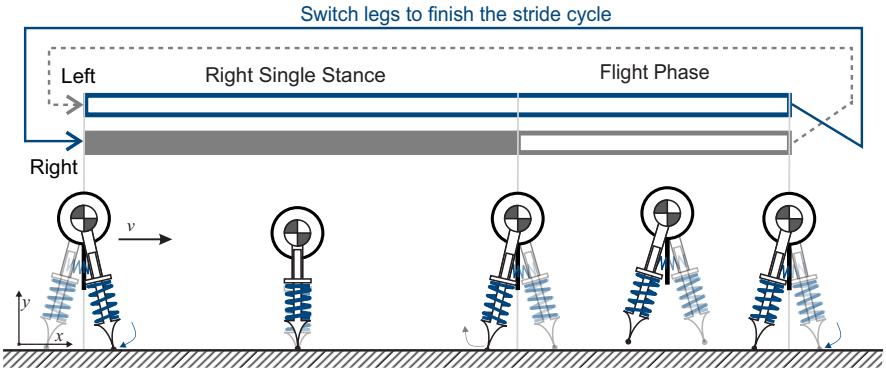

Figure 4.4: Key frames from an exemplary solution on the running branch ***R2*** (solution (c) in Fig. 4.3). Solutions on the other running branches have the same footfall pattern, but differ in their number of swing leg oscillations.

on ***R3***, the swing leg touches down while moving forwards (hence the large jump in velocity in Fig. 4.5b), while on ***R4*** it hits the ground while moving backwards (as for motions on ***R2***). The solutions on the next branches (***R5*** and ***R6***) are analogous to those on ***R3*** and ***R4***, but with the swing leg doing three oscillations during the flight phase. Overall, bifurcations along the ***RP*** branch arise whenever the hopping period is matched by the oscillation time of the swing leg or a multiple thereof. Many combinations are possible as flight time scales linearly with $\dot{y}_o$, while the swing leg has a constant frequency. Further solutions follow this pattern with even higher numbers of swing leg oscillations (up to 7 oscillations in this model). These solutions are not explicitly shown and discussed here.

In Fig. 4.3, one can see that the branches ***R5*** and ***R6*** join at another bifurcation point (point G) at high leg compression values. At this point, the swing leg velocity $\dot{\alpha}$ becomes zero at the moment of touchdown, thus essentially removing the difference between the motions in ***R5*** and ***R6***. Such a junction is not present for ***R3*** and ***R4***, as these two branches reach full leg compression before joining together. However, I can find a bifurcation (point F) along ***R2*** that corresponds to such a junction. It connects to another branch of running gaits, ***R1***, in which the swing leg performs a

Table 4.2: Initial states and eigenvectors associated with a Floquet multiplier of +1 at selected bifurcation points for motions emerging from *Asymmetrical Double Stance*.

States	S	I		J		P		Q		L		N	
$\dot{x}_o$	0	0.00		0.00		0.00		0.00		1.43		9.79	
$\dot{y}_o$	0	-0.70		-1.11		-1.19		-1.41		-1.13		-0.79	
$\alpha_{l,o}$	0	0.00		0.00		0.00		0.00		0.32		1.42	
$\alpha_{r,o}$	0	0.00		0.00		0.00		0.00		0.32		1.42	
eVec	$\boldsymbol{v}_S$	$\boldsymbol{v}_{I1}$	$\boldsymbol{v}_{I2}$	$\boldsymbol{v}_{J1}$	$\boldsymbol{v}_{J2}$	$\boldsymbol{v}_{P1}$	$\boldsymbol{v}_{P2}$	$\boldsymbol{v}_{Q1}$	$\boldsymbol{v}_{Q2}$	$\boldsymbol{v}_{L1}$	$\boldsymbol{v}_{L2}$	$\boldsymbol{v}_{N1}$	$\boldsymbol{v}_{N2}$
$\Delta\dot{x}$	0	0	0.94	0	0.95	0	0.00	0	0.00	0.97	0.22	0.99	0.54
$\Delta\dot{y}$	1	1	0.00	1	0.00	1	-0.01	1	0.00	-0.02	-0.02	-0.05	-0.36
$\Delta\alpha_l$	0	0	0.25	0	0.23	0	-0.71	0	-0.71	0.18	-0.78	-0.03	-0.71
$\Delta\alpha_r$	0	0	0.25	0	0.23	0	0.71	0	0.71	0.18	0.59	-0.03	0.26
Branch	***HP***	***HP***	***H1***	***HP***	***H2***	***HP***	***GP1***	***HP***	***GP2***	***H2***	***G1***	***H2***	***G1***

single oscillation and the foot strikes the ground in a forward motion (purple lines in Fig. 4.5). Solutions on the branch ***R1*** have the same footfall pattern as running in ***R2***, but shorter flight phases and lower COM profiles. At lower speeds on the ***R1*** branch, the aerial phase becomes shorter (see solution labeled (b) in Fig. 4.3) until it fully vanishes at a velocity of $0.25\sqrt{\mathrm{gl_o}}$. As speed further decreases, the touch-down of the leading leg happens earlier than the lift-off of the trailing leg and the flight phase is replaced by a double stance phase (see solution labeled (a) in Fig. 4.3). These double-stance gaits are not running (there is no flight phase); but they retain a single-hump vGRF profile, similar to that of running. Therefore, motions like this have been referred to as *grounded running* gaits (***GR***) (*Rummel et al.*, 2009; *Martinez and Carbajal*, 2011). This type of solution only exists when the forward speed is larger than $0.24\sqrt{\mathrm{gl_o}}$. For lower speeds, the ***GR*** branch would require negative vGRFs during the double stance phase which is not physically realistic. This is the reason why the ***R1/GR*** branch does not connect to the ***RP*** branch.

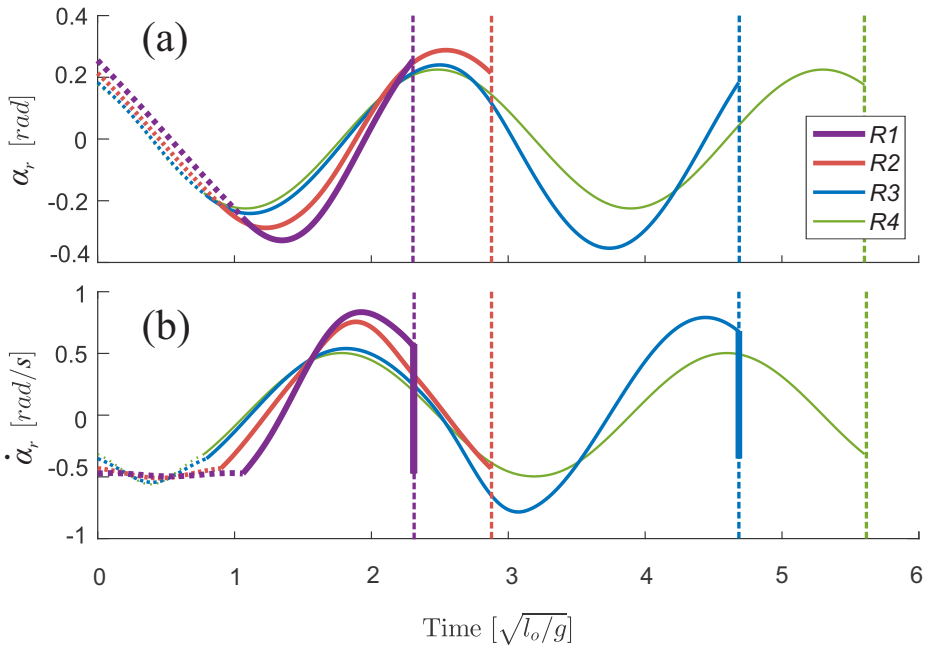

Figure 4.5: In this figure, I compare the right leg angle trajectory $\alpha_r(t)$ and right leg angle velocity $\dot{\alpha}_r(t)$ of solutions on the running branches (***R1*** - ***R4***). For each solution, I show a full stride with an average forward velocity of $0.5\sqrt{\mathrm{gl_o}}$. Stance phases are shown as dotted lines, while solid lines indicate flight phases. The solutions start and end at right leg touchdown. One can clearly see how the solutions differ in their number of oscillations and whether the swing leg hits the ground in a forward or backward motion. These differences are enabled by different durations of the flight phase.

4.3.2 Asymmetrical Double Stance

The periodic motions emerging from the asymmetrical double stance footfall pattern are shown in Fig. 4.6. Again, they originate from bouncing-in-place (point S, red circle) and can be generally classified as *hopping-in-place* (branch ***HP***), *hopping forward/backward* (branches ***H1*** and ***H2***), *galloping-in-place* (branches ***GP1*** and ***GP2***), and *galloping* (branches ***G1*** and ***G2***).

4.3.2.1 Hopping-in-place (Branch HP):

Starting from bouncing-in-place on two legs, the eigenvector $\boldsymbol{v_S}$ corresponding to the eigenvalue of $+1$ is pointing in the $\dot{y}$ direction (see Table 4.2). By varying the vertical speed $\dot{y}$ at touch-down, I find the hopping-in-place branch ***HP*** (grey line in Fig. 4.6). In this gait, the two legs are fully synchronized and always vertical. The ***HP*** branch extends to $\dot{y}_o = \sqrt{2k_{\mathrm{leg}} l_o^2/M - 2gl_o} = -6.16\sqrt{\mathrm{gl_o}}$, where the legs fully compress during stance. This value is larger than for the symmetrical single stance, as now both legs provide forces in the stance phase. (Note again that Fig. 4.6 only shows part of this branch for $\dot{y}_o > -2\sqrt{gl_o}$). I find 16 bifurcations along the ***HP*** branch. The first two bifurcations (points I and J) identified along the ***HP*** branch are pointing to the forward/backward hopping branches. They are at the vertical speeds $-0.70\sqrt{\mathrm{gl_o}}$ and $-1.11\sqrt{\mathrm{gl_o}}$, respectively. The corresponding eigenvectors are provided in Table 4.2. As with the running gaits, 6 additional hopping branches with multiple periods of swing leg oscillations appear in pairs along ***HP*** (not shown in the figure). The remaining bifurcations, including the next two bifurcations that are found at the vertical speeds $-1.19\sqrt{\mathrm{gl_o}}$ and $-1.41\sqrt{\mathrm{gl_o}}$ (points P and Q), are the starting points of galloping-in-place gaits.

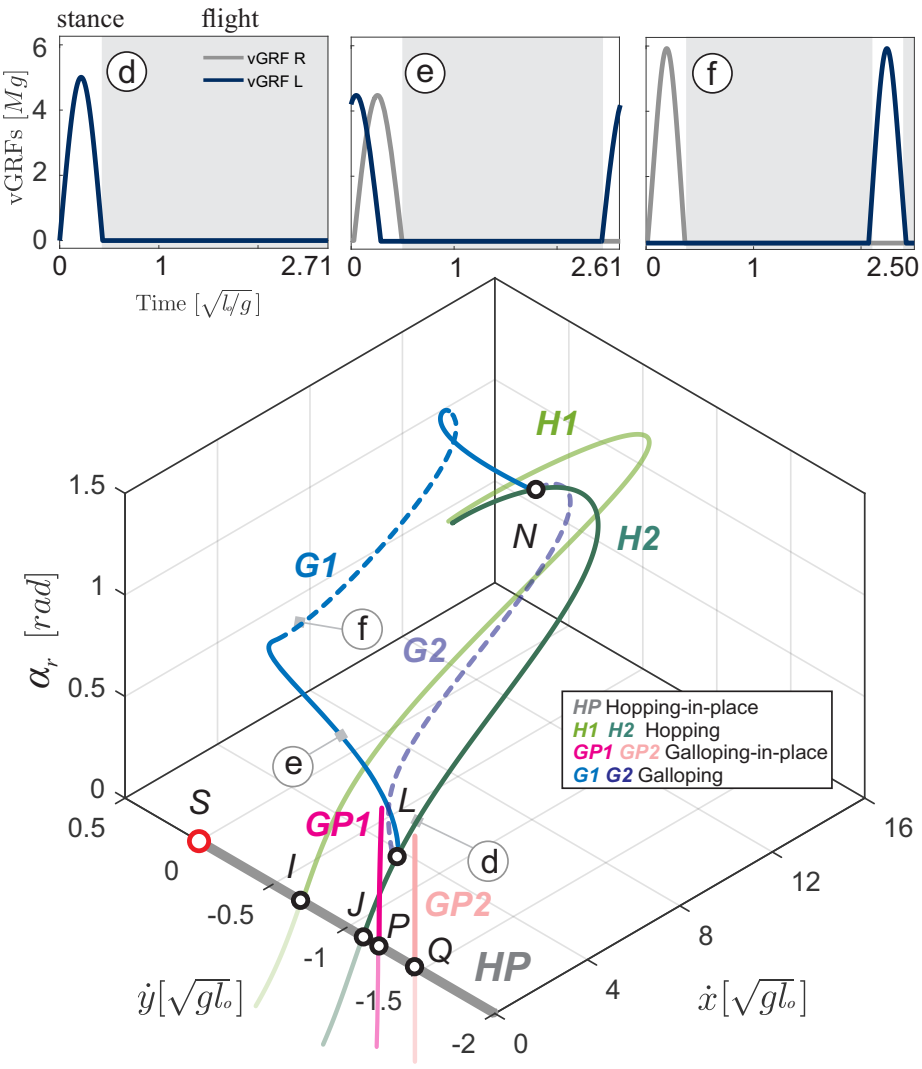

Figure 4.6: Visualization of periodic motions that emerge from bouncing-in-place (red circle, S) with an *asymmetrical double stance* (as shown in Fig. 4.2c). Solutions can be classified into hopping-in-place gaits with different vertical heights (grey line, ***HP***), hopping forward/backward gaits (***H1*** & ***H2***), galloping-in-place gaits (***GP1*** & ***GP2***), and galloping gaits (***G1*** & ***G2***). The black circles (I,J,L,N,P & Q) denote bifurcations that connect the solution branches. The inserts show the ground reaction forces of a typical hopping gait along the ***H2*** branch (d), as well as the transition from galloping (e) to an asymmetrical running gait (f) as an additional flight phase appears along ***G1***. Key motion frames from the solutions (d) and (e) are shown in Fig. 4.7 and Fig. 4.8.

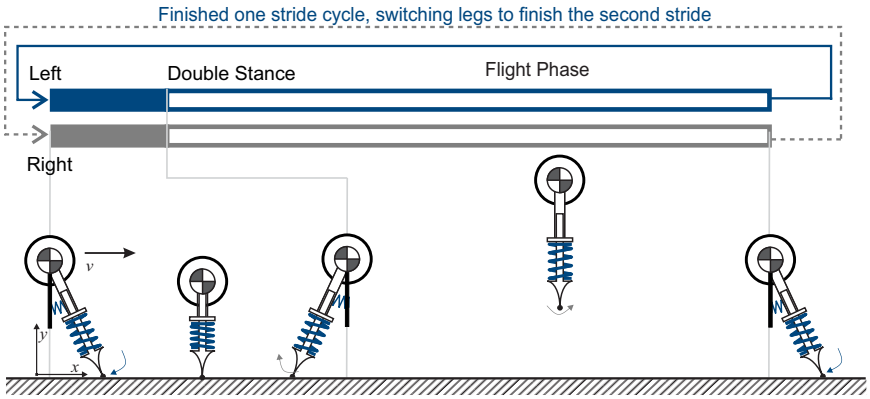

Figure 4.7: Key frames from an exemplary solution on the hopping branch ***H2*** (solution (d) in Fig. 4.6). In this hopping forward/backward gait, the two leg are always fully synchronized and act essentially as a single (yet stiffer) leg.

4.3.2.2 Forward/Backward Hopping (Branches H1 and H2):

The additional eigenvectors with an eigenvalue of +1, $\boldsymbol{v}_{I2}$ and $\boldsymbol{v}_{J2}$ at the bifurcations I and J, have components in the $\dot{x}$ and α_i directions. Notably, the values for α_l and α_r are identical, suggesting that these gaits emerge with the same initial angle and angular velocity for both legs. The resulting branches (labeled ***H1*** and ***H2***) extend symmetrically for both negative and positive velocities and correspond to *hopping* gaits. Along the hopping forward/backward branches, the legs remain together throughout the stride. The difference between the branches ***H1*** and ***H2*** is similar to that between ***R1*** and ***R2***. For solutions on ***H1***, touch-down is triggered while the legs swing forward, while for solutions on ***H2***, the legs hit the ground while swinging backward. The vGRFs of an exemplary solution along ***H2*** gait at a speed of $2.0\sqrt{\mathrm{gl_o}}$ are shown in Fig. 4.6, solution labeled (d). Fig. 4.7 shows several key frames from this solution. Both ***H1*** and ***H2*** terminate when the legs reach their full compression during stance (and before the branches can merge together). Along the branch ***H2***, two bifurcations (points L and N) are found when the forward speed reaches $1.43\sqrt{\mathrm{gl_o}}$ and $9.79\sqrt{\mathrm{gl_o}}$, respectively.

4.3.2.3 Galloping-in-place (Branches GP1 and GP2):

At points P and Q two *galloping-in-place* gaits (***GP1*** and ***GP2***) bifurcate from the hopping-in-place branch ***HP***. These two branches extend in almost the same direction: both leg angles increase equally in magnitude, but in opposite directions while the vertical speed $\dot{y}$ and the horizontal speed $\dot{x}$ remain the same (see $\boldsymbol{v}_{P2}$ and $\boldsymbol{v}_{Q2}$ in Table 4.2) . Solutions on these branches are hopping-in-place motions with leg swing. That is, at lift-off, the legs are split apart and perform a full oscillation during swing to return to the original orientation at touch-down. The branches ***GP1*** and ***GP2*** have different swing leg motions in the air: in ***GP1***, the leg hits the ground while extending outward, and in ***GP2***, the leg reaches its maximal extension and retracts inward before touching the ground. Both ***GP1*** and ***GP2*** terminate when they reach an unstable equilibrium point in the middle of the double-support phase. When the branches are extended in the negative $\boldsymbol{v}_{P2}$ and $\boldsymbol{v}_{Q2}$ directions, the roles of the left and right leg are simply switched. These gaits are equivalent to the skipping-in-place gaits that are discussed in more detail later in this section. The main difference is that in asymmetrical galloping, the legs perform a full oscillation during flight, while in symmetrical bounding, they perform only half an oscillation. A total of 6 galloping-in-place branches with multiple periods of swing leg oscillations appear in pairs along ***HP***. These additional branches are not shown here.

Along the two branches, solutions have the same vertical speeds and the COM only moves in the vertical direction with $\dot{x} = 0$ during the whole stride cycle. I find 3 bifurcation points that emerge along the ***GP1*** branch and two bifurcation points along the ***GP2*** branch. They are neither shown nor discussed here.

4.3.2.4 Galloping (Branches G1 and G2):

As provided in Table 4.2, at bifurcation L, in addition to moving along the hopping branch ***H2*** (direction $\boldsymbol{v}_{L1}$) where the legs are fully synchronized, there exist additional

solutions in direction $\boldsymbol{v}_{L2}$, away from ***H2***. For these new solutions, the leg motions become desynchronized: one leg slightly moves backward and becomes the trailing leg, while the other leg moves forward acting as the leading leg. Either leg can be the leading leg which corresponds to moving in either the positive or negative direction of $\boldsymbol{v}_{L2}$ (right leg in front: branch ***G1***; left leg in front: branch ***G2***). The gaits along ***G1*** and ***G2*** are referred to as *bipedal galloping*. An exemplary solution labeled (e) of this gait is shown in Fig. 4.8. Compared to the running and hopping gaits, the two legs have distinct angles at touch-down and follow different trajectories. Since each leg swings forward to its original angle after each stride, the leading and the trailing legs remain the same along the galloping branches. At high speeds, both ***G1*** and ***G2*** revert back to the hopping branch ***H2*** and merge with it at another bifurcation (point N), where the legs become synchronized again.

Close to the point L, galloping is similar to hopping, with only a slight desynchronization between the motion of the two legs. Moving away from ***H2***, the legs become less synchronized, with an increasing difference in their angles of attack. The double stance phase becomes shorter and eventually disappears. It is replaced by a brief flight phase after the speed reaches $3.31\sqrt{\mathrm{gl_o}}$ (see solution (f) in Fig. 4.6). Such galloping with two distinct flight phases can be thought of as *asymmetrical running*: it has the same footfall pattern as a running gait, but different touch-down angles of the two legs and different step durations. This gait is shown as the dashed line portion in the middle of ***G1*** in Fig. 4.6. Closer to the point N, the additional flight phase gets shorter again and is eventually replaced again by a double stance phase.

4.3.3 Symmetrical Double Stance

The periodic motions emerging from symmetrical double stance are shown in Fig. 4.9. The solution branches include hopping-in-place ***HP*** and hopping forward/backward ***H1*** and ***H2***, identical to those presented in Section 4.3.2. In addi-

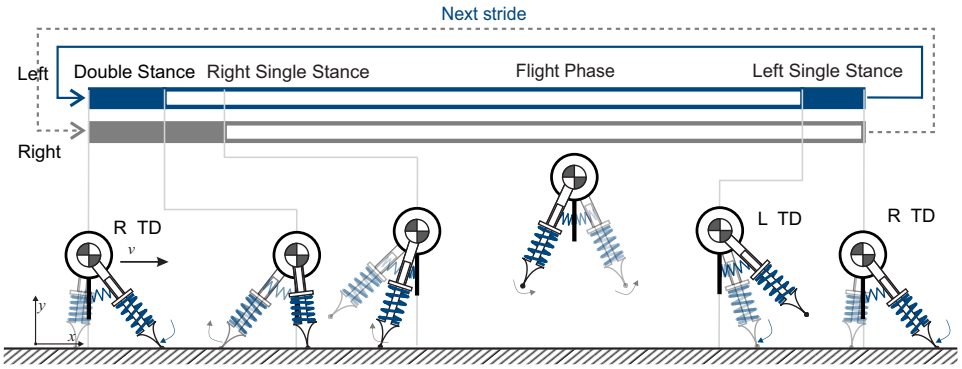

Figure 4.8: Key frames from an exemplary solution on the hopping branch ***G1*** (solution (e) in Fig. 4.6). In such a galloping gait, the trailing leg always touches down on the ground first. The ground contact of the leading leg follows shortly after. In contrast to the skipping gait, the leading leg and trailing leg never switch roles. Galloping is thus an asymmetrical gait. However, both the left leg and right leg can serve as the leading leg, corresponding to the left galloping ***G1*** and right galloping ***G2*** branches.

tion, I find skipping gaits along the new branches ***SP1***, ***SP2***, ***S1***, and ***S2***.

4.3.3.1 Hopping (Branches HP, H1, and H2):

As long as the motion of the two legs is synchronized, gaits emerging from symmetrical double stance remain the same after leg switching and are thus identical to those emerging from asymmetrical double stance, as discussed in Section 4.3.2. Therefore, starting from symmetrical bouncing at S, the hopping branches ***HP***, ***H1***, and ***H2*** are found again at the same locations. However, I find a new bifurcation point H on the ***HP*** branch, when the vertical speed $\dot{y}_o$ equals $-0.58\sqrt{\mathrm{gl_o}}$. Also, at the point I ($\dot{y}_o = -0.70\sqrt{\mathrm{gl_o}}$) where the ***H1*** branch connects to ***HP***, two additional Floquet multipliers cross the unit circle at $+1$ with the corresponding eigenvectors $\boldsymbol{v}_{I3}$ and $\boldsymbol{v}_{I4}$ reported in Table 4.3. That is, two additional branches connect to ***HP*** at point I.

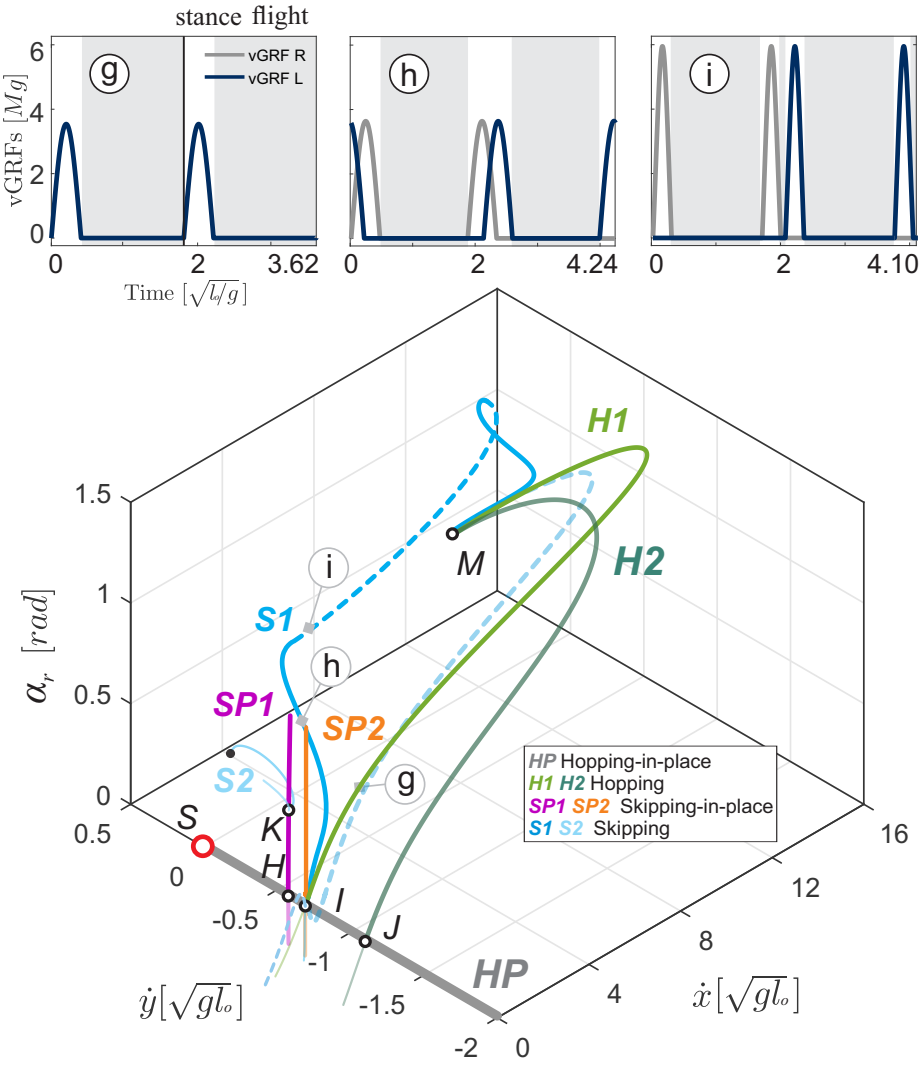

Figure 4.9: Visualization of periodic motions that emerge from bouncing-in-place (red circle, S) with a *symmetrical double stance* (as shown in Fig. 4.2c). Solutions include the same hopping gaits observed in Fig. 4.6, as well as a number of skipping gaits. The branches ***SP1*** and ***SP2*** correspond to skipping-in-place with split legs. Branch ***S1*** corresponds to a forward skipping gait. The solid line represents this gait as started from the touch-down event of the leading leg whereas the dashed line represents the same gait as started from the touch-down of the trailing leg. Branch ***S2*** is one of many examples of a forward skipping gait that emerges from in-place skipping. It eventually connects to solutions that can be classified as walking. The black circles (H-K & M) denote bifurcations that connect the solution branches. The inserts show the ground reaction forces of a typical hopping gait along the ***H1*** branch (g), as well as the transition from skipping (h) to an asymmetrical running gait (i) as an additional flight phase appears along ***S1***. Several key frames from the solution (h) are shown in Fig. 4.11.

Table 4.3: Initial states and eigenvectors associated with a Floquet multiplier of +1 at selected bifurcation points for motions emerging from *Symmetrical Double Stance*.

States	S	H				I		J		K		M		O	
$\dot{x}_o$	0	0.00				0.00		0.00		0.00		6.31		0.00	
$\dot{y}_o$	0	-0.58				-0.70		-1.11		-0.59		-0.70		-0.05	
$\alpha_{l,o}$	0	0.00				0.00		0.00		-0.44		1.45		0.00	
$\alpha_{r,o}$	0	0.00				0.00		0.00		0.44		1.45		0.00	
eVec	$\boldsymbol{v}_S$	$\boldsymbol{v}_{H1}$	$\boldsymbol{v}_{H2}$	$\boldsymbol{v}_{I1}$	$\boldsymbol{v}_{I2}$	$\boldsymbol{v}_{I3}$	$\boldsymbol{v}_{I4}$	$\boldsymbol{v}_{J1}$	$\boldsymbol{v}_{J2}$	$\boldsymbol{v}_{K1}$	$\boldsymbol{v}_{K2}$	$\boldsymbol{v}_{M1}$	$\boldsymbol{v}_{M2}$	$\boldsymbol{v}_{O1}$	$\boldsymbol{v}_{O2}$
$\Delta\dot{x}$	0	0	0.00	0	0.56	0.00	0.61	0	0.95	0.00	0.83	0.99	0.18	0	0.50
$\Delta\dot{y}$	1	1	0.00	1	0.00	0.00	0.00	1	0.00	-0.01	-0.29	-0.13	0.61	1	0.09
$\Delta\alpha_l$	0	0	-0.71	0	0.59	-0.71	-0.38	0	0.23	-0.71	0.26	-0.00	-0.39	0	-0.36
$\Delta\alpha_r$	0	0	0.71	0	0.59	0.71	0.70	0	0.23	0.71	0.40	-0.00	0.67	0	0.78
Branch	***HP***	***HP***	***SP1***	***HP***	***H1***	***SP2***	***S1***	***HP***	***H2***	***SP1***	***S2***	***H1***	***S1***	***4H***	***4W***

4.3.3.2 Skipping-in-place (Branches SP1 and SP2):

At points H and I periodic solutions ***SP1*** and ***SP2*** bifurcate from the hopping-in-place branch ***HP***. Their corresponding eigenvectors $\boldsymbol{v}_{H2}$ and $\boldsymbol{v}_{I3}$ (see Table 4.3) indicate that these two branches extend in the same direction: both leg angles increase equally in magnitude but in opposite directions, while the vertical speed $\dot{y}$ and the horizontal speed $\dot{x}$ remain the same. Solutions on these branches are bouncing-in-place motions in which the two legs move symmetrically with opposite angles and velocities. During swing, the front leg moves backward and hits the ground in the back, and vice versa. If the roles of the left and right leg are switched (right leg is initially behind and left leg in front), the branches extend in the negative $\boldsymbol{v}_{H2}$ and $\boldsymbol{v}_{I3}$ directions (not fully shown in the figure). Several frames of a typical motion on ***SP1*** are illustrated in Fig. 4.10. As the leg angle α_i at touch-down increases, the duration of the flight phase also increases. Both ***SP1*** and ***SP2*** terminate when they reach the unstable equilibrium point in the middle of the double-support phase, when the sum of the leg forces is equal to the weight of the main body, $Mg = 2k_{\text{leg}}\cos(\alpha_i)(l_o - l_i)$.

Similar to the running gaits ***R1*** and ***R2***, the branches ***SP1*** and ***SP2*** differ in how the swing leg hits the ground: in ***SP1*** the leg moves forward just before touch-

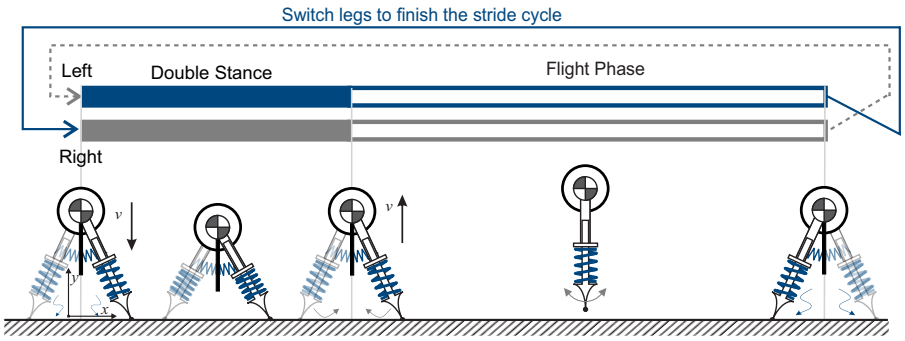

Figure 4.10: Key frames from the first half of a typical solution (at bifurcation point K in Fig. 4.9) on the skipping-in-place ***SP1*** branch. In this gait, the two legs always have the same angles and angular velocities but move in opposite directions. Both legs touch down and leave the ground at the same time. During the flight phase, the roles of trailing leg and leading leg are switched. This is a symmetrical gait and it thus takes another hop to finish a full stride cycle.

down and in ***SP2*** backward. Also, just like for the running gaits, additional skipping branches with multiple periods of swing leg oscillations appear in pairs along ***HP*** which are neither shown nor discussed here.

Along the two branches, solutions have roughly the same vertical speeds and the COM only moves in the vertical direction with $\dot{x} = 0$ during the whole stride cycle. I find 5 bifurcation points that emerge along the ***SP1*** and ***SP2*** branches. Most of them lead to skipping gaits with unequal vGRFs and these branches eventually become single-leg hopping gaits. They are neither shown nor discussed here. Only one of them leads to a gait with the same maximal vGRFs in both legs and has a continuation to a walking gait. This is shown in Fig. 4.9 at point K (Table 4.3). I describe this gait ***S2*** below.

4.3.3.3 Forward/Backward Skipping (Branch S1):

At point I, there is another eigenvalue of $+1$, associated with the eigenvector $\boldsymbol{v}_{I4}$. Hence, another set of solutions ***S1*** emerges from the hopping-in-place branch ***HP***. Along $\boldsymbol{v}_{I4}$ the leg angles change in opposite directions but, in contrast to $\boldsymbol{v}_{I3}$,

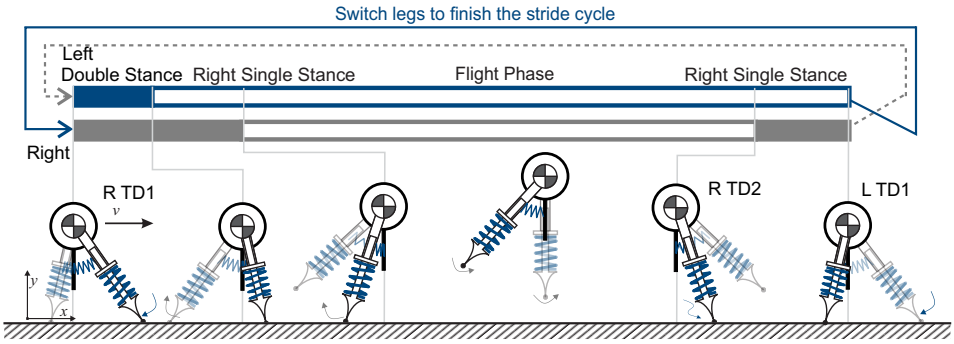

Figure 4.11: Key frames from the first half of a typical skipping gait on the ***S1*** branch (solution (h) in Fig. 4.9). This gait starts in the double stance phase, with the right leg acting as the leading leg. During the aerial phase, the right leg moves back and becomes the trailing leg. It takes another step for the right leg to move forward and finish the whole stride cycle. In order to find this gait, the two legs need to have different angles at their respective touch-down.

by different amounts. This difference in the initial angle magnitudes results in the COM moving forward/backward. The footfall pattern of this gait is demonstrated in Fig. 4.11 and it includes all possible combinations of leg phases (double stance, right leg single stance, left leg single stance, and flight). This gait is known as *skipping* (*Minetti*, 1998). In contrast to the hopping gaits where the legs move simultaneously, in skipping one leg moves faster than the other, causing the legs to hit the ground with different angles of attack. The two legs alternately act as the leading and trailing leg. As a result, skipping gaits are represented by two lines in Fig. 4.9, the solid ***S1*** line (right leg in front) and the dashed ***S1*** line (left leg in front), and each particular motion 'jumps' between them. At low speeds, skipping gaits from ***S1*** are similar to the skipping-in-place gait ***SP2***. As the speed increases, however, touch-down angles of both legs increase to positive values, but the trailing leg angle is always smaller than that of the leading leg (see Fig. 4.9, solution labeled (h)). When the forward speed reaches $3.74\sqrt{gl_o}$, the double stance phase is replaced by a short flight phase as shown in Fig. 4.9, solution (i). As I further increase the forward speed, this brief flight phase disappears and phases of the legs tend to synchronize again. Eventually,

S1 connects back to the hopping branch ***H1*** at point M, as shown in Fig. 4.9. It should be noted that as the forward speed becomes negative, this branch extends symmetrically to the opposite side on the Poincaré section. In these solutions, the roles of left and right leg are simply switched and the model skips backwards.

4.3.3.4 Transition to Walking (Branch S2):

A similar skipping gait ***S2*** bifurcates from the branch ***SP1*** at point K, as shown in Fig. 4.9. For solutions along ***S2***, both leg angles increase, but at different rates, and both the horizontal and vertical speed magnitudes increase (see eigenvector $\boldsymbol{v}_{K2}$ in Table 4.3). In ***S2*** gaits, the footfall sequence is exactly the same as in ***S1***. Swing legs rotate away from the COM and retract back to the center before hitting the ground. At low speeds, the legs are fully synchronized. As the forward speed grows, the duration of the flight phase decreases and the phase delay between the legs gets bigger. Shortly after reaching the fastest speed $0.462\sqrt{\mathrm{gl_o}}$ along ***S2***, the flight phase disappears. The branch thus vanishes at the solution labeled (o) (see Fig. 4.13) when the two adjacent single stance phases of the same leg merge together. A single stance phase with two maxima in the leg forces appears as a natural smooth continuation of ***S2*** skipping. The resulting double-humped vGRF motion is the most common walking gait, which I discuss below along with other types of walking that I found.

4.3.4 Symmetrical Single/Double Stance

4.3.4.1 4-Beat Hopping (Branch 4H):

Following the footfall pattern shown in Fig. 4.2d at point S and varying the vertical speed $\dot{y}$, a hopping-in-place gait including both a single stance phase and a double stance phase is found. Fig. 4.13 shows that at point O, the same footfall pattern can be used to locomote the COM forward/backward at low speeds (branch ***4H***). An exemplary motion of the ***4H*** gait (solution (j) in Fig. 4.13) is shown in

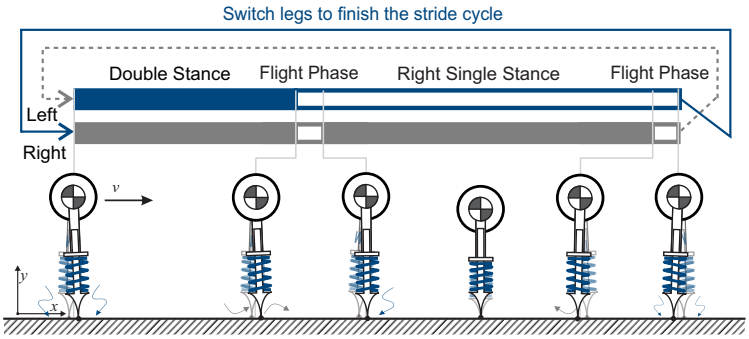

Figure 4.12: Key frames from the first half of solution labeled (j) in Fig. 4.13. This is a symmetrical gait that includes single stance phase, double stance phase, and short flight phases. At higher energies, this gait ***4H*** transitions into the typical bipedal walking gait ***W***.

Fig. 4.12. As the horizontal speed increases, the durations of the flight phases in this gait get shorter. Eventually, the three adjacent stance phases of the same leg are joined together as a prolonged stance phase, leading to the same footfall sequence as in walking. This happens when the horizontal velocity reaches $0.04\sqrt{gl_o}$ (see solution (k) in Fig. 4.13).

4.3.4.2 Triple-humped Walking:

This prolonged-stance walking gait is called *triple-humped walking*. As shown in an exemplary solution (l) in Fig. 4.13, each leg undergoes three compressions in the entire stance phase: one compression in each of the two double stance phases and a third compression during the single stance in between. At higher speeds, as the stance phase gets shorter, these oscillations become less pronounced and the peak forces approach the body weight Mg. Eventually all oscillations along the stance leg settle down to just one compression.

4.3.4.3 Level Walking:

The single compression during stance of such walking gait results in a prolonged, single humped shape of the vGRFs (see solution (m) in Fig. 4.13). This gait is

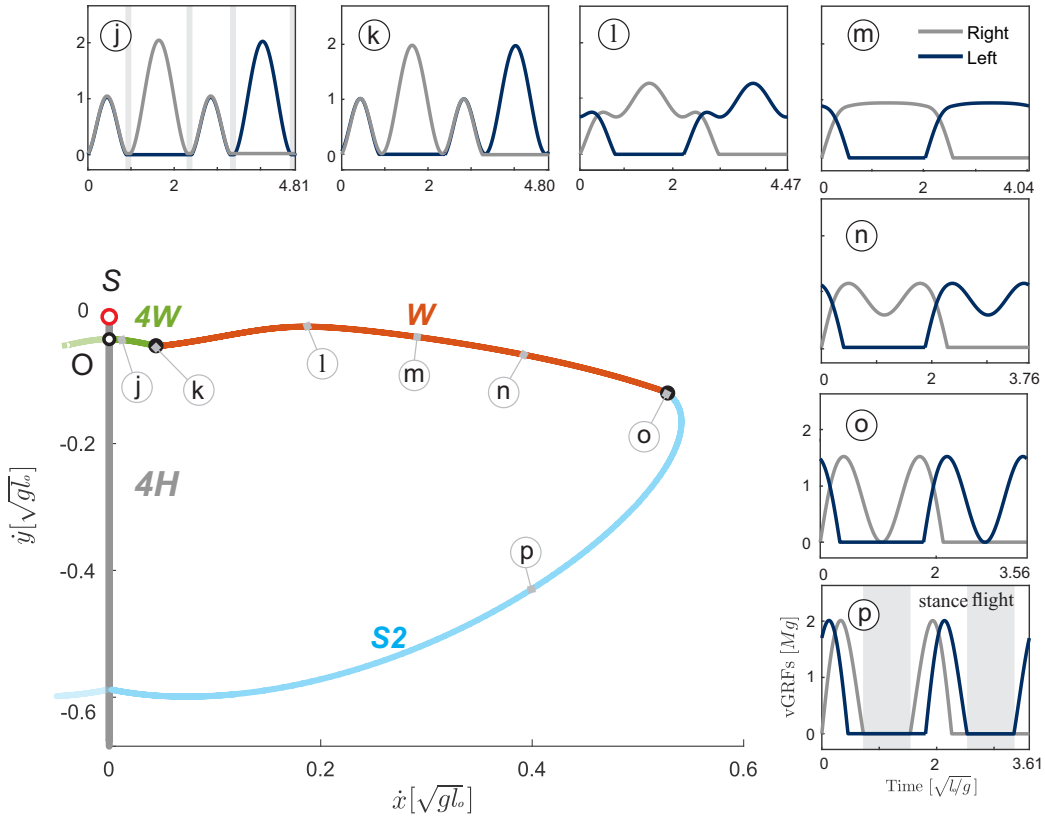

Figure 4.13: Visualization of periodic motions that emerge from bouncing-in-place (red circle, S) with a *symmetrical single/double stance* (as shown in Fig. 4.2d). A forward/backward speed is introduced at bifurcation point O, and at solution (k) all air phases vanish, leading to walking with triple-hump ground reaction forces. This gait undergoes a substantial change in its ground reaction force profile and gradually transitions to level walking, and eventually walking with double-hump ground reaction forces. At solution labeled (o), an additional lift-off arises and the walking gait smoothly changes to the previously identified skipping gait on branch ***S2***. The inserts show how the ground reaction forces profiles evolves along this branch. Several successive motion frames of 4-beat hopping (j) and double-humped walking (n) are shown in Fig. 4.12 and Fig. 4.14.

sometimes referred to as *level walking* (*Rummel et al.*, 2009). It has the smallest vertical excursion of the COM trajectory, $0.93{-}0.95\,l_o$, compared to all other walking gaits.

4.3.4.4 Double-humped Walking:

Starting from the level walking, as the forward speed increases, I found the most human-like walking gait (*Pandy*, 2003). This walking gait has two maxima in the leg forces during stance (Fig. 4.13, solution labeled (n)) and a local minimum in the leg forces appears at exactly the middle of the single stance phase. In contrast to all other gaits in which the COM moves to the lowest position (maximum leg compression) at mid-stance, in the double-humped walking gait, the COM vaults to the highest point when the leg is vertical (see Fig. 4.14). As I increase the forward speed, the leg force tends to decrease in single stance. When the speed gets to $0.52\sqrt{gl_o}$, the minimal leg compression becomes zero with no forces in the stance leg (see solution (o) in Fig. 4.13). A flight phase appears as a natural continuation after passing this solution, and the gait smoothly transitions to the symmetrical skipping ***S2***. Thus, the double-humped walking spans only a small range of speeds $0.27{-}0.45\sqrt{gl_o}$ in this passive model.

4.4 Discussion & Conclusion

In this chapter, I systematically investigated passive dynamic gaits that emerge from the natural mechanical dynamics of a bipedal legged system. To this end, I developed an energetically conservative, yet complete dynamical model of a biped. I achieved this by extending the established SLIP model to include two legs and by adding a foot mass and a hip spring to enable passive swing leg dynamics. By letting the foot mass and hip stiffness go to zero while keeping their ratio (and thus the leg swing frequency ω_{swing}) constant, I prevented energy losses at touchdown.

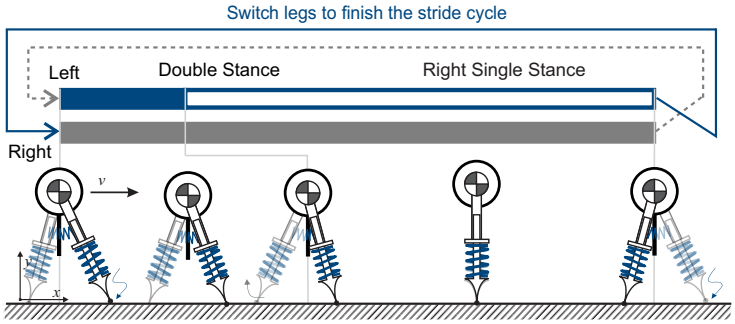

Figure 4.14: Key frames from the first half of a typical double-humped walking gait $\boldsymbol{W}$ (solution (n) in Fig. 4.13). This is a symmetrical gait and it thus takes another hop to finish a full stride cycle. All walking solutions along this branch have the same footfall pattern, but differ in the number of COM oscillations during the stance phase.

Through a targeted continuation of periodic motions, I showed that a range of different bipedal gaits emerged in this model from a simple bouncing-in-place motion with different discrete footfall patterns. Among others, these passive dynamic gaits included walking, running, hopping, skipping, and galloping. The different gaits arose along one-dimensional manifolds of solutions. These manifolds bifurcated into different branches with distinctly different types of motions (as shown in Figs. 4.3, 4.6, 4.9, and 4.13). That is, the gaits were obtained as different oscillatory motions (or nonlinear modes) of a single mechanical system with a single set of parameters.

As this biped model has neither actuation nor control, it supports the hypothesis that different gaits are primarily a manifestation of the underlying natural mechanical dynamics of a legged system. The occurrence and prevalence of certain gaits in nature are thus possibly the consequence of animals exploiting passivity based gaits in order to move in an energetically economical fashion. The same argument should hold for legged robots: the passive motions derived in this chapter establish a blueprint of how to move economically. In the absence of losses, the passive dynamic gaits constitute the only feasible way of locomoting without performing any actuator work. As losses are introduced, such as losses due to friction and collision impacts, the motions will

have to change and will, of course, require some actuation. However, staying close to the original passive motions might reduce the need for motor torques and for negative actuator work, and might hence reduce the energetic cost of locomotion.

On some level, I can consider all gaits found in this chapter to originate from a bipedal model that is completely at rest, standing either on one or both legs with the main body supported by a lightly compressed leg spring that balances gravity. One can think of this equilibrium as a state of maximal symmetry. It is invariant with regards to any time shift (temporal symmetry), to switching the forward and backward directions (symmetrical to the frontal plane), and (for the case of double support) to switching of the left and right legs (symmetrical to the sagittal plane). Different gaits arise from this equilibrium through a sequence of breaks in symmetry that occur at bifurcations (*Stewart and Golubitsky*, 1992). The first is the introduction of a vertical oscillation that breaks the temporal symmetry and introduces a periodic motion. This oscillation is linear for small amplitudes. However, beyond a certain point, the legs will fully extend, and the model will enter a flight phase which renders the dynamics nonlinear. This is the point where this study begins to track the motion as either running (***RP***) or hopping (***HP***, ***H4***) in place. The gaits that branch out from these motions further reduce the symmetry. For example, hopping gaits (***H1***, ***H2***) break the frontal plane symmetry, while the left and right legs still can be switched without changing the motion. This sagittal plane symmetry is then broken in another bifurcation as the galloping gaits (***G1***, ***G2***) emerge. A similar process leads to all the other gaits. Skipping-in-place (***SP1***, ***SP2***), for example, has a mixed symmetry: solutions remain invariant to switching both forward/backward and left/right at the same time. Again, this symmetry is broken as soon as forward motion is introduced. This is shown, for example, in the ***S2*** branch. A similar consideration holds for the running gaits (***R1***-***R6***) which introduce a forward/backward motion into an already left/right asymmetric running-in-place ***RP***. The breaks in symmetry

happen whenever the vertical motion of the model is matched to the leg swing. Since the swing legs are undergoing quasi-sinusoidal motions dictated by the torsional spring at the hip, the same leg angles can be reached with a different number of oscillation periods. This creates several branches of the same gait, such as the running branches ***R2***, ***R4***, and ***R6*** as illustrated in Fig. 4.5. Furthermore, contact can happen either in a forward or backward motion of the swing leg. All gaits, including all of the running gaits ***R1-R6***, hopping forward/backward ***H1-H2***, and skipping in place ***SP1-SP2***, thus appear in pairs.

I have shown that this unified model can reproduce most of the common bipedal gaits that are observed in nature. The motions obtained from the model seem qualitatively similar to gaits of animals. This similarity includes the footfall sequences that are characteristic of each gait, the shape of the vertical ground contact forces, as well as details such as swing leg retraction. For example, the proposed model can produce a double-humped ground reaction force profile along the ***W*** branch of solutions that is characteristic of walking in nature (*Pandy*, 2003). Yet, while this approach provides a reason why many bipeds in nature use similar gaits (and do not locomote in arbitrarily different ways), it cannot explain why a certain biped walks at slow speeds, runs at high speeds, and reverts to hopping, skipping, and galloping only in very special situations. In order to explain these choices among the passivity-based gaits, I might need to be able to explain which of the provided motions are more efficient at a given speed in systems that have losses. This is obviously not possible in a passive model, and would require further considerations about the energetic impact of each motion.

As a further limitation, the gaits found in this study do not necessarily constitute the complete set of all possible periodic motions of this model. While the continuation/bifurcation approach finds all period-one gaits that originate from bouncing in place with the given footfall patterns, there might be other gaits that do not connect

to these starting motions, or that connect to them under conditions that are not considered valid in this study. It is possible that other branches exist, but remain undetected. Other examples that are omitted from this study include motions with different footfall sequences, such as single leg hopping. Furthermore, in this study, I limited myself to trace only simple bifurcation points. Other types of bifurcation exist, and could lead to other types of gaits. For example, I found that asymmetrical running gaits with different angles of attack at each step emerge as period-doubling (PD) bifurcations from the period-one running gaits ***R1-R6***. On these branches of period-two solutions, further running gaits with periods of four steps are found. As the PD bifurcations keep emerging, they eventually lead to chaotic effects that are similar to those found in passive dynamic walkers (*Garcia*, 1998). Including all these solutions was simply out the scope of this work, yet could provide an interesting avenue for further explorations, For all results presented here, I used a fixed parameter set for the model. In particular, I had to make a somewhat arbitrary choice about how to select the leg stiffness and swing leg frequency. It remains an open question how these results may or may not change for different parameter values. Hence, another natural continuation of this work is a parameter study that systematically tracks how locations of the bifurcation points and branches on the Poincaré section change. This information would be particularly valuable from a design point of view. In a preliminary parameter study, I have already found that changes in parameter values can induce structural changes in the solution landscape. For example, when increasing ω_{swing}, the grounded running ***GR*** and walking ***W*** branches merge together at about $\omega_{\text{swing}} = \sqrt{35}\,\sqrt{\text{g}/\text{l}_\text{o}}$. For higher swing frequencies, grounded running and level walking become the same gait and a smooth transition from walking to running can be observed. This is similar to the result by (*Rummel et al.*, 2009), who reported that there was no speed gap between running and walking.

CHAPTER V

On the Dynamic Similarity between Bipeds and Quadrupeds

5.1 Introduction

[1] Broadly speaking, animals gaits can be categorized into two classes: symmetrical and asymmetrical gaits (*Hildebrand*, 1977; *Alexander*, 1984). In symmetrical gaits, the left and right half of the animal performs the exact same motion, half a stride out of phase. This includes, for example, walking and running for bipeds and trotting for quadrupeds. In contrast, in asymmetrical gaits, the motions of the left and right legs show a different phase shift. For bipeds, these asymmetrical gaits include *hopping* and *bipedal galloping* or *leaping* (*Franz et al.*, 2005). In hopping, both legs strike and leave the ground simultaneously. When the synchronization is lost, one leg will hit the ground earlier than the other which becomes leaping. In contrast to bipeds, quadrupeds can utilize a much larger variety of asymmetrical gaits. Among other gaits, quadrupeds can *pronk*, *bound*, and *gallop*. Within these broad definitions, subclasses of gait exist. *Hildebrand* (1977), for example, further classified the bound into four categories according to the durations of the flight phases (suspensions) between the front and back contact: 1) gaits with *no suspension*, 2) gaits with *gathered*

[1] This chapter has been previously published in 2018 IEEE Robotics and Automation Letters (RA-L 2018) and presented at IROS (*Gan et al.*, 2018a).

suspension, 3) gaits with *extended suspension*, and 4) gaits with *two suspensions*. Animals with varying body weights and agility use different categories of bounding: heavier animals such as the bison and giraffe tend to locomote in gaits with gathered suspension or no suspension. While some fast moving animals like the cheetah and greyhound prefer to use the gait with two suspensions at their highest speeds (*Hudson et al.*, 2012).

It is notable, that despite the vast differences in morphology, the gaits of bipedal and quadrupedal animals share some important similarities. *Heglund et al.* (1982) investigated the *dynamic similarity* between *walking* in bipeds and quadrupeds and hypothesized that they utilize the same mechanism similar to an inverted pendulum in which kinetic energy is exchanged for potential (gravitational) energy and vice versa. This implies that fluctuations in kinetic and potential energy happen out of phase. These energy-based observations can be extended to other gaits: in bipedal *running* or *hopping* and in quadrupedal *trotting*, fluctuations of potential and kinetic energy happen in phase and both are exchanged for elastic energy (*Farley et al.*, 1993). However, this analysis breaks down for asymmetrical gaits of quadrupeds. Due to the lack of the additional pair of legs, a biped cannot move in a fashion that is dynamically similar to a galloping quadruped (*Alexander and Jayes*, 1983).

In this chapter, I explore the dynamic similarity between bipedal gaits and asymmetrical quadrupedal gaits by using *simplistic passive models* as illustrated in Fig. 5.1. These models are built on an extensive body of previous work that investigates the passive dynamics of legged locomotion (*Mochon and McMahon*, 1980a; *Blickhan*, 1989). In the present work, I employ our two models to reveal potential dynamic relationships between bipedal gaits on the one side and quadrupedal asymmetrical gaits on the other. For our quadrupedal model, I only focus on *bounding* gaits and neglect the phase difference within the fore/hind leg pairs which is characteristic of different forms of quadrupedal *galloping*. By letting the inertia of the torso in the

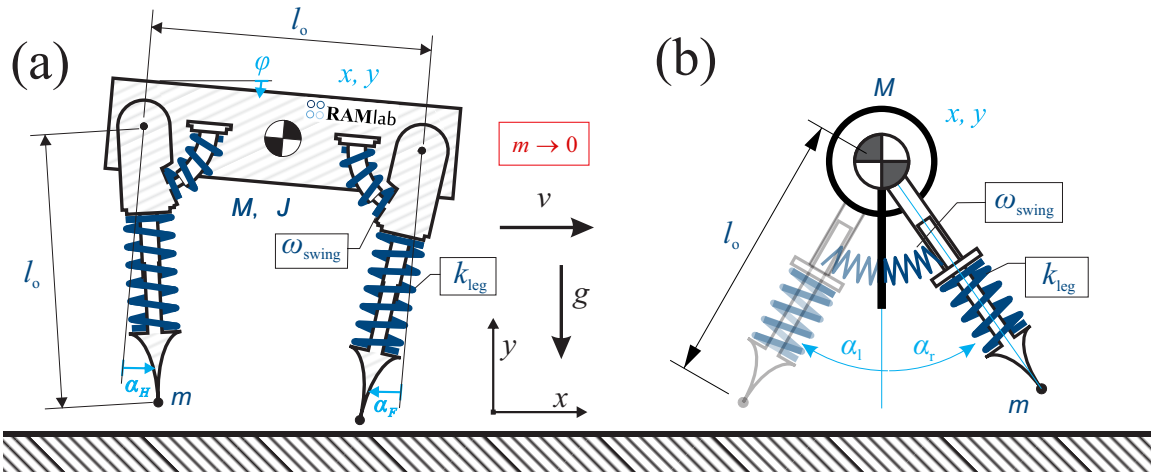

Figure 5.1: The well-known SLIP model is extended to include passive swing leg dynamics with constant swing leg frequency ω_{swing} and similar mechanism is applied to a quadrupedal bounding model with main body mass M and inertia J (a). Our results are contrasted against a similar bipedal model with a point mass as the main body (b).

quadrupedal model vary from zero to infinitely large, I explicitly connect the two models and link all bounding gaits of the quadrupedal model to the two-legged gaits of the bipedal model.

I believe these results to be of importance to the robotics community, as roboticists have already developed a large number of legged machines that rely on asymmetrical gaits. *Talebi et al.* (2001), for example, designed the quadruped robot Scout II and used a simple open-loop controller to reset contact angles to demonstrate stable bounding at a range of speeds. Wildcat developed by Boston Dynamics can bound and gallop at 28 mph. Similarly, MIT Cheetah 2 (*Park et al.*, 2017) can bound at a large range of speeds using impulse-based controller. *Eckert et al.* (2015) also found that with different spine designs, Lynx-robot demonstrates bounding gaits with different footfall patterns and duty factors. Most closely related to the aims of this chapter, *De* (2017) found different bounding and pronking gaits by tuning the main body inertia of the Minitaur robot.

5.2 Methods

5.2.1 Model Description

The quadrupedal model used in this study consists of an extended main body with mass M and inertia J (Fig. 5.1a). The vertical and horizontal positions of the COM of the main body, and the main body's pitch angle were given by the variables x, y, and ϕ, respectively. Each pair of legs (with index $i \in [H, F]$) was modeled as a massless linear spring with length l_i, rest leg length l_o, total spring stiffness k_{leg}, no damping, and a point mass m at the foot. The leg pairs were connected to the main body through frictionless rotational joints with joint angle α_i. The hip joint (back leg pair) was located at a distance of $l_{b,H}$ behind the Center of Mass (COM) of the main body and the shoulder joint at a distance of $l_{b,F}$ in front of the COM. I defined the value of $l_{b,H}$ to have a negative sign. Torsional springs with stiffness k_{swing} and no damping were added to these joints. The springs are uncompressed at zero leg angles when the main body and the respective leg are perpendicular to each other. Similar to the bipedal model defined in Chapter IV, rather than defining a value for k_{swing} directly, I prescribed a leg swing frequency $\omega_{\text{swing}} = \sqrt{\frac{k_{\text{swing}}}{ml_o^2}}$. While this model is energetically conservative during flight, it would lose energy when a foot's velocity is brought to zero in a touch-down collision. With such losses, it would be impossible to identify passive periodic gaits. To resolve this issue, I took the limit of m going towards zero ($m \to 0$), similar to the method used in (*Garcia*, 1998; *O'Connor*, 2009). This implies that $k_{\text{swing}} \to 0$ as the swing frequency ω_{swing} remains unchanged. During swing, dynamics along the legs are ignored and the leg length remains as a constant value of their uncompressed length l_o. To focus on the dynamics of the proposed model, I assume the ground to be flat and rigid, and that there is no foot slipping during the stance phase.

When the main body inertia of this quadrupedal model approaches infinity ($J \to$

∞), the torso would stop to perform any pitching motion. At this point, and when started with a pitch of zero, the model can behave exactly as a bipedal model in which the front and back legs of the bounding model move like the left and right legs of the bipedal model. Such a bipedal model was examined in detail in the prior chapter (Fig. 5.1b).

5.2.2 Equations of Motion

The Equations of Motion (EOM) are given for the main body as:

$$\ddot{x} = F_x/M, \quad \ddot{y} = F_y/M - g, \quad \ddot{\phi} = \tau/J, \tag{5.1}$$

where F_x, F_y, and τ are the net forces and torques created by the leg pairs (see Appendix B). Depending on whether the leg pairs are in the air or in contact with the ground, their dynamics differ. During the swing phase, the leg length is set to $l_i = l_o$ and the leg angle accelerations are given by:

$$\begin{aligned} \ddot{\alpha}_i = -\ddot{\phi} - {}^1\!/_{l_o} \Big(& \cos(\alpha_i + \phi)\, \ddot{x} + \sin(\alpha_i + \phi)\, (g + \ddot{y}) \\ & - l_b \sin(\alpha_i)\, \ddot{\phi} + l_b \cos(\alpha_i)\, \dot{\phi}^2 + {}^1\!/_{l_o} k_{swing} \alpha_i \Big). \end{aligned} \tag{5.2}$$

During stance, the leg angle and leg length are computed from kinematic constraints, as I assume no sliding of the foot. The leg length is given by $l_i = \frac{y + l_{b,i} \sin(\phi)}{\cos(\alpha_i + \phi)}$, and the leg angle follows from

$$x + l_b \cos(\phi) + \tan(\alpha_i + \phi)\, (y + l_b \sin(\phi)) = x_{foot,i}, \tag{5.3}$$

where $x_{foot,i}$ is the horizontal position of the foot on the ground. I solved this equation explicitly for leg velocities and accelerations, allowing us to express the leg angle in both stance and swing phase as a second order differential equation (see Appendix B for details).

5.2.3 Footfall Sequence

In order to determine the footfall pattern of a stride, I introduced four timing variables t_j, ($j \in [Htd, Hlo, Ftd, Flo]$) for the touch-down and lift-off events. To enable solutions with different footfall patterns, the order of these events can be arbitrary, but their values are confined within the time interval of one stride $[0, t_{stride})$. These timing variables are used to determine whether a leg pair is in the air or on the ground at a given time t. The timing vector $\boldsymbol{e}^T = [t_{Htd}, t_{Hlo}, t_{Ftd}, t_{Flo}]$ thus breaks the whole stride into 5 distinct intervals, each next interval with a different contact configuration. Using the position and velocity vector $\boldsymbol{q}^T := [x, y, \phi, \alpha_F, \alpha_H]$, $\dot{\boldsymbol{q}}^T := [\dot{x}, \dot{y}, \dot{\phi}, \dot{\alpha}_F, \dot{\alpha}_H]$ to describe the state of the system, I express the dynamics as a time variant differential equation $\ddot{\boldsymbol{q}} = f\left(\boldsymbol{q}, \dot{\boldsymbol{q}}, t, \boldsymbol{e}\right)$ which is parameterized by $\boldsymbol{e}$. In addition, at the moments of touch-down t_k, ($k \in [Htd, Ftd]$), I need to reset the leg velocities according to the derivative of equation (5.3) resulting in the additional discrete dynamics $\dot{\boldsymbol{q}}\left(t_k^+\right) = h\left(\boldsymbol{q}\left(t_k^-\right), \dot{\boldsymbol{q}}\left(t_k^-\right)\right)$.

5.2.4 Gait Creation

Similar to (*Hermann and Saravi*, 2016), I stated the gait creation as a Boundary Value Problem (BVP). I defined a gait as a periodic motion in which all states except for the horizontal position x return to their original values after one full *stride*. Without loss of generality, the apex transition ($\dot{y} = 0$) was selected as the Poincaré section for this limit cycle analysis. Finding a gait in this model was thus equivalent to solving the following problem:

$$\mathrm{T}(\boldsymbol{Z}^*) := \begin{bmatrix} \ddot{\boldsymbol{q}} - \mathrm{f}(\boldsymbol{q}, \dot{\boldsymbol{q}}, t, \boldsymbol{e}) \\ \dot{\boldsymbol{q}}\left(t_k^+\right) - h\left(\boldsymbol{q}\left(t_k^-\right), \dot{\boldsymbol{q}}\left(t_k^-\right)\right) \\ \mathrm{R}_{1\text{-}14}(\boldsymbol{q}, \dot{\boldsymbol{q}}, \boldsymbol{e}, t_{stride}) \end{bmatrix} = \mathbf{0}. \tag{5.4}$$

The solution vector of this equation, $\boldsymbol{Z}^* := (\boldsymbol{q}, \dot{\boldsymbol{q}}, \boldsymbol{e}, t_{stride})$, combines the generalized positions and velocities of the model ($\boldsymbol{q}$ and $\dot{\boldsymbol{q}}$) with the vector of footfall timings $\boldsymbol{e}$ and the overall stride time t_{stride}. The boundary and interior-point conditions in $\mathrm{R}_{1\text{-}14}$ were used to enforce (I) that all positions except x are periodic (R_{1-4}), (II) that all velocities are periodic (R_{5-9}), (III) that the stride ends at the Poincaré section (R_{10}), and (IV) that the legs are fully extended at touchdown and liftoff (R_{11-14}):

$$\begin{aligned} R_{1-4} &= \bar{\boldsymbol{q}}\left(t_{stride}\right) - \bar{\boldsymbol{q}}\left(t=0\right), \\ R_{5-9} &= \dot{\boldsymbol{q}}\left(t_{stride}\right) - \dot{\boldsymbol{q}}\left(t=0\right), \\ R_{10} &= \dot{y}(t_{stride}), \\ R_{11-14} &= y(t_j) + l_{b,i}\sin(\phi(t_j)) \\ &\quad - l_o\cos(\phi(t_j) + \alpha_i(t_j)). \end{aligned} \tag{5.5}$$

5.2.5 Continuation and Bifurcations

I found all solutions of eq. (5.4) through numerical continuation and bifurcation analysis. That is, starting from an initial solution $\boldsymbol{Z}_1$, I computed branches of solutions iteratively. Assuming that $\boldsymbol{Z}_n^*$ is the n^{th} solution that I found, I numerically search for an adjacent solution $\boldsymbol{Z}_{n+1}^*$ in a two-step predictor-corrector process (Fig. 5.2): first I determine an initial guess $\boldsymbol{Z}_{n+1}^o = \boldsymbol{Z}_n^* + d\cdot\left(\boldsymbol{Z}_n^* - \boldsymbol{Z}_{n-1}^*\right)$, by continuing to move with a fixed step length of d tangentially along the existing solution branch. I then identify the exact solution $\boldsymbol{Z}_{n+1}^*$ by numerically solving the following constrained problem:

$$\mathrm{T}\left(\boldsymbol{Z}_{n+1}^*\right) = \boldsymbol{0}, \tag{5.6a}$$

$$\left\|\boldsymbol{Z}_{n+1}^* - \boldsymbol{Z}_n^*\right\| = d, \tag{5.6b}$$

$$\left(\boldsymbol{Z}_{n+1}^* - \boldsymbol{Z}_n^*\right)^T\left(\boldsymbol{Z}_n^* - \boldsymbol{Z}_{n-1}^*\right) > 0. \tag{5.6c}$$

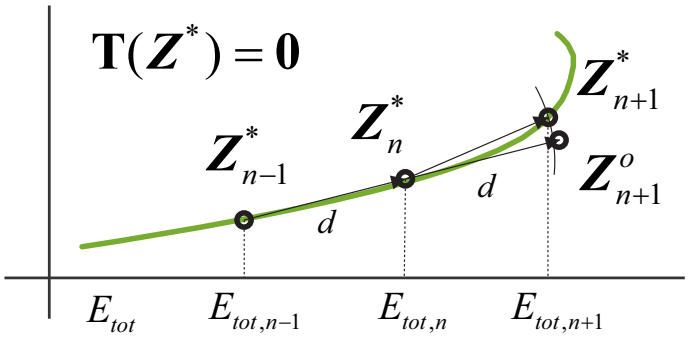

Figure 5.2: The continuation algorithm used in this work employs a prediction-correction process. I first determine an initial guess $\boldsymbol{Z}^o_{n+1}$ of a new solution by moving tangentially along the branch with a step length of d. I then numerically solve eq. (5.6) to find an exact new solution $\boldsymbol{Z}^*_{n+1}$.

Here, eq. (5.6a) ensures that the new solution fulfills (5.4), eq. (5.6b) ensures that I move with a constant step length along the branch, and eq. (5.6c) ensures that I are not stepping backwards. For computational efficiency, I used a backward finite difference method to find the tangent direction $\boldsymbol{v}_n$. By iteratively repeating these two steps, I can identify complete solution branches.

In some cases, eq. (5.6) has more then one solution. At such *bifurcation points*, new solution branches emerge, which I track in a similar fashion. I explicitly detect these instances by tracking a change in the null space dimension of the fréchet derivative of T. I categorized bifurcations by simply considering the changes in stability and the number of solutions in the neighborhood of the bifurcation. Please see (*Merker et al.*, 2015; *Hermann and Saravi*, 2016) for more details of this process.

Solutions obtained through this process can be characterized by the amount of total energy E_{tot} stored in the system. Since the model is energetically conservative, this value is constant throughout a stride and a good metric to distinguish different solutions.

5.2.6 Parameter Study

In order to keep our solutions general, I normalized all state and parameter values with respect to M, g, and l_o (*Hof*, 1996). I set the leg pair stiffness to $k_{\text{leg}} = 20\,{}^{Mg}/_{\text{l}_\text{o}}$ and the swing frequency to $\omega_{\text{swing}} = \sqrt{5}\,\sqrt{{}^{g}/_{\text{l}_\text{o}}}$. The front leg pair and the hind leg pair were attached symmetrically to the center of the body with $l_{b,F} = 0.5\,\text{l}_\text{o}$ and $l_{b,H} = -0.5\,\text{l}_\text{o}$. These dimensionless values are comparable to our existing hardware (*Smit-Anseeuw et al.*, 2017a). The parameter of interest in this paper was the main body inertia J. I started our investigation with the extremal case of an infinite main body inertia $J = \infty$. While this case is highly contrived, it allows us to draw the dynamic connections between the gaits of a biped and the asymmetrical gaits of a quadruped, as the two models are dynamically equal for $J = \infty$. When then gradually reduced the value of J and iteratively re-computed all primary solution branches, ignoring motions with multiple leg-swing oscillations during swing in the process.

5.3 Results

In this section, I visualize different solution branches by showing how selected states $\boldsymbol{Z}^*$ on the Poincaré section evolve as a function of energy E_{tot}. Furthermore, I visualize and numerically report bifurcation points (Table 5.1). I also illustrate typical solutions along branches by showing a series of key-frames of an animation of the motion .

In order to highlight the dynamic similarities between the bipedal model and quadrupedal model and show how do they diverge from each other, I also conducted an detailed parameter study on the body inertia. In the bipedal model (Fig. 5.1b) the legs are massless and the COM motion and the swing leg rotations are fully decoupled. That is, for any finite value of the body inertia J, the main body orientation will

remain the same during the whole stride. In other words, the solution branches of the bipedal gaits are invariant under different values of J. As shown in the following sections, this will not hold for the quadrupedal model. I first report on the extremal case of $J = \infty$, then establish the correspondence between asymmetrical quadrupedal gaits and the gaits of a biped, and finally report how these solutions change as a function of J. For some selected periodic motions, I also present a visualization of the motion[2].

5.3.1 Infinite Main Body Inertia, $J = \infty$

5.3.1.1 Pronking and Bounding in Place

The most basic periodic motions of this model and the starting point for our exploration are simple *pronking in place* (***PP***) and *bounding in place* (***BP***) gaits. In both gaits, the model moves purely vertically and the legs are pointing straight down during the entire gait cycle. The primary difference between pronking and bounding is the contact sequence. In pronking (Fig. 5.3a), the front and hind leg pairs strike and leave the ground simultaneously with a single flight phase in between, whereas in bounding (Fig. 5.3b), there exist two flight phases and the front and hind leg pairs are in contact at separate times. Strictly speaking, there are two versions of this bounding gait, one in which the front contact happens first and one in which it happens second in the stride that I consider. Since I assume an infinite main body inertia, the off-center loading during bounding does not induce any pitching motion and the main body remains horizontal. Increasing E_{tot} increases the apex height y_o during flight and leads to more compression of the legs during stance. The theoretical limit for the maximal pronking height is $20\,\mathrm{l_o}$ and for the maximal bounding height it is $10\,\mathrm{l_o}$. For higher apex heights, the legs would become fully compressed during

[2]Please see the multimedia file at https://youtu.be/bKDJXu5RqNA for a video showing these motions.

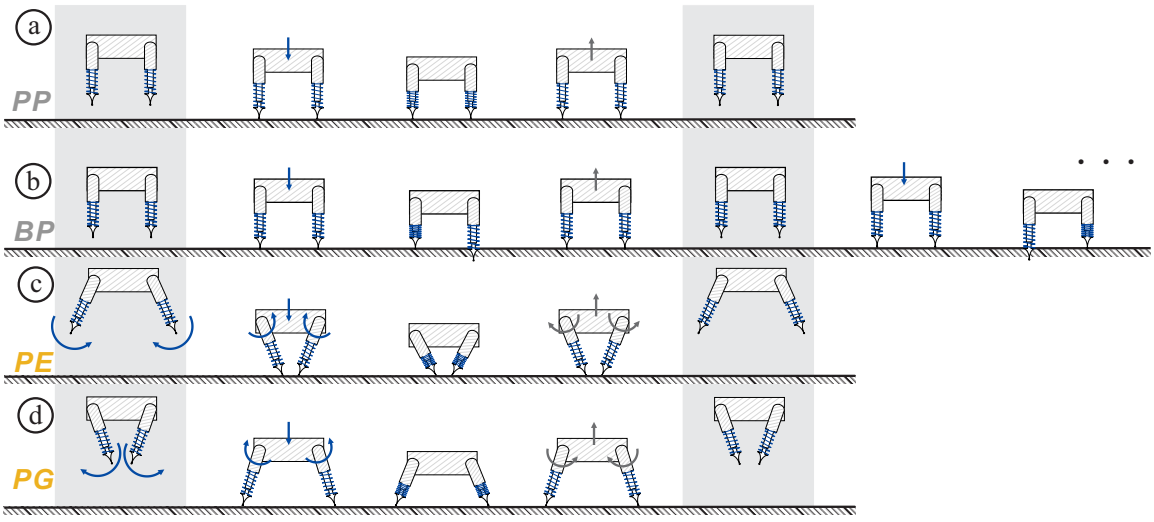

Figure 5.3: Shown are the motions of pronking in place (***PP***, a), bounding in place (***BP***, b), pronking with extended suspension (***PE***, c), and pronking with gathered suspension (***PG***, d) of the quadrupedal model. The motions are independent of the main body inertia J. Note that for ***BP***, only the first half of a full stride is shown.

stance. Apart from the contact sequence, the solution branches overlap. They are illustrated for $y_o < 2\,\mathrm{l_o}$ in Fig. 5.4.

5.3.1.2 Pronking in Place with Leg Swing (PE and PG)

Along the ***PP*** branch, a pitchfork (PF) bifurcation occurs at point A at an apex height of $y_o = 1.71\,\mathrm{l_o}$. The two new branches break the front/hind symmetry of the ***PP*** motions and correspond to two in-place gaits in which the leg pairs swing against each other: *in-place pronking with extended suspension* (***PE***, Fig. 5.3c) and *in-place pronking with gathered suspension* (***PG***, Fig. 5.3d). As the ***PE*** branch moves away from the bifurcation point with increasing E_{tot}, the leg pairs in the corresponding solutions rotate outward, reach their maximal excursion at apex, and then move back inward again before hitting the ground pointing towards each other. The opposite happens on the ***PG*** branch, as the leg pairs gather towards the center during the flight phase and are extended during stance. At the same apex height, the main

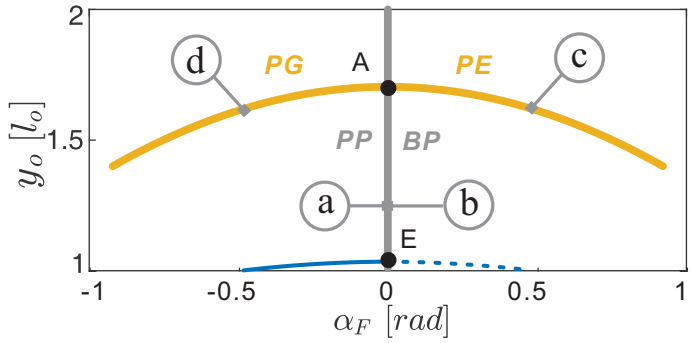

Figure 5.4: This visualization of the solution branches shows the initial main body height y_o and front leg angle $\alpha_{F,o}$ at the Poincaré section for the ***PP***, ***BP***, ***PE***, and ***PG*** gaits. The ***PE*** and ***PG*** branches bifurcate from the ***PP*** branch at point A. The solutions are independent of the main body inertia J. The labels (a)-(d) refer to specific solutions that are shown in Fig. 5.3.

body motions of these two branches are exactly the same. Yet, their leg motions are inverted. That is, at any instant of motion, the angles and angle rates of the hind legs on ***PE*** are identical to those of the front legs on ***PG***, and vice versa. The two branches terminate when the main body COM reaches an unstable equilibrium point during stance, where the sum of the leg forces is equal to the weight of the main body, $Mg = 2k_{\text{leg}}\cos(\alpha_i + \phi)(l_o - l_i)$. Increasing the energy even further would result in the COM 'dropping' all the way into the ground.

5.3.1.3 Pronking Forward (PF)

Breaking the frontal symmetry, I found a *pronking forward* (***PF***, Fig. 5.5e) gait that branches off the in-place pronking ***PP*** solutions with a PF bifurcation at point B (Fig. 5.7). This bifurcation happens at an apex height of $y_o = 1.61\,\text{l}_\text{o}$. In this gait, the two leg pairs simultaneously strike and leave the ground and exhibit the same leg angles throughout the motion. Along this branch, an increase in E_{tot} leads to an increased forward speed with larger contact angles, until a turning point with the maximal energy $E_{tot} = 61.43\,\text{Mgl}_\text{o}$ ($\dot{x}_o = 11.02\,\sqrt{\text{gl}_\text{o}}$) is reached. Solutions further

Table 5.1: Initial states $\boldsymbol{X}_o$ and event timings at the bifurcation points A - F.

BP	unit	A	B	C	D	E	F
$\dot{x}_o$	$\sqrt{\mathrm{g l_o}}$	0	0	1.41	9.71	0	4.34
y_o	$\mathrm{l_o}$	1.71	1.61	1.58	0.45	1.02	1.09
$\dot{y}$	$\sqrt{\mathrm{g l_o}}$	0	0	0	0	0	0
ϕ_o	$[\cdot]$	0	0	0	0	0	0
$\dot{\phi}_o$	$\sqrt{\mathrm{g/l_o}}$	0	0	0	0	0	0.20
$\alpha_{H,o}$	$[\cdot]$	0	0	0	0	0	1.30
$\dot{\alpha}_{H,o}$	$\sqrt{\mathrm{g/l_o}}$	0	0	1.22	3.25	0	1.38
$\alpha_{F,o}$	$[\cdot]$	0	0	0	0	0	-1.30
$\dot{\alpha}_{F,o}$	$\sqrt{\mathrm{g/l_o}}$	0	0	1.22	3.25	0	1.38
t_{htd}	$\sqrt{\mathrm{l_o/g}}$	1.19	1.11	1.13	0.79	0.21	0.72
t_{hlo}	$\sqrt{\mathrm{l_o/g}}$	1.73	1.65	1.60	1.01	1.28	1.04
t_{ftd}	$\sqrt{\mathrm{l_o/g}}$	1.19	1.11	1.13	0.79	1.69	1.56
t_{flo}	$\sqrt{\mathrm{l_o/g}}$	1.73	1.65	1.60	1.01	2.76	1.88
t_{apx}	$\sqrt{\mathrm{l_o/g}}$	2.91	2.76	2.73	1.80	2.97	2.60

along the branch have lower energy and lower forward speeds. The gait vanishes when the leg springs are fully compressed during stance, which happens at a forward speed of $\dot{x}_o = 6.43\sqrt{\mathrm{g l_o}}$. One should note that there also exists a corresponding pronking backward gait that branches off in the opposite $\dot{x}_o$ direction.

5.3.1.4 Bounding with Gathered/Extended Suspension (BG and BE)

Along the ***PF*** branch, I found a PF bifurcation at point C (Fig. 5.7. On the new branches, the front/hind symmetry of the ***PF*** motions breaks, and the two leg pairs loose their synchronization as they either gather inwards or extend outwards during the flight phase. The corresponding gaits are called *bounding with gathered suspension* (***BG***, Fig. 5.5f) and *bounding with extended suspension* (***BE***, Fig. 5.5g). Moving along these branches, first with increasing energy E_{tot} and after a turning point with decreasing energy, I can observe that they eventually merge back to the ***PF*** branch at another PF bifurcation at point D. These two bounding branches thus form a closed loop, which is symmetrical with regard to the motion of the front and hind leg pairs. That is, the motion of hind legs in ***BG*** resembles the motion of

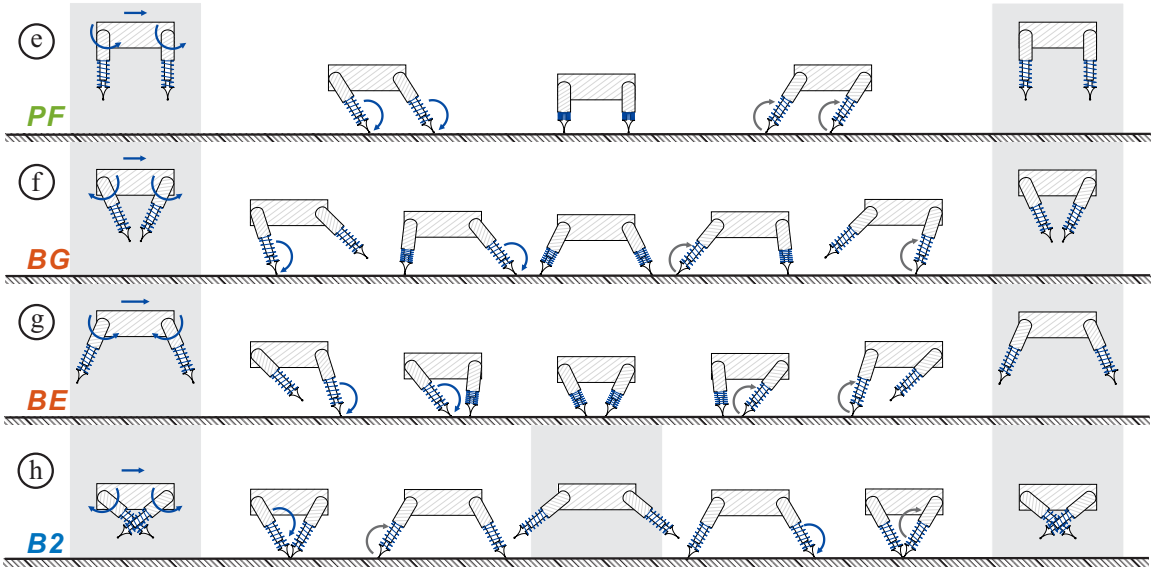

Figure 5.5: Shown are the motions of pronking forward (***PF***, e), bounding with gathered suspension (***BG***, f), bounding with extended suspension (***BE***, g), and bounding with two suspensions (***B2***, h) of the quadrupedal model with infinite inertia ($J = \infty$).

front legs in ***BE*** and vice versa. Despite the differences in leg motions, the COM moves along the same trajectories in both branches. One should note that along these branches, the footfall sequence does change. In the central part of the branches (dashed lines in Fig. 5.7), a second flight phases arises, as the order of touchdown and lift-off of the leg pairs change in the middle of the stride.

5.3.1.5 Bounding with Two Suspensions B2

The ***BP*** branch has no front/hind symmetry due to the staggered contact sequence. It thus bifurcates directly into branches that include forward/backward motion (Fig. 5.7). Such a PF bifurcation was found at point E at an apex height of $y_o = 1.02\,\mathrm{l_o}$. The resulting motion is *bounding with two suspensions* (***B2***, Fig. 5.5h). In this bounding gait, after lift-off, the swing leg pair first continues to extend backward until it reaches zero speed and the hip spring starts pulling it forward.. Then the leg pair swings forward, reaches its maximal forward extension, and strikes the

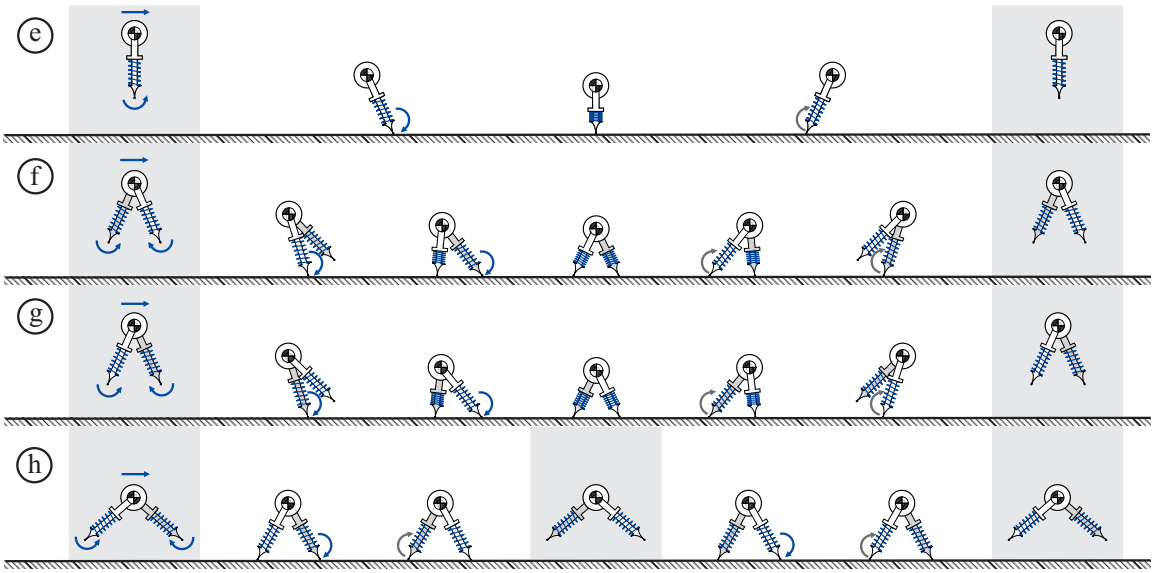

Figure 5.6: This figure highlights the correspondence between bipedal gaits and quadrupedal bounding with infinite inertia (as shown in Fig. 5.5). In particular, bipedal hopping (e) corresponds to quadrupedal pronking (***PF***), bipedal leaping (f, g) to bounding with gathered/extended suspension (***BE***, ***BG***), and bipedal running (h) to bounding with two suspensions (***B2***). These solution branches of the bipedal gaits are invariant under different values of J in the bipedal model.

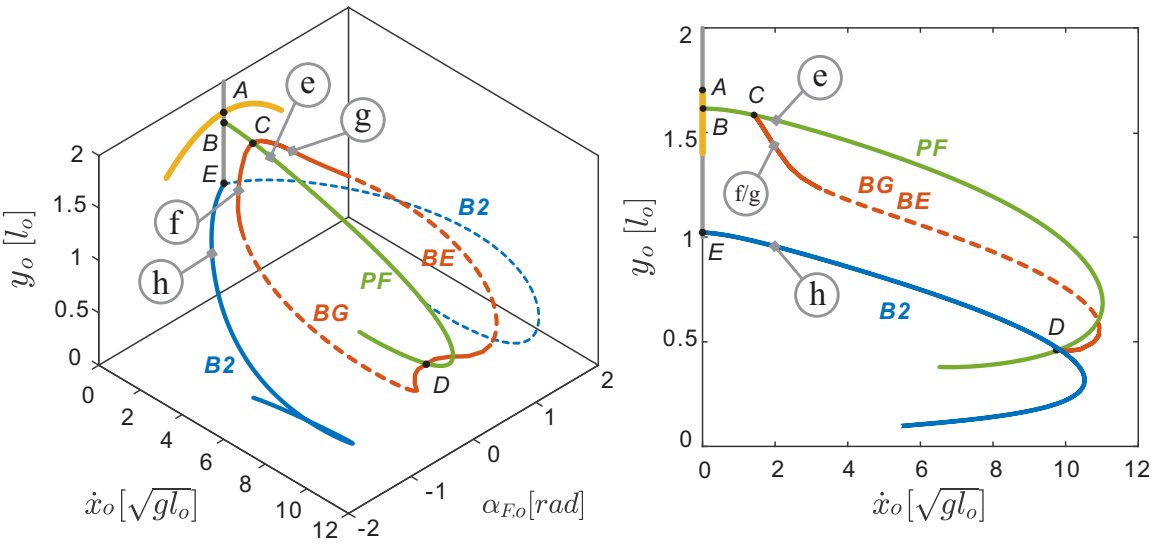

Figure 5.7: This visualization of the solution branches shows the initial main body height y_o, forward speed $\dot{x}_o$, and front leg angle $\alpha_{F,o}$ at the Poincaré section for all gaits of the quadrupedal model with infinite inertia. The bipedal branches are invariant with the main body inertia J and are identical to the quadrupedal branches with infinite inertia. The PF branch (green) bifurcates from the ***PP*** branch (grey) at point B. The ***BG*** and ***BE*** branches (red) form a closed loop that bifurcates from the ***PF*** branch a points C and D. Along the ***BG*** and ***BE*** branches, the contact sequence changes and a second flight phase is introduced (dashed section). Finally, the ***B2*** branch (blue) bifurcates from the ***BP*** branch at point E. A second version of this branch (dotted line) can be obtained by redefining the Poincaré section to the second apex transit. The labels e-h refer to specific solutions that are shown in Fig. 5.5 and Fig. 5.6.

ground during the backward retraction. Because of the infinite body inertia, the main body remains horizontal within the whole stride cycle, the two flight phases have equal durations, and the motion of the front and hind leg pairs is exactly the same, just half a stride apart. Because of the two air-phases, the ***B2*** branch is represented by two curves in Fig. 5.7: the solid line corresponds to the apex transit after the front leg stance (legs pointing inward at apex), and the dotted line to the apex after the back leg stance (legs pointing outward). Similar to the ***PF*** branch, increasing E_{tot} along the ***B2*** branch increases forward speed until a turning point is reached at $E_{tot} = 55.58\,\mathrm{Mgl_o}$ ($\dot{x}_o = 10.52\sqrt{\mathrm{gl_o}}$). The branch terminates when full leg compression is reached at a speed of $\dot{x}_o = 5.35\sqrt{\mathrm{gl_o}}$. Similar to pronking, there exist corresponding backward gaits that branch off in the negative $\dot{x}_o$ direction.

5.3.2 Correspondence to Bipedal Gaits

As the main body does not pitch in the case of the infinite body inertia, I can identify direct correspondences between the asymmetrical bounding gaits of the quadrupedal model and the gaits of the bipedal model (Fig. 5.6). To this end, I let the front leg pair of the quadrupedal model correspond to the left leg of the bipedal model, and the hind leg pair correspond to the right leg. In particular, *pronking* corresponds to *bipedal hopping* (Fig. 5.6e). *Bounding with gathered suspension* corresponds to *bipedal leaping* with the left leg leading (Fig. 5.6f) and *bounding with extended suspension* to *bipedal leaping* with the right leg leading (Fig. 5.6g). Finally, *bounding with two suspensions* corresponds to *bipedal running* (Fig. 5.6h).

5.3.3 Finite Main Body Inertia, $J < \infty$

Since in the pronking gaits (***PG***, ***PE***, and ***PF***), all legs strike and leave the ground simultaneously and the front and hind leg pairs have either the same or opposite angles, the pitch torques on the main body are always balanced. In these

motions, the main body will remain horizontal, independent of the value of J. In the following, I thus focus on the bounding branches (***BG***, ***BE***, and ***B2***) which are indeed influenced by the choice of the main body inertia J.

5.3.3.1 Large Inertia, $J \in [1.047\,\mathrm{Ml}_\mathrm{o}^2, \infty)$

As the value of J gradually decreases from infinity, the structure of the bounding gaits remains roughly the same until $J = 1.047\,\mathrm{Ml}_\mathrm{o}^2$. The net torque on the torso creates an angular acceleration and the main body pitches accordingly. This pitching motion is superimposed with the bounding motion, yet the general motion and footfall sequence remain the same (Fig. 5.8). What is lost, is the symmetry between the ***BG*** and ***BE*** branches. That is, the motion of the hind legs in ***BG*** does not longer resemble the motion of the front legs in ***BE*** and vice versa. This can also be observed in the solution branches (Fig. 5.9), where the ***BG*** and ***BE*** are no longer symmetrical with respect to the ***PF*** branch. Notably, a new turning point arises along the ***BG*** branch near Point C, as the energy level along the branch now initially decreases. Similarly, I can observe an asymmetry in the two different apex transits in *bounding with two suspensions* (***B2***).

In the *bounding with two suspensions* gait, I can also observe that, as the inertia value decreases, the gathered suspension becomes longer than the extended suspension. The main body motions along the ***B2*** branch therefore become similar to the solutions with two flight phases along the ***BG*** branch; in particular with regard to the timing of these flight phases and in the sense that they both have a positive pitching velocity at the start of each stride and a negative rotational velocity in the middle of that stride (Figs. 5.8h & 5.8j). As a result, the ***BG*** and ***B2*** branches approach each other for decreasing values of J and eventually merge at a critical inertia value of $1.047\,\mathrm{Ml}_\mathrm{o}^2$ (Point F).

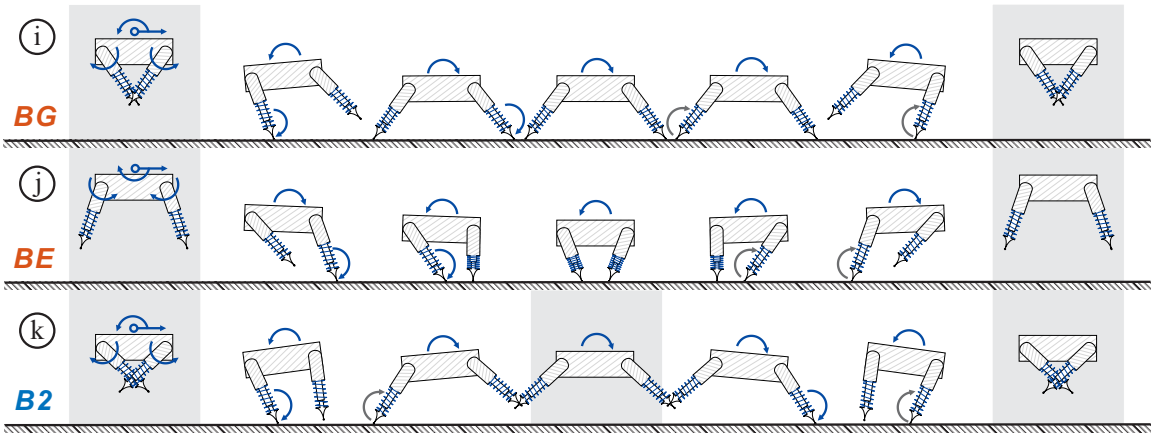

Figure 5.8: Shown are the motions of bounding with gathered suspension (***BG***, i), bounding with extended suspension (***BE***, j), bounding with two suspensions (***B2***, k) of the quadrupedal model with a main body inertia of $J = 1.047\,\mathrm{Ml_o^2}$.

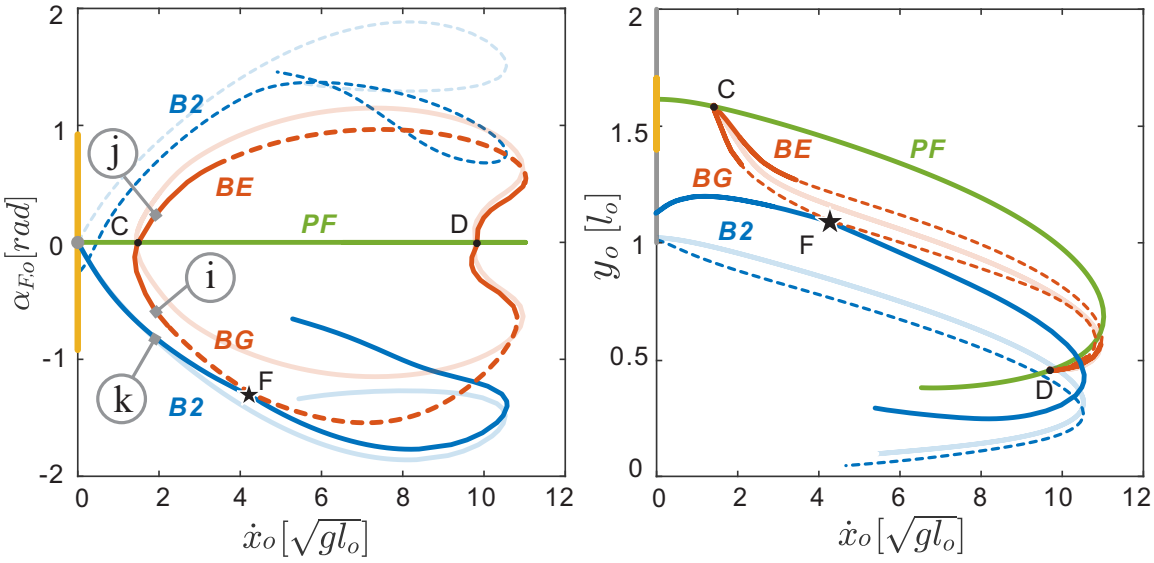

Figure 5.9: This figure shows how the quadrupedal gait branches evolve as the inertia goes from $J = \infty$ (faded lines) to $J = 1.047\,\mathrm{Ml_o^2}$ (solid lines). At this critical inertia value, the ***B2*** and ***BG*** branches merge at bifurcation point F. The labels i-k refer to specific solutions that are shown in Fig. 5.8.

5.3.3.2 Intermediate Inertia, $J \in [0.501\,\mathrm{Ml}_\mathrm{o}^2, 1.047\,\mathrm{Ml}_\mathrm{o}^2)$

As the main body inertia is decreased below $1.047\,\mathrm{Ml}_\mathrm{o}^2$, the ***BG*** and ***B2*** break apart at the bifurcation point F (Fig. 5.10) but stay connected with each other. As a result, I now get a seamless continuation from the ***B2*** branches onto the ***BG*** branches at two new turning points (F_1 and F_2, Fig. 5.10). These two turning points move away from each other as the inertia J keeps decreasing. F_1 moves towards lower forward speeds and F_2 towards higher forward speeds. As a result, bounding with gathered suspension (***BG***) and bounding with two suspensions (***B2***) cease to exist at the intermediate speed range and bounding with an extended suspension (***BE*** branch) becomes the only passive bounding gait for certain speeds. The pronking branch ***PF*** and the bifurcation points (C and D) remain in the same locations on the Poincaré section.

When the inertia value drops below $0.501\,\mathrm{Ml}_\mathrm{o}^2$, the turning points F_1 and F_2 disappear (Fig. 5.11). They merge with the existing turning points on the ***BG*** and ***B2*** branches. Energy now monotonically decreases when moving along ***BG*** starting from point C, and only a single turning point remains on the ***BG*** branch starting from point D. With this, it is not possible anymore to do a formal distinction between the ***BG*** and ***B2*** branches. In a sense, the original bounding gait with double suspension (***B2***) ceases to exist. In contrast, the ***BE*** branch does not undergo any fundamental changes and remains strikingly similar to bipedal leaping. The branch leaves pronking at point C and joins back to the pronking branch at point D after going through a turning point.

5.3.3.3 Small Inertia, $J \in (0, 0.501\,\mathrm{Ml}_\mathrm{o}^2)$

As the inertia value keeps decreasing from $0.501\,\mathrm{Ml}_\mathrm{o}^2$, the rotations of the main body are getting smaller within one stride. In the meantime, the branches ***BG*** and ***BE*** are approaching the pronking branch ***PF***. When the main body in the model

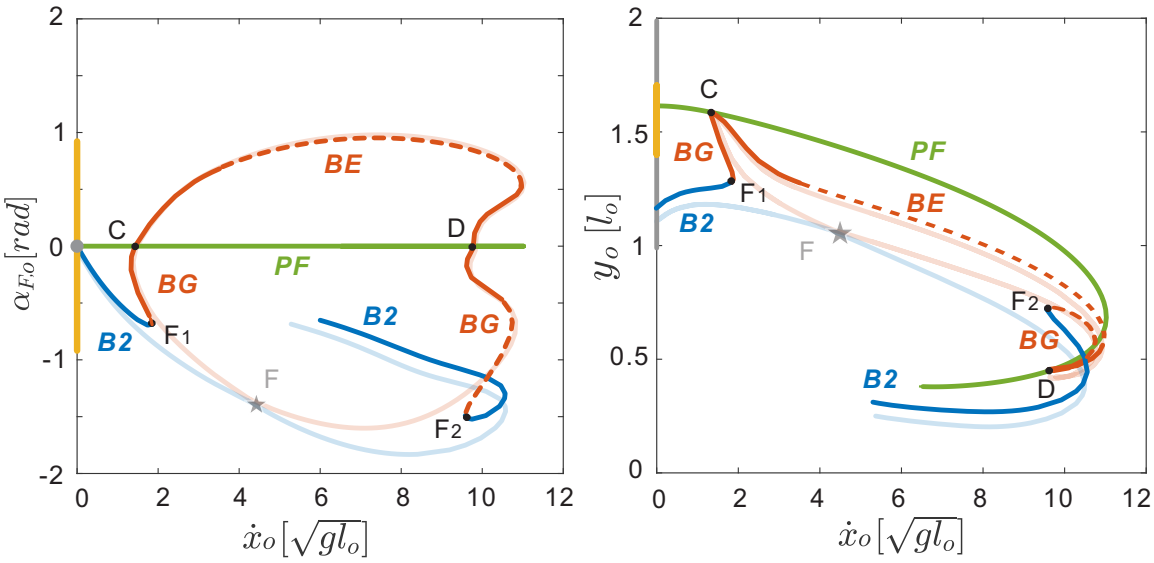

Figure 5.10: This figure shows how the quadrupedal gait branches evolve as the inertia goes from $J = 1.047\,\mathrm{Ml_o^2}$ (faded lines) to $J = 0.9\,\mathrm{Ml_o^2}$ (solid lines). The ***BG*** and ***B2*** branches join and bifurcation point F forms two turning points F_1 and F_2 that move away from each other.

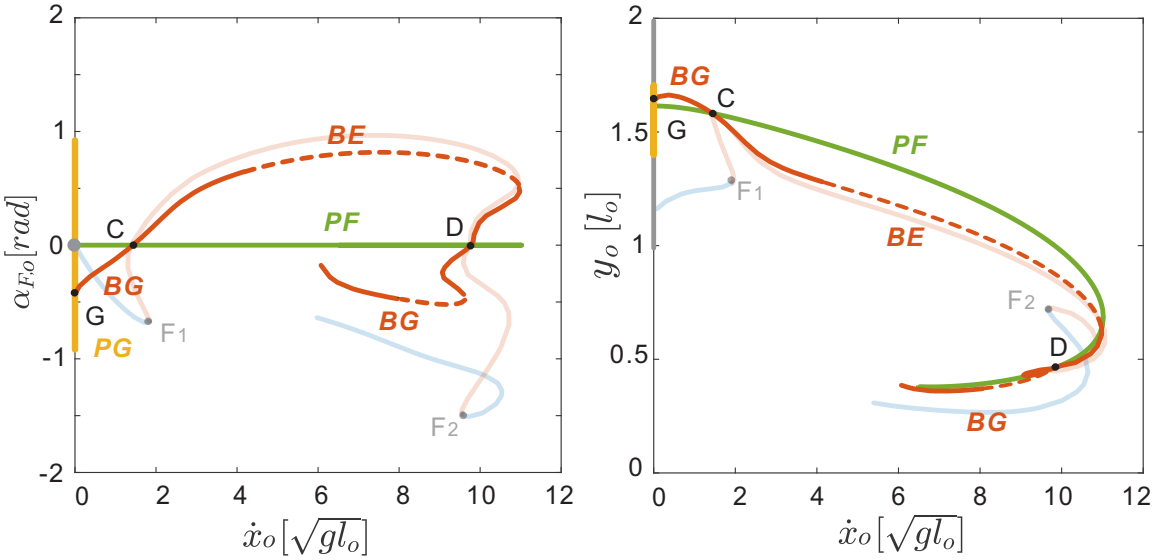

Figure 5.11: This figure shows how the quadrupedal gait branches evolve as the inertia goes from $0.9\,\mathrm{Ml_o^2}$ (faded lines) to $0.501\,\mathrm{Ml_o^2}$ (solid lines). The turning points F_1 and F_2 merge with other turning points and disappear at this point, the ***B2*** branches cease to exist.

has zero inertia, any time lag in the touch-downs will cause infinite acceleration of the main body. Therefore all bounding branches vanish, and the pronking branch ***PF*** becomes the only gait with nonzero speeds.

5.4 Discussion & Conclusion

In this chapter, I have identified passive dynamic bounding gaits, and have investigated the dynamic similarity between bipedal and asymmetrical quadrupedal gaits. I did so by studying the passive motions of a simplistic energetically-conservative quadrupedal model. Since there is no control in this model, its motion is fully determined by its mechanical dynamics. Still, by using numerical continuation techniques, I were able to identify the most prevalent bounding gaits found in nature: pronking, bounding with extended support, bounding with gathered support, and bounding with two flight phases. These motions emerge completely passively, and may serve as a template to develop energetically economical motions for legged robotic systems. While an actual robot would need to compensate for energetic losses due to friction, damping, and contact collisions, staying close to these passive motions would ensure that the robot avoids negative actuator work. This is because the energetic fluctuations that happen during locomotion can be fully realized by the dynamics of the mechanical system.

As a starting point of our analysis, I assumed an infinite inertia of the robot's main body. Since this prevents any main body pitch, I were able to draw direct connections between the gaits of a biped and those of a quadruped. In fact, comparing the results presented in this work with our prior work on bipeds in Chapter IV,, showed that for the same set of parameters and the same choice of the Poincaré section the two models behave exactly identical: quadrupedal pronking is equal to bipedal hopping, quadrupedal bounding with a gathered/extended suspension is equal to bipedal leaping, and bounding with two suspensions is equal to bipedal running.

Such similarities between bipedal and quadrupedal gaits have been long postulated and have been studied previously using the established SLIP model. However, due to the large dimensions of solutions in the SLIP model, previous research only focused on symmetrical gaits, such as the correspondence of running and trotting (*Alexander*, 1984; *Farley et al.*, 1993). Knowing about the connections between the bipedal and quadrupedal model, and also about the connections between the different types of quadrupedal bounding gaits may help the design of robots and controllers that can switch between different gaits.

Naturally, the similarities between bipeds and quadrupeds become less evident as the main body inertia in the quadruped decreases and the solutions change. In the bipedal model, because the legs are all connected to the COM, the main body stays horizontal in all gaits and for all values of the main body inertia. On the other hand, the two leg pairs in the quadrupedal model are mounted at two ends of the torso, which results in a nonzero torque when the footfalls of these two leg pairs are not simultaneous. Therefore, the quadrupedal gaits start to differ as the main body begins to oscillate. Most notably are the changes in bounding with a gathered suspension. For low values of the main body inertia, these solutions disappear almost completely, leaving bounding with an extended suspension and bounding with two suspensions as the only passive modes of locomotion for a wide range of speeds.

In this work, I limited ourselves to bounding; that is, to gaits in which leg pairs move together. While this greatly reduced the complexity of the analysis, it should be noted that bounding is not a particularly common or efficient gait. In fact, in our prior work, I have shown that bounding is energetically inferior in quadrupedal robotic locomotion (*Xi et al.*, 2015). This holds both for quadrupeds with and without an articulated spine (*Yesilevskiy et al.*, 2018). A natural extension of this work is thus to expand our approach to discover half-bound (3-beat) and galloping (4-beat) gaits in which the footfalls of the front and hind legs are not necessarily synchronized

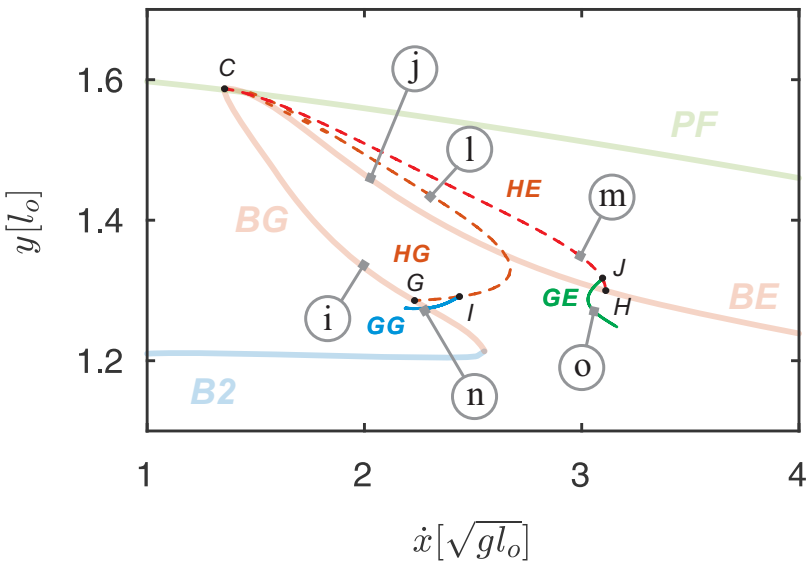

Figure 5.12: This figure shows how the half-bound (***HG*** and ***HE***) and gallop (***GG*** and ***GE***) branches evolve from the bounding gaits (***BG*** and ***BE***). Several key frames of each exemplary gait are shown in Fig. 5.13.

(*Hildebrand*, 1977). As these gaits include bounding as a special case, our preliminary results suggest that half-bound and galloping gaits emerge through additional bifurcations from the solution branches that have been presented in this paper. As indicated by dash lines in Fig. 5.12, the branches of half-bound (***HE*** with extended suspension, and ***HG*** with gathered suspension) are bifurcated from the bounding branches at G and H respectfully. The other side of ***HE*** and ***HG*** are all connected to pronking branch ***PF*** at point C. In addition, 4-beat galloping gaits (***GE*** with extended suspension, and ***GG*** with gathered suspension) are identified on the half-bound branches at point J and I. For each gait mentioned above, a exemplary periodic solution is in Fig. 5.13. It is worth noting that the galloping gaits shown in this figure have *transverse* footfall pattern (*Hildebrand*, 1989). Since this is a 2D model, one can easily find the *rotary* galloping by switching the initial angles and angular speed for only one pair of the legs (fore or hind pair). If switching both legs pairs, another branch of transverse galloping gait with different leading legs will be obtained. In this sense, there are *four* identical branches with different footfall

sequences laying together for ***HG*** and ***HE*** in Fig. 5.12.

Our work shows that all asymmetrical gaits can be generated with a single passive model and a single set of parameters. In a sense, the different gaits are just different oscillation modes of a single mechanical framework. Our model therefore has the potential to serve as a general template (*Full and Koditschek*, 1999) for the study of quadrupedal locomotion. It might also explain, why our past optimization studies (*Xi and Remy*, 2014) have converged to similar motions with varying flight phases. Furthermore, the approach could be extended to be used in the gait design of legged systems. In order to reproduce desired gaits efficiently, one can tune the parameter values of their specific hardware, such as the body mass, leg length, or the body inertia, to ensure the gaits are passively available.

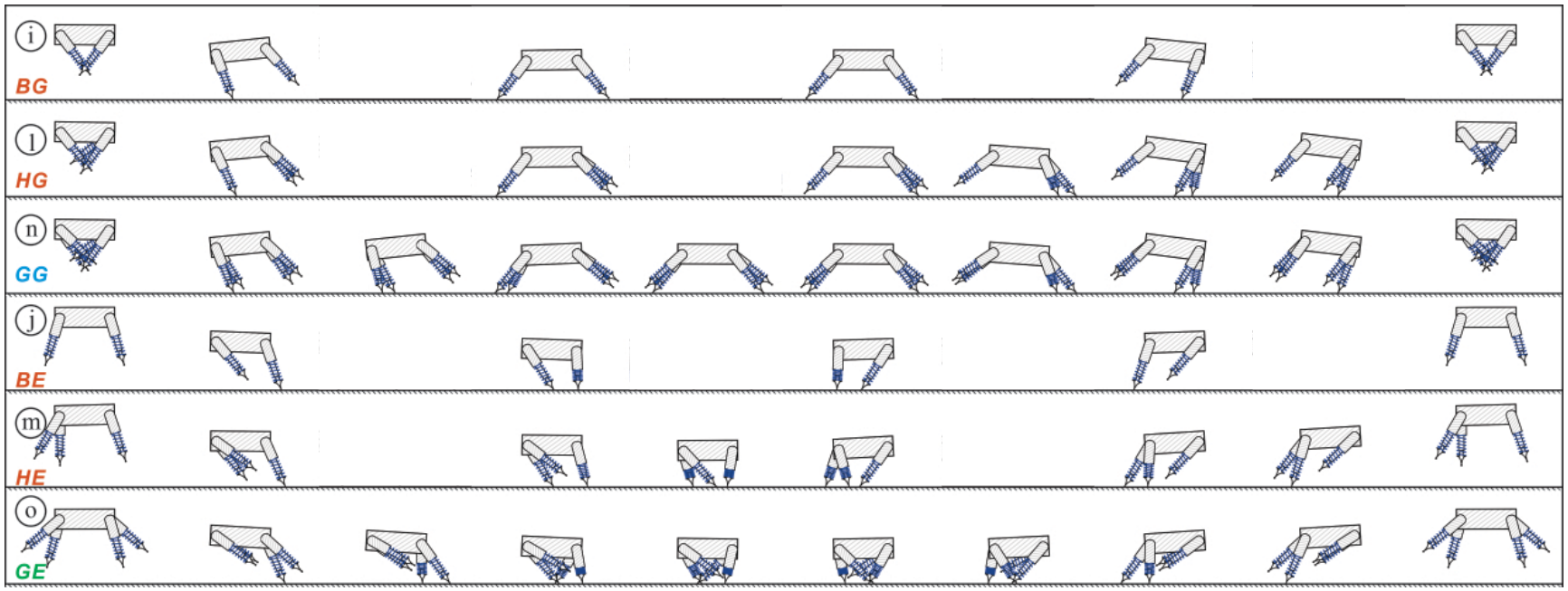

Figure 5.13: This figure compares several key frames of bound (***BG***, ***BE***), half-bound (***HG***, ***HE***), and gallop (***GG***, ***GE***) from the passive quadrupedal model with the same set of parameter values as indicated in Fig. 5.12. At the apex, according to their leg orientations these gaits can be categorized into two classes: the gaits with gathered suspension (***BG***(i), ***HG***(l), ***GG***(n)) and the gaits with extended suspension (***BE***(j), ***HE***(m), ***GE***(o)). Within each class, the main body moves in a similar fashion. As the symmetry in leg motions gradually breaks, legs hit the ground in quick successions which leads to all these gaits.

CHAPTER VI

General Conclusions and Future Directions

Throughout this dissertation, I have shown that it is possible to use a single model to reproduce almost all bipedal and quadrupedal animal gaits observed in nature. By restoring passive dynamics of swing leg motions to the SLIP models with instantaneous leg reset, the solution manifold is simplified to one-dimensional branches with varying total energy levels. These solution branches represent distinct gaits with various footfall patterns; they are all originated from simple hopping in-place motions and connected to each other through continuations and bifurcations. Therefore, the proposed models may explain why animals in nature with different morphology move in similar ways. They also have the potential to serve as the locomotion planning tool for hardware design or as the gait selection tool to improve energetic economy of the existing hardware.

6.1 Discussion and Contributions of Presented Work

In Chapter II & III, I extended the concept of the unified model from Geyer's bipedal SLIP model to quadrupeds. The proposed simplistic model generated a variety of different gaits primarily by altering the initial continuous and discrete states of the system. The resulting motions, footfall patterns, and GRFs emerge from these initial conditions through a numerical integration of the dynamics. The result suggests

that quadrupedal gaits are merely different dynamic modes of the same structural system and that we can interpret different gaits as different nonlinear elastic oscillations that propel an animal forward. These different oscillation modes create a large number of locomotion types and allow for varying properties (such as different locomotion velocities) that can be exploited by the animal. Despite its simplicity, the model does not only produce qualitatively different motion patterns, but can quantitatively reproduce the recorded vertical GRFs with high accuracy. Particularly the GRFs of trotting and tölting can be predicted with high R-square values. Larger residuals were only obtained in walking, but could be alleviated by adding a head-neck segment to the model.

Despite the simplicity of the dynamics, the structure of all periodic gaits of the SLIP models without swing leg motions are complex. This is mainly caused by the control parameter AOA for each leg during swing. In order to reveal the fundamental structure of gaits from bipedal systems, in Chapter IV, I extended the Geyer SLIP model with passive swing leg dynamics and explored all periodic solutions using numerical continuation method. This work consolidates a number of previous efforts to explain different gaits through mechanical dynamic models (*Mochon and McMahon*, 1980a; *Full and Koditschek*, 1999; *Blickhan*, 1989; *Farley et al.*, 1993; *Geyer et al.*, 2006; *Rummel et al.*, 2009). To the best of my knowledge, this is the first time it has been shown that a single model with fixed parameters can generate all common bipedal gaits at once. Furthermore, my results provide a new point of view on the relationships among different gaits, as we show that they are all connected to in-place bouncing through breaks in symmetry. My model therefore has the potential to serve as a general template (*Full and Koditschek*, 1999) for the study of bipedal locomotion. Previous models were either only able to produce a single gait (such as passive dynamic walking (*McGeer*, 1990)) or relied on a (control) parameter that had to be adjusted to obtain different motions (such as the AOA in the traditional SLIP model

(*Geyer et al.*, 2006; *Rummel et al.*, 2009)). In the case of the Geyer SLIP model, for example, a series of similar solutions can be found for the same AOA by varying the total energy of the model (*Geyer et al.*, 2006; *Rummel et al.*, 2009). Yet, the value of the AOA has to change for the same gait at various speeds and it has to take on different values to enable the two gaits, walking and running, that the Geyer SLIP model can exhibit (*Rummel et al.*, 2009). Moreover, since these models are essentially controlled, infinitely many solutions can be produced by gradually changing the AOA, leading to a high-dimensional solution space with no clear boundaries on individual gaits. In contrast, in the present work, the different gaits are found along distinct one-dimensional manifolds that are only connected through a series of discrete bifurcations. That is, while my results extend the range of gaits that can be explained by the mechanical dynamics of a single model, they also define these gaits in a more precise manner. For the individual running branches, for example, the solutions found within my study form a well-defined subset of the solution range of the SLIP model. In particular, they contain only solutions that can be achieved with passive swing dynamics and thus exclude, for example, motions that require unreasonably fast leg swing or are otherwise not physically achievable with an actual legged system. This work thus has the potential to provide a new definition of a gait: a distinct nonlinear dynamic mode of the underlying passive mechanical system.

In Chapter V, I extended the concept of passive swing leg motions to quadrupeds. Various bounding gaits with distinct footfall patterns have been identified. Similar to the bipedal model, since there is no control in this system, for a given initial state its motion is fully determined by the mechanical dynamics. Using numerical continuation techniques, I was to identify the most prevalent bounding gaits found in nature, such as pronking, bounding with extended support, bounding with gathered support, and bounding with two flight phases. These motions emerge completely passively, and may serve as a template to develop energetically economical motions for legged robotic

systems. While an actual robot would need to compensate for energetic losses due to friction, damping, and contact collisions, staying close to these passive motions would ensure that the robot avoids negative actuator work. This is because the energetic fluctuations that happen during locomotion can be fully realized by the dynamics of the mechanical system. In addition, the dynamic similarity between these bounding gaits and the bipedal gaits found in Chapter IV has been investigated. It has been shown that when the main body inertia in the models is infinite, the gaits of these two models are identical. As the body inertia gradually decreases, the main body from the quadrupedal model starts to oscillate and the resulting gaits become less similar.

6.2 Future Research

6.2.1 Symmetrical Gaits of Quadrupeds

In the end of Chapter V, I showed the solution manifold of several asymmetrical gaits of the quadrupedal model with passive swing leg motions. An immediate extension of this work would be studying the *symmetrical gaits* according to the Hildebrand's classification (*Hildebrand*, 1967). Symmetrical gaits are often used by animals at relatively low speeds, for example, walking, tölting, trotting, and pacing. The proposed quadrupedal model in Chapter V can be utilized directly to identify this type of gaits by simply enforcing additional constraints such that the phase delay within each leg pair (fore or hind) is one half of the stride cycle. Using the same methods, some preliminary results of symmetrical gaits are shown in Fig. 6.1 & 6.2.

As I have shown in Chapter II, trot is a 2-beat gait in which the diagonal leg pairs move simultaneously. In this gait, the main body of the model barely rotates within the whole stride. As a result, this type of gait resembles the running gait found in the bipedal model as shown in Fig. 4.3. Similar to the bipedal running, multiple

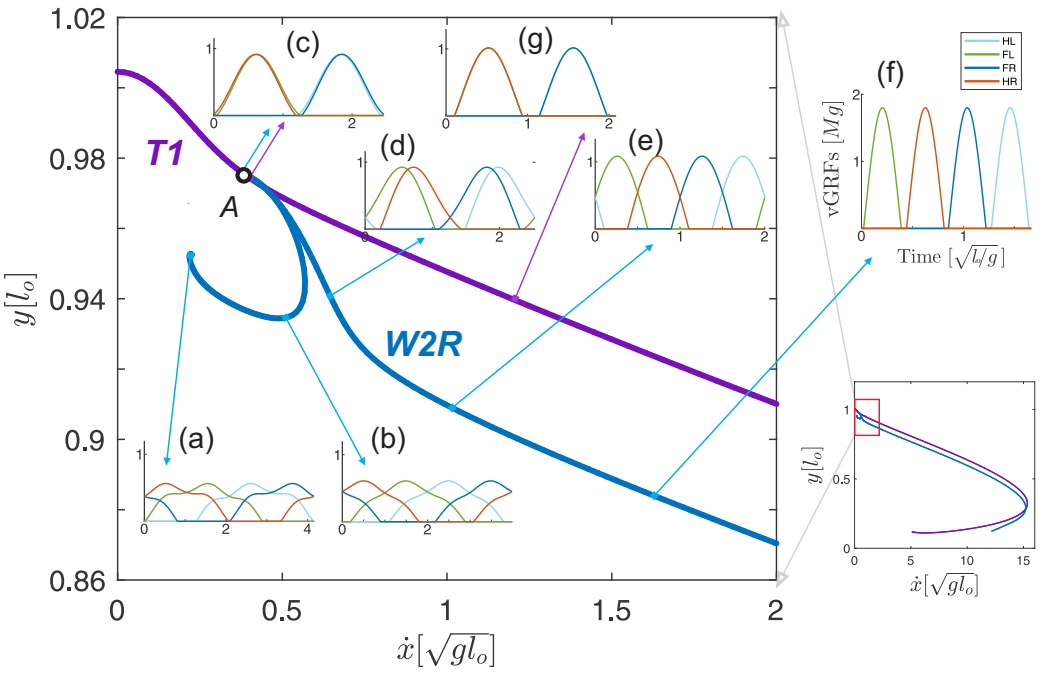

Figure 6.1: This figure demonstrates how the footfall patterns and the vertical GRFs change along the branches of symmetrical gaits ***T1*** and ***W2R***.

trotting branches ***T1*** and ***T2*** with different swing leg motions are found. Similar to the branches ***R1*** and ***R2***, solutions from ***T1*** have the same type of velocity reset at the moment of touchdown, while continuous leg velocities are observed in solutions from ***T2***.

Along the first trotting branch ***T1***, all solutions have the same footfall pattern in which the two leg pairs always strike the ground at the same time. As the forward speed increases, the magnitude of the largest vertical GRFs also increases, as shown in Fig. 6.1c & g. However, starting at point A, the two leg pairs gradually loose their synchronization along the branch ***T1***. This leads to two types of 4-beat gaits: walking with *diagonal* sequence (hind leg footfall followed by the footfall of the diagonal front leg) at low speeds as shown in Fig. 6.1a & b and running with *lateral* sequence (hind leg footfall followed by the footfall of the ipsilateral front leg) at high speeds e & f. At the other bifurcation point B on branch ***T2***, the 4-beat lateral walking and diagonal running are discovered as illustrated in Fig. 6.2. Even though all these

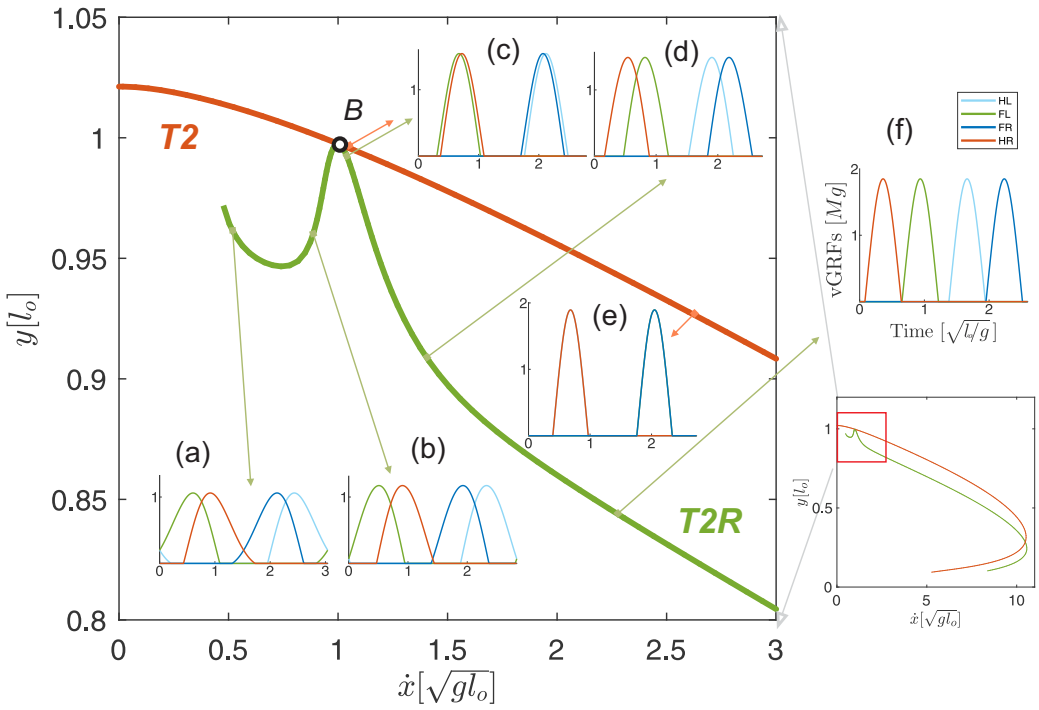

Figure 6.2: This figure demonstrates how the footfall pattern and the vertical GRFs change along the symmetrical gait branches ***T2*** and ***T2R***.

gaits merge into trotting around the bifurcation points, the changes in the footfall sequences are distinct. In the first case, at low speeds, the hind leg touch-down joins the *subsequent* touch-down of the front leg (Fig. 6.1b & c). On the other hand, the hind legs synchronize with the stance phase of the *prior* front leg (Fig. 6.2b & c).

It is also interesting to think about these branches if we switch the left and right legs in one of the leg pairs (fore or hind). In this case, because this is just a 2D model, the main body motion will remain the same. Therefore, the locations of the branches shown in Fig. 6.1 & 6.2 will not change. However, along the branches ***T1*** and ***T2***, legs on the same side of the body will move in the same fashion, which corresponds to a pacing gait. In addition, the original 4-beat gaits with lateral footfall pattern will change to diagonal sequence and visa versa.

6.2.2 Compare All Passive Quadrupedal gaits with Animal Gaits in Nature

So far, I have shown the proposed quadrupedal model is able to reproduce a large number of symmetrical gaits (Section 6.2.1) and asymmetrical gaits (Section 5.4) with a single set of parameter values. It could be interesting to compare these passive gaits with the gait graph in Fig. 1.3 and see to what extent this model can explain animal gaits in nature. For the symmetrical gaits with the selected values of model parameters, the proposed model creates a continuum with four branches similar to that in the gait graph as shown in Fig. 6.3a. However, due to the absence of realistic constraints such as the maximal leg compression or the largest limb force, many more solutions are identified in my model at high speeds as shown on the right of the figure. Additionally, even though many 4-beat running gaits with diagonal footfall pattern are found to connect the pacing gaits (dashed lines in the bottom of Fig. 6.3a) in the passive model, animals in nature rarely use these gaits might because of the stability concerns.

For the asymmetrical gaits, only those with small duty factors are identified in the passive model (Fig. 6.3b). Animals in nature, however, are able to maintain the same footfall pattern at slower speeds, especially large animals such as the bison or giraffe. Therefore, the region of asymmetrical gaits of the passive model may be expanded by exploring effects of different morphology, for example, different values of the main body inertia or the ratio between the body length and uncompressed leg length. Another potential reason for such small regions of asymmetrical gaits might be the fixed swing leg oscillation frequency used in the model. As a result, the solutions with varying forward speeds from the proposed model have roughly the same flight phase duration but different apex heights. Nevertheless, it is very common to see that as animals move faster, they also recirculate their limbs faster. Therefore, one can also scan different values of the swing leg oscillation frequency to see if the gaits branches

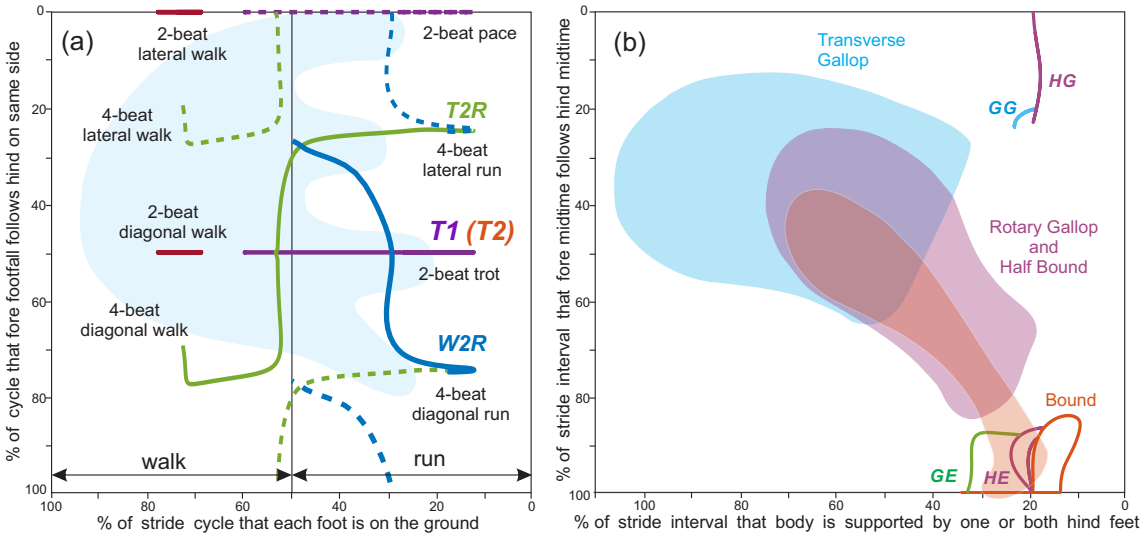

Figure 6.3: These two figures illustrate the symmetrical gaits (a) and asymmetrical gaits (b) obtained from the proposed passive quadrupedal model overlaid with animals gaits from the Gait Graph (*Hildebrand*, 1989). Dashed lines in figure (a) indicate the pacing branches obtained by switching one of the leg pairs in the trotting branches as shown in Fig. 6.1 & 6.2.

have smaller duty factors.

6.2.3 Including Damping or Other Sources of Losses into the Model

Another pertinent question of implementing the proposed conceptual models on hardware is, how would some physical constraints such as damping of springs, mechanical friction in joints, or collision losses, change the identified gait structure? And how to include these components into the gait analysis in a meaningful way? As for the spring damping alone, one can adopt a similar approach as what I have done for the swing leg torsional spring. That is, one can gradually decrease the value of damping coefficient c at the same rate of the foot mass m. In the limit of zero foot mass ($m \to 0$), the damping in the springs will not consume any energy ($c \to 0$) but it will still affect the trajectory of the swing leg motion. Since c/m will be a constant value in the EOM of the swing leg.

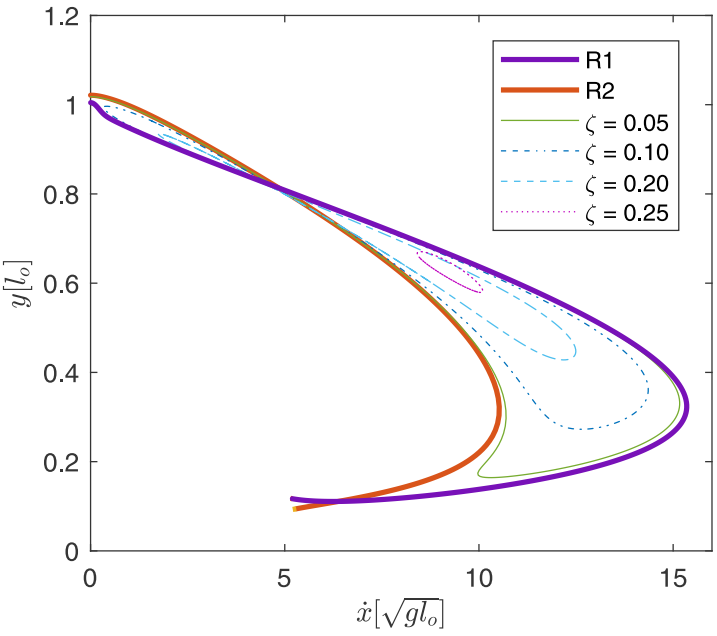

Figure 6.4: Branches of bipedal running solutions with different values of damping ratios are shown in this figure. Apex transition is selected as the Poincaré section. As the value of damping ratio ζ in the torsional spring at the hip increases, this two running branches merge together as a loop and shrinks.

I have identified some of the damped solutions for the bipedal running branches ***R1*** and ***R2*** discussed in Chapter IV. As shown in Fig. 6.4, by choosing different values of the damping ratio for the torsional spring at the hip, these two branches merge together as a loop. As the value of the damping ratio increases, this combined loop shrinks. On the other hand, with negative damping, periodic solutions also exist. In this case, these two branches will move away from each other as two independent curves which is not shown in the figure. Therefore, the damping in the system will not only dissipate the total energy of the system, but also affect the motion of the swing leg and the locations of the limit cycles. Thus, in order to implement the identified solutions of the undamped models on a hardware, it is important to compensate for the effect of physical damping.

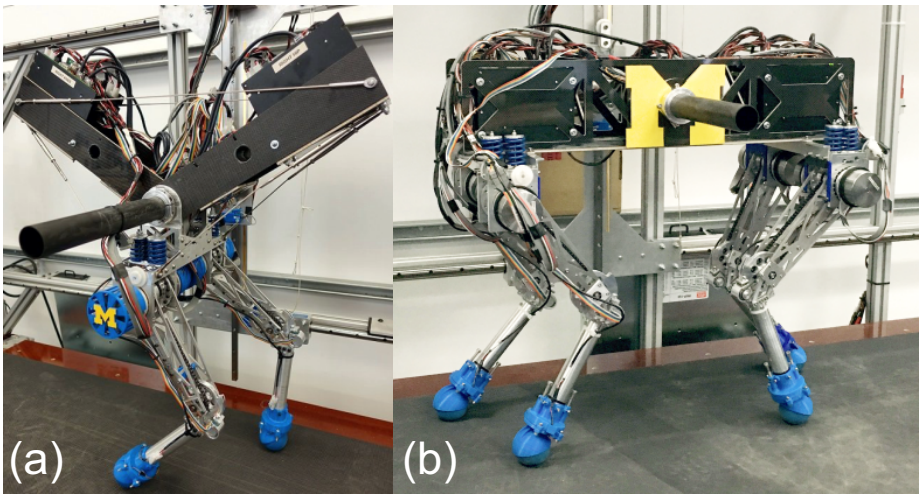

Figure 6.5: The robot RAMone (a) and RAMbi (b) developed at Robotics and Motion Laboratory (RAMlab) of the University of Michigan are designed with compliant legs.

6.2.4 Applications to Legged Systems

From the perspective of a roboticist, the most exciting aspect of the work in this thesis lies in its potential as a design tool for legged systems. The proposed passive models can be used directly to develop energetically economical motions that exploit the natural dynamics of the system. It might also explain, why the past optimization studies (*Xi and Remy*, 2014; *Xi et al.*, 2015; *Smit-Anseeuw et al.*, 2017a) have converged to motions that closely resemble gaits found in nature. Furthermore, the approach could be extended to be used in the development of new hardware that incorporates suitable dynamic elements, for example the planar bipedal and quadrupedal robots, RAMone and RAMbi developed in our lab. In both robots, there are two rotational joints (hip and knee) in each leg which are motorized by Series Elastic Actuators (SEAs) through harmonic drives. In order to utilize the passive gaits generated by the proposed simplistic models, several physical constraints have to be taken into considerations. First problem is the ground clearance enforced by the unilateral constraint of the ground. Since the feet of a robot in reality cannot penetrate the

ground, it is important to shorten the leg length during leg swing to avoid foot scuffing or premature touchdown collisions. Therefore, articulated knee joints as shown in Fig. 6.5 or prismatic sliders (see Fig. 1.2(c)) are usually adopted in hardware to achieve this task. Another concern is the stability and the robustness of the identified gaits. For example, what will happen if the actual values of the parameters in the hardware can not be obtained accurately? Also, what should the controller do if the legs strike the ground at a different time due to an external disturbance. To address these problems, additional feedback controllers or online optimization algorithms are required to ensure the desired periodic solution is attractive. With these problems solved, the complicated multibody dynamics of the actual robots could be tuned on the simplified model to yield beneficial natural dynamics that enable economical locomotion on a full robot. The results in this thesis also suggest that swing leg motions in legged systems can be simplified to be a nearly passive spring oscillation which has the same natural frequency for all gaits at different speeds. The fact that the model relies on a single set of parameters for all motions, also provides some reasoning that fixed stiffness actuators might be a sufficient choice for legged robots and that variable stiffness actuation is not necessarily required to achieve energetic economy.

Additionally, the continuation method and the bifurcation study can be used as a gait selection tool for a specific robot. As shown in Chapter V, quadrupeds with different main body inertia also have passive gaits with distinct footfall patterns. These results are supported by recent experiments on hardware. For example, *De* (2017) has shown that the stable phase relationship of two leg pairs in the Minitaur robot is highly dependent on the body inertia. In the results presented in this thesis, when the body inertia is smaller than $1\,\mathrm{Ml}_\mathrm{o}^2$, the leg pairs are weakly coupled and bounding is stable. As the body inertia increases, the two leg pairs are strongly coupled and the robot exhibits a stable pronking gait. Similar results were also observed on the MIT Cheetah 2, when the gait pattern stabilizer was not enforced,

the phase difference in the resulting gait became smaller (*Park et al.*, 2017). These results suggest that different morphology and varying body inertia of robots may affect the stability and availability of their gaits. One may test this hypothesis on a specific robot such as RAMbi to see whether or not these passive gaits are energetically optimal.

6.3 Concluding Remarks

In this thesis, several simplistic models with compliant legs and passive swing leg motions have been proposed for both bipeds and quadrupeds. By using numerical continuations, the structure of periodic solutions for these models have been systematically explored to reveal the fundamental relationships among different gaits. Parameter studies of these models demonstrate that some passive gaits are strongly affected by the morphology of the legged system. This work may provide some insights into understanding of the underlying dynamics of legged locomotion and may help design of more economical controllers for legged machines.

APPENDIX

APPENDIX A

EOM of the Headed Model

The equations of motion of the headed model were derived using the Euler-Lagrange equations. The mass matrix is given as:

$$M = \begin{bmatrix} m_1 + m_2 & 0 & C_1 & -m_2 l_2 \sin(\varphi + \theta) \\ 0 & m_1 + m_2 & C_2 & m_2 l_2 \cos(\varphi + \theta) \\ C_1 & C_2 & C_3 & C_4 \\ -m_2 l_2 \sin(\varphi + \theta) & m_2 l_2 \cos(\varphi + \theta) & C_4 & m_2 l_2^2 + j_2 \end{bmatrix}, \qquad \text{(A.1)}$$

with

$$\begin{aligned} C_1 &= -m_2 d_F \sin(\varphi) - m_2 l_2 \sin(\varphi + \theta), \\ C_2 &= m_2 d_F \cos(\varphi) + m_2 l_2 \cos(\varphi + \theta), \\ C_3 &= m_2 d_F^2 + m_2 l_2^2 + 2 m_2 d_F l_2 \cos(\theta) + j_1 + j_2, \\ C_4 &= m_2 l_2^2 + m_2 d_F l_2 \cos(\theta). \end{aligned}$$

The Coriolis, centrifugal, and gravitational terms are given as:

$$h = -\begin{bmatrix} \left(\dot{\varphi}+\dot{\theta}\right)^2 l_2 m_2 \cos(\varphi+\theta) + \dot{\varphi}^2 d_F m_2 \cos(\varphi) \\ \left(\dot{\varphi}+\dot{\theta}\right)^2 l_2 m_2 \sin(\varphi+\theta) + \dot{\varphi}^2 d_F m_2 \sin(\varphi) - (m_1+m_2)g \\ m_2\dot{\theta}^2 d_F l_2 \sin(\theta) + 2m_2\dot{\varphi}\dot{\theta} d_F l_2 \sin(\theta) - m_2 g d_F \cos(\theta) - m_2 g l_2 \cos(\varphi+\theta) \\ -m_2\dot{\varphi}^2 l_2 d_F \sin(\theta) - m_2 g l_2 \cos(\varphi+\theta) \end{bmatrix}. \tag{A.2}$$

The generalized forces additionally include the torque M_{head} that is produced by the head and neck spring-damper. The leg forces and the neck torque are projected into the generalized coordinates according to:

$$\tau = \sum_i J_i^T F_i + J_{head}^T M_{head} \tag{A.3}$$

$$\begin{aligned} \mathbf{J}_i &= [-\sin(\gamma_i),\ \cos(\gamma_i),\ d_i \cdot cos(\varphi-\gamma_i),\ 0] \\ \mathbf{J}_{head} &= \begin{bmatrix} 0 & 0 & 1 & 1 \end{bmatrix} \end{aligned} \tag{A.4}$$

APPENDIX B

EOM of the Quadrupedal Model with Swing Leg Motion

F_x, F_y, and τ are the net forces and torques created by the leg pairs in the EOM of the main body:

$$F_x = -\sum_i \sin(\alpha_i + \phi) F_i, \tag{B.1a}$$

$$F_y = +\sum_i \cos(\alpha_i + \phi) F_i, \tag{B.1b}$$

$$\tau = +\sum_i l_{b,i} \cos(\alpha_i) F_i, \tag{B.1c}$$

$$F_i = k_{\text{leg}} \cdot (l_o - l_i),$$

The equations used to solve for stance leg velocities and accelerations are listed in (B.2) and (B.3).

$$\dot{\alpha_i} = -\frac{2\dot{\phi}\left(l_{b,i}\cos\left(\alpha_i\right)\sin\left(\alpha_i+\phi\right)+y\right)+2\dot{x}\cos^2\left(\alpha_i+\phi\right)+\dot{y}\sin\left(2\left(\alpha_i+\phi\right)\right)}{2\left(l_{b,i}\sin(\phi)+y\right)} \tag{B.2}$$

$$
\begin{aligned}
\ddot{\alpha}_i \; = & \frac{1}{2\left(l_{b,i}\sin(\phi)+y\right)^{\,2}}\left(l_{b,i}\dot{\phi}\cos(\phi)+\dot{y}\right)\Big(2\dot{\phi}\left(l_{b,i}\cos\left(\alpha_i\right)\sin\left(\alpha_i+\phi\right)+y\right) \\
& \qquad +2\dot{x}\cos^2\left(\alpha_i+\phi\right)+\dot{y}\sin\left(2\left(\alpha_i+\phi\right)\right)\Big) \\
& -\left(l_{b,i}\sin(\phi)+y\right)\Big(2\dot{\phi}\Big(l_{b,i}(\dot{\phi}\cos\left(\alpha_i\right)\cos\left(\alpha_i+\phi\right)+\dot{\alpha_i}\cos\left(2\alpha_i+\phi\right))+\dot{y}\Big) \\
& \qquad +2\ddot{\phi}\left(l_{b,i}\cos\left(\alpha_i\right)\sin\left(\alpha_i+\phi\right)+y\right) \\
& \qquad +2\ddot{x}\cos^2\left(\alpha_i+\phi\right)-2\dot{x}(\dot{\alpha_i}+\dot{\phi})\sin\left(2\left(\alpha_i+\phi\right)\right) \\
& \qquad +\ddot{y}\sin\left(2\left(\alpha_i+\phi\right)\right)+2\dot{y}(\dot{\alpha_i}+\dot{\phi})\cos\left(2\left(\alpha_i+\phi\right)\right)\Big)
\end{aligned}
\tag{B.3}
$$

BIBLIOGRAPHY

Bibliography

Alexander, R. M. (1980), Optimum walking techniques for quadrupeds and bipeds, *Journal of Zoology*, *192*(1), 97–117, doi:10.1111/j.1469-7998.1980.tb04222.x.

Alexander, R. M. (1982), *Locomotion of Animals*, Springer Netherlands, doi:10.1007/978-94-011-6009-4.

Alexander, R. M. (1984), The gaits of bipedal and quadrupedal animals, *The International Journal of Robotics Research*, *3*(2), 49–59, doi:10.1177/027836498400300205.

Alexander, R. M., and A. S. Jayes (1983), A dynamic similarity hypothesis for the gaits of quadrupedal mammals, *Journal of Zoology*, *201*(1), 135–152, doi:10.1111/j.1469-7998.1983.tb04266.x.

Allgower, E. L., and K. Georg (2003), *Introduction to Numerical Continuation Methods*, Society for Industrial and Applied Mathematics, doi:10.1137/1.9780898719154.

Bhounsule, P. A., J. Cortell, and A. Ruina (2012), Design and control of ranger: an energy-efficient, dynamic walking robot, in *Adaptive Mobile Robotics*, pp. 441–448, World Scientific, doi:10.1142/9789814415958_0057.

Blickhan, R. (1989), The spring-mass model for running and hopping, *Journal of Biomechanics*, *22*(11-12), 1217–1227, doi:10.1016/0021-9290(89)90224-8.

Bogisch, S., K. G.-V. Peinen, T. Wiestner, L. Roepstorff, and M. Weishaupt (2014), Influence of velocity on horse and rider movement and resulting saddle forces at walk and trot, *Comparative Exercise Physiology*, *10*(1), 23–32, doi:10.3920/cep13025.

Buchner, H., H. Savelberg, H. Schamhardt, and A. Barneveld (1997), Inertial properties of dutch warmblood horses, *Journal of Biomechanics*, *30*(6), 653–658, doi:10.1016/s0021-9290(97)00005-5.

Cavagna, G. A., and M. Kaneko (1977), Mechanical work and efficiency in level walking and running, *The Journal of Physiology*, *268*(2), 467–481, doi:10.1113/jphysiol.1977.sp011866.

Cavagna, G. A., H. Thys, and A. Zamboni (1976), The sources of external work in level walking and running., *The Journal of Physiology*, *262*(3), 639–657, doi:10.1113/jphysiol.1976.sp011613.

Chatzakos, P., and E. Papadopoulos (2007), Parametric analysis and design guidelines for a quadruped bounding robot, in *2007 Mediterranean Conference on Control & Automation*, IEEE, doi:10.1109/med.2007.4433668.

Clayton, H. M., H. C. Schamhardt, M. A. Willemen, J. L. Lanovaz, and G. R. Colborne (2000), Kinematics and ground reaction forces in horses with superficial digital flexor tendinitis, *American Journal of Veterinary Research*, *61*(2), 191–196, doi:10.2460/ajvr.2000.61.191.

Collins, S., A. Ruina, R. Tedrake, and M. Wisse (2005), Efficient bipedal robots based on passive-dynamic walkers, *Science*, *307*(5712), 1082–1085, doi:10.1126/science.1107799.

Dankowicz, H., and F. Schilder (2013), *Recipes for Continuation*, Society for Industrial and Applied Mathematics, doi:10.1137/1.9781611972573.

Dawson, T. J., and C. R. Taylor (1973), Energetic cost of locomotion in kangaroos, *Nature*, *246*(5431), 313–314, doi:10.1038/246313a0.

De, A. (2017), Modular hopping and running via parallel composition, Ph.D. thesis, University of Pennsylvania.

Demes, B., J. Fleagle, and W. Jungers (1999), Takeoff and landing forces of leaping strepsirhine primates, *Journal of Human Evolution*, *37*(2), 279–292, doi:10.1006/jhev.1999.0311.

Eckert, P., A. Spröwitz, H. Witte, and A. J. Ijspeert (2015), Comparing the effect of different spine and leg designs for a small bounding quadruped robot, in *2015 IEEE International Conference on Robotics and Automation (ICRA)*, IEEE, doi:10.1109/icra.2015.7139629.

Farley, C. T., J. Glasheen, and T. A. McMahon (1993), Running springs: speed and animal size, *Journal of Experimental Biology*, *185*(1), 71–86.

Fiers, P., D. D. Clercq, V. Segers, and P. Aerts (2012), Biomechanics of human bipedal gallop: asymmetry dictates leg function, *Journal of Experimental Biology*, *216*(7), 1338–1349, doi:10.1242/jeb.074690.

Franz, T. M., B. Demes, and K. J. Carlson (2005), Gait mechanics of lemurid primates on terrestrial and arboreal substrates, *Journal of Human Evolution*, *48*(2), 199–217, doi:10.1016/j.jhevol.2004.11.004.

Full, R., and D. Koditschek (1999), Templates and anchors: neuromechanical hypotheses of legged locomotion on land, *Journal of Experimental Biology*, *202*(23), 3325–3332.

Gan, Z., and C. D. Remy (2014a), A passive dynamic quadruped that moves in a large variety of gaits, in *2014 IEEE/RSJ International Conference on Intelligent Robots and Systems*, pp. 4876–4881, IEEE, doi:10.1109/iros.2014.6943255.

Gan, Z., and C. D. Remy (2014b), A simplistic model for quadrupedal walking and trotting, Dynamic walking meeting, Zürich, Switzerland.

Gan, Z., T. Wiestner, M. A. Weishaupt, N. M. Waldern, and C. D. Remy (2015), Passive dynamics explain quadrupedal walking, trotting, and tlting, *Journal of Computational and Nonlinear Dynamics*, *11*(2), 021,008, doi:10.1115/1.4030622.

Gan, Z., Z. Jiao, and C. D. Remy (2018a), On the dynamic similarity between bipeds and quadrupeds:a case study on bounding, *IEEE Robotics and Automation Letters*, *accepted*.

Gan, Z., Y. Yesilevskiy, P. Zaytsev, and C. D. Remy (2018b), All common bipedal gaits emerge from a single passive model, *Journal of The Royal Society Interface*, *under review*.

Garcia, M. (1998), The simplest walking model: Stability, complexity, and scaling, *Journal of Biomechanical Engineering*, *120*(2), 281, doi:10.1115/1.2798313.

Geyer, H., A. Seyfarth, and R. Blickhan (2006), Compliant leg behaviour explains basic dynamics of walking and running, *Proceedings of the Royal Society B: Biological Sciences*, *273*(1603), 2861–2867, doi:10.1098/rspb.2006.3637.

Griffin, T. M. (2004), Biomechanical and energetic determinants of the walk-trot transition in horses, *Journal of Experimental Biology*, *207*(24), 4215–4223, doi:10.1242/jeb.01277.

Heglund, N. C., G. A. Cavagna, and C. R. Taylor (1982), Energetics and mechanics of terrestrial locomotion. iii. energy changes of the centre of mass as a function of speed and body size in birds and mammals, *Journal of Experimental Biology*, *97*(1), 41–56.

Hereid, A., S. Kolathaya, M. S. Jones, J. V. Why, J. W. Hurst, and A. D. Ames (2014), Dynamic multi-domain bipedal walking with atrias through SLIP based human-inspired control, in *Proceedings of the 17th international conference on Hybrid systems: computation and control - HSCC 14*, pp. 263–272, ACM Press, doi:10.1145/2562059.2562143.

Hermann, M., and M. Saravi (2016), *Nonlinear Ordinary Differential Equations*, Springer India, doi:10.1007/978-81-322-2812-7.

Herr, H. M., and T. A. McMahon (2000), A trotting horse model, *The International Journal of Robotics Research*, *19*(6), 566–581, doi:10.1177/027836490001900602.

Hildebrand, M. (1965), Symmetrical gaits of horses, *Science*, *150*(3697), 701–708, doi:10.1126/science.150.3697.701.

Hildebrand, M. (1967), Symmetrical gaits of primates, *American Journal of Physical Anthropology*, *26*(2), 119–130, doi:10.1002/ajpa.1330260203.

Hildebrand, M. (1977), Analysis of asymmetrical gaits, *Journal of Mammalogy*, *58*(2), 131–156, doi:10.2307/1379571.

Hildebrand, M. (1985), Walking and running, in *Functional Vertebrate Morphology*, chap. 3, pp. 38–57, Harvard University Press, doi:10.4159/harvard.9780674184404.c3.

Hildebrand, M. (1989), The quadrupedal gaits of vertebrates, *BioScience*, *39*(11), 766–775, doi:10.2307/1311182.

Hof, A. L. (1996), Scaling gait data to body size, *Gait & Posture*, *4*(3), 222–223, doi:10.1016/0966-6362(95)01057-2.

Holmes, P., R. J. Full, D. Koditschek, and J. Guckenheimer (2006), The dynamics of legged locomotion: Models, analyses, and challenges, *SIAM Review*, *48*(2), 207–304, doi:10.1137/s0036144504445133.

Hudson, P. E., S. A. Corr, and A. M. Wilson (2012), High speed galloping in the cheetah (acinonyx jubatus) and the racing greyhound (canis familiaris): spatio-temporal and kinetic characteristics, *Journal of Experimental Biology*, *215*(14), 2425–2434, doi:10.1242/jeb.066720.

Kuo, A. D. (2001), A simple model of bipedal walking predicts the preferred speed–step length relationship, *Journal of Biomechanical Engineering*, *123*(3), 264, doi:10.1115/1.1372322.

Lee, C. R., and C. T. Farley (1998), Determinants of the center of mass trajectory in human walking and running., *Journal of Experimental Biology*, *201*(21), 2935–2944.

Martinez, H. R., and J. P. Carbajal (2011), From walking to running a natural transition in the SLIP model using the hopping gait, in *2011 IEEE International Conference on Robotics and Biomimetics*, pp. 2163–2168, IEEE, doi:10.1109/robio.2011.6181612.

McGeer, T. (1990), Passive dynamic walking, *The International Journal of Robotics Research*, *9*(2), 62–82, doi:10.1177/027836499000900206.

McGuigan, M. P. (2003), The effect of gait and digital flexor muscle activation on limb compliance in the forelimb of the horse equus caballus, *Journal of Experimental Biology*, *206*(8), 1325–1336, doi:10.1242/jeb.00254.

Merker, A., D. Kaiser, and M. Hermann (2015), Numerical bifurcation analysis of the bipedal spring-mass model, *Physica D: Nonlinear Phenomena*, *291*, 21–30, doi:10.1016/j.physd.2014.09.010.

Minetti, A. E. (1998), The biomechanics of skipping gaits: a third locomotion paradigm?, *Proceedings of the Royal Society B: Biological Sciences*, *265*(1402), 1227–1233, doi:10.1098/rspb.1998.0424.

Mochon, S., and T. A. McMahon (1980a), Ballistic walking, *Journal of Biomechanics*, *13*(1), 49–57, doi:10.1016/0021-9290(80)90007-x.

Mochon, S., and T. A. McMahon (1980b), Ballistic walking: an improved model, *Mathematical Biosciences*, *52*(3-4), 241–260, doi:10.1016/0025-5564(80)90070-x.

Mombaur, K. D., H. G. Bock, J. P. Schlder, and R. W. Longman (2005), Stable walking and running robots without feedback, in *Climbing and Walking Robots*, pp. 725–735, Springer Berlin Heidelberg, doi:10.1007/3-540-29461-9_71.

Mordatch, I., M. de Lasa, and A. Hertzmann (2010), Robust physics-based locomotion using low-dimensional planning, in *ACM SIGGRAPH 2010 papers on - SIGGRAPH 10*, vol. 29, p. 71, ACM Press, doi:10.1145/1833349.1778808.

Muybridge, E. (2012a), *The Human Figure in Motion*, Dover Publications.

Muybridge, E. (2012b), *Animals in Motion*, Dover Publications.

O'Connor, S. M. (2009), The relative roles of dynamics and control in bipedal locomotion, Ph.D. thesis, University of Michigan.

Pandy, M. G. (2003), Simple and complex models for studying muscle function in walking, *Philosophical Transactions of the Royal Society B: Biological Sciences*, *358*(1437), 1501–1509, doi:10.1098/rstb.2003.1338.

Park, H.-W., P. M. Wensing, and S. Kim (2017), High-speed bounding with the MIT cheetah 2: Control design and experiments, *The International Journal of Robotics Research*, *36*(2), 167–192, doi:10.1177/0278364917694244.

Pavei, G., C. M. Biancardi, and A. E. Minetti (2015), Skipping vs. running as the bipedal gait of choice in hypogravity, *Journal of Applied Physiology*, *119*(1), 93–100, doi:10.1152/japplphysiol.01021.2014.

Poulakakis, I., J. A. Smith, and M. Buehler (2005), Modeling and experiments of untethered quadrupedal running with a bounding gait: The scout II robot, *The International Journal of Robotics Research*, *24*(4), 239–256, doi:10.1177/0278364904050917.

Raibert, M., M. Chepponis, and H. Brown (1986), Running on four legs as though they were one, *IEEE Journal on Robotics and Automation*, *2*(2), 70–82, doi:10.1109/jra.1986.1087044.

Remy, C. D., K. Buffinton, and R. Siegwart (2009), Stability analysis of passive dynamic walking of quadrupeds, *The International Journal of Robotics Research*, *29*(9), 1173–1185, doi:10.1177/0278364909344635.

Remy, C. D., M. Hutter, and R. Siegwart (2010), Passive dynamic walking with quadrupeds - extensions towards 3d, in *2010 IEEE International Conference on Robotics and Automation*, IEEE, doi:10.1109/robot.2010.5509408.

Remy, C. D., K. Buffinton, and R. Siegwart (2011), A MATLAB framework for efficient gait creation, in *2011 IEEE/RSJ International Conference on Intelligent Robots and Systems*, pp. 190–196, IEEE, doi:10.1109/iros.2011.6094452.

Remy, C. D., M. Hutter, M. Hoepflinger, M. Bloesch, C. Gehring, and R. Siegwart (2012), Quadrupedal robots with stiff and compliant actuation, *at - Automatisierungstechnik*, *60*(11), 682–691, doi:10.1524/auto.2012.1042.

Rezazadeh, S., C. Hubicki, M. Jones, A. Peekema, J. V. Why, A. Abate, and J. Hurst (2015), Spring-mass walking with ATRIAS in 3d: Robust gait control spanning zero to 4.3 KPH on a heavily underactuated bipedal robot, in *Proceedings of the ASME 2015 Dynamic Systems and Control Conference*, p. V001T04A003, ASME, doi:10.1115/dscc2015-9899.

Rosa, N., and K. M. Lynch (2014), Extending equilibria to periodic orbits for walkers using continuation methods, in *2014 IEEE/RSJ International Conference on Intelligent Robots and Systems*, IEEE, doi:10.1109/iros.2014.6943076.

Rummel, J., Y. Blum, and A. Seyfarth (2009), From walking to running, in *Autonome Mobile Systeme 2009*, pp. 89–96, Springer Berlin Heidelberg, doi:10.1007/978-3-642-10284-4_12.

Rummel, J., Y. Blum, H. M. Maus, C. Rode, and A. Seyfarth (2010), Stable and robust walking with compliant legs, in *2010 IEEE International Conference on Robotics and Automation*, IEEE, doi:10.1109/robot.2010.5509500.

Seyfarth, A., H. Geyer, M. Gnther, and R. Blickhan (2002), A movement criterion for running, *Journal of Biomechanics*, *35*(5), 649–655, doi:10.1016/s0021-9290(01)00245-7.

Seyfarth, A., H. Geyer, and H. Herr (2003), Swing-leg retraction: a simple control model for stable running, *Journal of Experimental Biology*, *206*(15), 2547–2555, doi:10.1242/jeb.00463.

Smit-Anseeuw, N., R. Gleason, R. Vasudevan, and C. D. Remy (2017a), The energetic benefit of robotic gait selection—a case study on the robot RAMone, *IEEE Robotics and Automation Letters*, *2*(2), 1124–1131, doi:10.1109/lra.2017.2661801.

Smit-Anseeuw, N., R. Gleason, P. Zaytsev, and C. D. Remy (2017b), RAMone: A planar biped for studying the energetics of gait, in *2017 IEEE/RSJ International Conference on Intelligent Robots and Systems (IROS)*, pp. 4090–4095, IEEE, doi:10.1109/iros.2017.8206266.

Smith, A., and M. Berkemeier (1997), Passive dynamic quadrupedal walking, in *Proceedings of International Conference on Robotics and Automation, ICRA*, vol. 1, pp. 34–39, IEEE, Albuquerque, New Mexico, doi:10.1109/robot.1997.620012.

Stewart, I., and M. Golubitsky (1992), *Fearful Symmetry: Is God a Geometer?*, Blackwell Publishers.

Talebi, S., I. Poulakakis, E. Papadopoulos, and M. Buehler (2001), Quadruped robot running with a bounding gait, in *Experimental Robotics VII*, pp. 281–289, Springer Berlin Heidelberg, doi:10.1007/3-540-45118-8_29.

Vaughan, C. L., and M. J. O'Malley (2005), Froude and the contribution of naval architecture to our understanding of bipedal locomotion, *Gait & Posture*, *21*(3), 350–362, doi:10.1016/j.gaitpost.2004.01.011.

Vorstenbosch, M., H. Buchner, H. Savelberg, H. Schamhardt, and A. Barneveld (1997), Modeling study of compensatory head movements in lame horses, *American journal of veterinary research*, *58*(7), 713718.

Waldern, N. M., T. Wiestner, K. Peinen, C. G. G. Álvarez, L. Roepstorff, C. Johnston, H. Meyer, and M. A. Weishaupt (2009), Influence of different head-neck positions on vertical ground reaction forces, linear and time parameters in the unridden horse walking and trotting on a treadmill, *Equine Veterinary Journal*, *41*(3), 268–273, doi:10.2746/042516409x397389.

Weishaupt, M., N. Waldern, V. Kubli, and T. Wiestner (2014), Effects of shoeing on breakover forces in icelandic horses at walk, tlt and trot, *Equine Veterinary Journal*, *46*, 51–51, doi:10.1111/evj.12267_156.

Weishaupt, M. A., H. P. Hogg, T. Wiestner, J. Denoth, E. Stussi, and J. A. Auer (2002), Instrumented treadmill for measuring vertical ground reaction forces in horses, *American Journal of Veterinary Research*, *63*(4), 520–527, doi:10.2460/ajvr.2002.63.520.

Weishaupt, M. A., T. Wiestner, H. P. Hogg, P. Jordan, and J. A. Auer (2004), Vertical ground reaction force–time histories of sound warmblood horses trotting on a treadmill, *The Veterinary Journal*, *168*(3), 304–311, doi:10.1016/j.tvjl.2003.08.007.

Xi, W., and C. D. Remy (2014), Optimal gaits and motions for legged robots, in *2014 IEEE/RSJ International Conference on Intelligent Robots and Systems*, pp. 3259–3265, IEEE, doi:10.1109/iros.2014.6943015.

Xi, W., Y. Yesilevskiy, and C. D. Remy (2015), Selecting gaits for economical locomotion of legged robots, *The International Journal of Robotics Research*, *35*(9), 1140–1154, doi:10.1177/0278364915612572.

Yesilevskiy, Y., W. Yang, and C. D. Remy (2018), Spine morphology and energetics: how principles from nature apply to robotics, *Bioinspiration & Biomimetics*, *13*(3), 036,002, doi:10.1088/1748-3190/aaaa9e.